INFORMATION TO USERS

The most advanced technology has been used to photograph and reproduce this manuscript from the microfilm master. UMI films the text directly from the original or copy submitted. Thus, some thesis and dissertation copies are in typewriter face, while others may be from any type of computer printer.

The quality of this reproduction is dependent upon the quality of the copy submitted. Broken or indistinct print, colored or poor quality illustrations and photographs, print bleedthrough, substandard margins, and improper alignment can adversely affect reproduction.

In the unlikely event that the author did not send UMI a complete manuscript and there are missing pages, these will be noted. Also, if unauthorized copyright material had to be removed, a note will indicate the deletion.

Oversize materials (e.g., maps, drawings, charts) are reproduced by sectioning the original, beginning at the upper left-hand corner and continuing from left to right in equal sections with small overlaps. Each original is also photographed in one exposure and is included in reduced form at the back of the book. These are also available as one exposure on a standard 35mm slide or as a 17" x 23" black and white photographic print for an additional charge.

Photographs included in the original manuscript have been reproduced xerographically in this copy. Higher quality 6" x 9" black and white photographic prints are available for any photographs or illustrations appearing in this copy for an additional charge. Contact UMI directly to order.

UMI

University Microfilms International
A Bell & Howell Information Company
300 North Zeeb Road, Ann Arbor, MI 48106-1346 USA
313/761-4700 800/521-0600

Order Number 9009724

Thermally-induced agglomeration in fluidized beds

Compo, Peter C., Ph.D.

City University of New York, 1989

U·M·I
300 N. Zeeb Rd.
Ann Arbor, MI 48106

A

THERMALLY INDUCED AGGLOMERATION IN FLUIDIZED BEDS

by

PETER COMPO

A dissertation submitted to The Graduate Faculty in
Engineering in partial fulfillment of the requirements
for the degree of Doctor of Philosophy,
The City University of New York

1989

This manuscript has been read and accepted for the Graduate Faculty in Engineering in satisfaction of the dissertation requirement for the degree of Doctor of Philosophy.

Sept 19 1989
Date

G. Tesler
Chair of Examining Committee

9/19/89
Date

Jacques E. Bernieste
Executive Officer

Robert Pfeffer
Herbert Weinstein
Leslie L. Isaacs
Dominick N. Mazzone
Robert W. Sylvester

Supervisory Committee

The City University of New York

ABSTRACT

THERMALLY INDUCED AGGLOMERATION IN FLUIDIZED BEDS

By

Peter Compo

Advisers: Professor Gabriel Tardos and Professor Robert Pfeffer

The surfaces of particulate solids can become cohesive at temperatures as low as 40% of the material's absolute melting point. This "high temperature cohesion", frequently described as being due to sintering, occurs in a number of industrial fluidized bed systems and is in general a nuisance to be avoided. Siegell (1976) showed that dilatometry could be used to predict the temperature of incipient cohesion. In the present work, this technique is broadened so as to apply to a number of industrially important particle types and other materials which had not been previously tested. It is concluded that the surfaces of particles in the high temperature range exhibit liquid-like behavior which allows for instantaneous interparticle bonding of some strength. The minimum sintering temperatures of numerous materials are reported and the relative minimum sintering temperature is shown to decrease with the material's degree of ionic bonding.

Fluidized bed agglomeration is proposed to occur according to a survival mechanism in which the state of agglomeration is determined by the strength and nature of both the interparticle attraction and the breaking forces in the bed. It is shown that Geldart type "C" fluidization is a limiting case of agglomeration where the agglomerate structures are porous and very weak. The mechanism deviates from the two body models of agglomeration because two body models do not discriminate between agglomerate configurations. The minimum fluidization velocity and defluidization of agglomerating systems at high temperatures are also discussed.

To the memory of Dr. Samuel Kahn

ACKNOWLEDGEMENTS

I thank my mentors, Professors Gabriel Tardos and Robert Pfeffer for their guidance and help during the course of this work and for introducing me to many of their colleagues in the chemical industry. I appreciate also the helpful discussions with Professor Leslie Isaacs and Professor Herbert Weinstein over the course of my studies.

I thank Dr. Dominick Mazzone, Dr. Alan Avidan, and Professor Charles Maldarelli for their friendship and good advice.

I am grateful to the Chemical Engineering Department's technical staff, including Mr. Ivan Ortiz, Mr. Bill Hall, and Mr. Russel Smith for their assistance in designing and building the experimental equipment.

Finally, I would like to acknowledge the International Fine Particle Research Institute (IFPRI) for the funding of a large part of this work.

TABLE OF CONTENTS

LIST OF TABLES

LIST OF FIGURES

NOMENCLATURE

A_b	Cross sectional area of a fluidized bed [cm]
A_p	Projected area of a sphere [cm^2]
b	Bond neck diameter [cm]
Co	Cohesion number [-]
D_b	Diameter of fluidized bed [cm]
D_s	Dilatometer sample diameter [cm]
d_{agg}	Agglomerate diameter [cm]
d_p	Particle diameter [cm]
F_{ad}	Adhesion force between two particles [N]
F_d	Drag force on a body [N]
F_p	Interparticle compressive stress [N/m^2]
F_V	Vertical force [N]
F_v	Van der Waals force [N]
Ga	Gallileo number [-]
H_o	Bed height at rest [cm]
k	coordination number [-]; constant in Equation A.21 [-]; function in Equation (C.6)
L	Load on dilatometer sample [g]
L_o	Initial length of dilatometer sample [cm]
ΔL	Dilatometer sample length change [cm]
n	Number of primary particles in an agglomerate [-]; exponent in Equation (C.6) [-]
m	Exponent in Equation (C.6) [-]
ΔP	Pressure drop over the fluidized bed [cm H_2O]
ΔP_ℓ	Pressure drop over a differential height (ℓ) of the the fluidized bed [cm H_2O]
ΔP_{max}	Maximum pressure drop over the fluidized bed during refluidization [cm H_2O]; maximum pressure across an agglomerate [N/cm^2]
P_1	Pressure measured at the bottom of the bed [cm H_2O]
P_2	Pressure measured at the middle of the bed [cm H_2O]
Re	Reynolds number [-]

Re_{mf}	Reynolds number at minimum fluidization [-]
S	Adhesive stress [$g^2/cm \cdot s^2$]
T	Temperature [^oC]
T_m	Melting point [^oC]
T_s	Minimum sintering temperature [^oC]
T_{soak}	Temperature of isothermal soak [^oC]
t	Time [s]
U	Superficial velocity [cm/sec]
U_{mb}	Minimum bubbling velocity [cm/sec]
U_{mf}	Minimum fluidization velocity [cm/sec]
U_{mfo}	Minimum fluidization velocity at ambient conditions [cm/sec]
U_{mfs}	U_{mf} at the minimum sintering temperature [cm/sec]
W_{agg}	Weight of an agglomerate [g]
W_p	Weight of a particle [g]
W_b	Weight of a fluidized bed [g]

Greek Symbols:

α	Coefficient of thermal expansion [cm/cm/^oC]
β	Packing factor [-]
Γ	Surface tension [N/m]
ε	Voidage [-]
ε_{mf}	Voidage at minimum fluidization [-]
ℓ	Differential height of fluidized bed [cm]
Φ_a	Shape factor of a cluster made of spherical particles [-]
Φ_p	Shape factor of a single particle [-]
Φ	Shape factor of a cluster [-]
η	Surface viscosity [g/cm·s]
Ψ	Adhesive force (Equation A.7)
μ	Gas viscosity [g/cm·s]
ρ	Gas density [g/cm^3]
ρ_s	Particle density [g/cm^3]
σ_t	Tensile strength [N/m^2]
σ_y	Yield strength [N/m^2]
τ	Time constant for sintering [1/s]

EXECUTIVE SUMMARY

The principle aim of this study is to broaden the understanding of thermally induced agglomeration in fluidized beds and in particular to refine the methods used to predict its occurrence. Agglomeration at high temperatures occurs when the particle surface in some way becomes mobile allowing for the formation of interparticle bonds which can resist stress. The process of surface mobility development is closely related to sintering, but sintering in the traditional sense implies particle contact before heating (as in the fabrication of refractory metals and ceramics powders). In high temperature fluidized beds, however, particles are first contacted at elevated temperatures. Thermally induced cohesion is one of many processes by which particle systems become cohesive; others include van der Waals interactions, electrostatics, liquid bridging, and particle magnetization.

Interest in thermally induced particle agglomeration was stimulated by the development of agglomerating coal gasifiers in the 1970's. Siegell and Squires et al. (see Siegell, 1976) were the first to make a systematic study of the subject by performing controlled high temperature fluidization experiments in small scale equipment. They also developed the technique of using constant heating rate dilatometry to predict the temperature of incipient interparticle cohesion, coining the term "initial sticky temperature" (now commonly referred to as the "minimum sintering temperature", T_s). Siegell reported a fairly good correlation of initial shrinkage in the dilatometer with initial cohesion in the fluidized bed for various particle types. The importance of the minimum sintering temperature has been made more clear through the acquaintance of the author with a number of industrial cases of high temperature fluidization in which the principle objective was to avoid high temperature cohesion.

Details on Siegell's and the other studies which have been made of high temperature agglomeration are given in Chapter One. In addition, the various models of both bubbling bed agglomeration and agglomeration in systems meant to mimic gasifiers are discussed. These models range in complexity from simple correlations of the so called minimum

fluidization velocity to detailed models of particle interactions, particularly two body models of agglomeration.

In the present work, high temperature dilatometry and fluidization experiments have been performed using a number of particle types. The results are presented in Chapter Two. Some of these materials have been tested before such as glass beads, certain polymers, and coal ash powders. Results on inorganic salts, a titanium dioxide ore beneficiate, FCC catalysts, and a ferrous chloride powder are presented here for the first time. The materials are grouped into two categories: model materials (Section 2.2), of which more exhaustive investigations were made, and industrial materials (Section 2.3), labeled as such mainly because they were supplied by industrial contacts who were interested in the material's cohesive properties. The industrial materials had either been found to agglomerate in use or were being screened for potential cohesion in a developing process. The rational for choice of model materials is discussed in Section 2.2.1. Descriptions of the experimental procedures and equipment used are given in Section 2.1.

The results of high temperature experiments confirmed the general applicability of constant heating rate dilatometry to predicting the minimum sintering temperature. Some deviations were observed, however, particularly in the interpretation of inorganic salt data. For example, sodium chloride crystals were found to expand at even greater rates than predicted by thermal expansion data once the minimum sintering temperature was reached. Confusion arises when testing inorganic crystals which are hydrated at ambient temperature (Section 2.2.3). The crystals demonstrate shrinkage in the dilatometer which can not be attributable to interparticle bonding. Other deviations from the "ideal" dilatometry curve are noted, but none seem to be significant enough to suppress the usefulness of the method.

Data from the fluidization experiments clearly show that many properties of fluidized beds (i.e. voidage, minimum velocity for stable fluidization, etc.) are significantly altered by high temperature cohesion. The changes in these properties have been traditionally related to the formation of agglomerates, yet efforts to sample agglomerates were consistently unsuccessful. Strong (strong enough to survive the sampling process), distinguishable agglomerates comprised of

more than two or three primary particles were almost never obtained. This was surprising considering that the whole range of adhesive forces relative to dynamic breaking forces was traversed in the experimental procedures. In fact, experiments were attempted at temperatures so high that fluidization was impossible under any velocity conditions. These observations led to the interpretation of the state of agglomeration being dominated by the breakage of weak agglomerates and the survival of strong ones. This mechanism deviates from the two-body models of agglomeration in that agglomerate configuration must be taken into account. In addition, most models of agglomeration stress the importance of the collision process on agglomerate formation, while the mechanism expounded here stresses that many more agglomerates are formed than actually survive, and that it is differences in configuration strengths which decides the final outcome. These arguments are made in Section 3.1 where discussions of the minimum fluidization velocity and bed defluidization are also included.

The high temperature bonding mechanism is discussed in Section 3.2. It is argued that the surfaces of particles above the minimum sintering temperature are liquid-like which accounts for the development of interparticle cohesion on very short time scales. Properties of the minimum sintering temperature are discussed in Section 3.2.2.: the most important property discussed is an inversely proportional relationship between the relative minimum sintering temperature, $T_s/T_m(^oK/^oK)$, and the materials ionic bond character. The ionic character is approximated by the electronegativity difference of the elements comprising the material.

Conclusions and suggestions for future work are presented in Chapter four. Future work might include the study of interparticle cohesion in systems undergoing chemical reaction or transformation (for example, a solid-solid phase transformation). Appendix D contains a preliminary report of defluidization caused by reduction of phosphogypsum to calcium sulfide.

INTRODUCTION AND BACKGROUND

1.1 Cohesive Particle Systems

The surfaces of solid particles become cohesive at temperatures well below the bulk melting point of the material. This phenomena, referred to here as "high temperature cohesion" is one of many mechanisms by which particulate solids can become cohesive. Cohesiveness in gas-particle systems is defined in this dissertation as the phenomenon where particle motion is influenced by interparticle attracive forces. Some interparticle forces (e.g., van der Waals and electrostatic forces) are present in all particle systems to some extent, but it is clear from this definition that the presence of interparticle attractive forces does not alone render a gas-particle system cohesive. The interparticle forces must be of sufficient magnitude relative to the other forces which also influence particle motion.

Interparticle forces vary in strength, distance of interaction and dynamic behavior; they may also be dependent on the surrounding gas humidity, temperature and pressure. Generally, most interparticle attractions are electrical in nature or a result of material bridges between particles.

Clift (1985) has reviewed the three most common and best understood interparticle forces: those due to electrostatic, Van der Waals and capillary phenomena (see also Rietema, 1984 and Geldart et al., 1984). Electrostatic and Van der Waals forces are present in most particle systems to one degree or another with electrostatic charge usually resulting from triboelectrification. These forces are relatively weak but can have a significant effect on the fluidization quality of small particles.

Fluidization quality is typically described in terms of Geldart's (1973) classification (see Geldart,1986 for a more recent discussion). As an example, the presence of these forces is thought to be necessary for the stable, non-bubbling fluidized expansion of type A powders (Musters and Rietema, 1977; Seville and Clift, 1984). Anderson and Jackson's (1967) analysis showed particulate expansion to be an unstable state if only hydrodynamic effects are in control. (For an alternative view of the importance of cohesion in bed stabilization see Foscolo et al.,[1985] who propose a theory of particulate bed expansion based purely on hydrodynamic considerations.) Clift cites the work of Agbin et al.(1971) who showed that permanent magnetization of metal particles could change fluidization behavior from type B to type A.

Pendular liquid bridges between particles result in interparticle capillary forces. Seville and Clift(1985) were able to change the behavior of a type B powder to type A and then type C by progressively adding layers of a non-volatile liquid to the bed. Capillary forces are stronger than those due to Van der Waals and electrostatic interations.

Fine, type C powders, have been shown to fluidize well because of the formation of agglomerates which are closer in properties to type A or B particles. Chaoki et al.(1985) reported stable fluidization of agglomerated, fine aerogel powders (primary particle size of about one micron). The interesting aspect is that the stable agglomeration only occurred when the gas velocity was raised far in excess of the minimum fluidization velocity as calculated from the primary particle diameter. The agglomerate size was estimated to be about 700 microns. Kono et al.(1987) and Morooka et al.(1987) reported similar effects with various fine metal and metal oxide powders. Also, Kono found that these same powders could serve as binders for type A FCC catalyts. In all three of these papers it was clearly shown that at low fluidization velocities the powders showed type C behavior and were unfluidizable but that at very high gas velocities (high with respect to the minimum fluidization velocity of the primary particles) the powders agglomerated and fluidized well as agglomerates.

1.2 Solid Surfaces at High Temperatures and Classical Sintering

Sintering is a powder metallurgical term which encompasses a wide range of high temperature particle bonding mechanisms. The surfaces of solids behave differently than the bulk of the material because of the excess free energy of the interface. At high temperatures, but below the melting point of a material, the activation energies needed for substantial material migration are attained allowing for atom mobility and surface rearrangement to more favorable equilibrium conditions. The

driving force for sintering is the reduction of high energy surface area.

The process of sintering is used as a method of metal fabrication because of the difficulties with melting refractories. Currently, sintering is an important technique in ceramic powder processing in addition to the well known metallurgical applications. Instead of melting these high melting point materials to form larger structures, fine powders are compacted and then heated to temperatures usually about two-thirds of the absolute melting point. Under suitable conditions the particles begin to bond and coalesce until the desired density and strength is obtained.

The physics of sintering is discussed by Yan(1987 and 1982), Waldron and Daniell(1978), Hirschhorn(1976), and Kuczynski(1972). Yan's(1982) paper is resricted to ceramic powders. Sintering has been defined by Kuczynski as "the process of approach to equilibrium which eventually should result in the coalescence of two spheres into one of double volume". But the term sintering implies no particular mechanism of particle bonding and many mechanisms have been shown to occur.

The dynamics of classical sintering are usually described in terms of stages of which as many as six have been proposed. Hirschhorn describes the first stage as grain bondary formation resulting in a bond neck between the two contacted particles and the second as the growth of the bond neck. Kuczynski does not differentiate initial bond formation from neck growth and considers the two processes to together constitute the first stage. Bond neck growth can proceed in two ways as shown schematically in Figure 1.1 taken from Kuczynski. In the first case

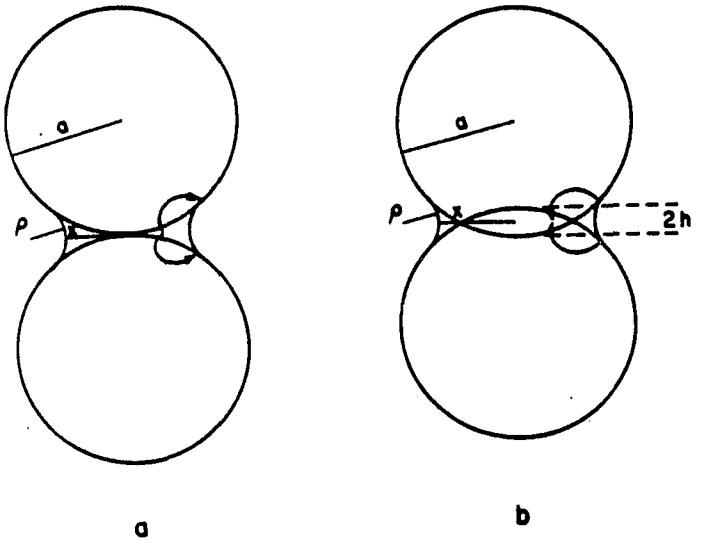

Figure 1.1. Schematic representation of the first stage of sintering. (a) spheres tangential (b) spheres interpenetrating. (From Kuczynski, 1972).

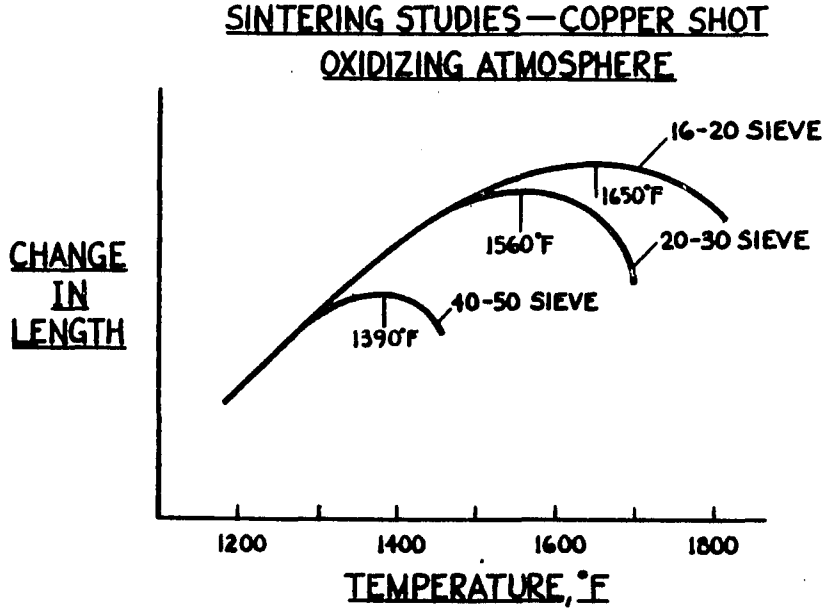

Figure 1.2. Siegell's (1976) dilatometry data for copper shot.

(Figure 1.1a) there is no change in the center to center distance between particles. Surface diffusion and evaporation-condensation through the vapor phase are mechanisms which can produce this result. Viscous flow, volume diffusion, and grain boundary diffusion are mechanisms which result in a decrease of the distance between particles as shown in Figure 1.1b. Hircshhorn states that the initial stage of bond formation will not result in a decrease of the distance between particles.

Following bond neck formation, sintering proceeds with changes in the geometry of the interstitial pores. These stages occur only after significant densification of the powder compact has occurred by bond neck growth and are sometimes difficult to achieve. The later stages begin with pore closure, where the void space is no longer connected, followed by pore rounding, pore shrinkage, and possibly pore coarsening.

1.3 High Temperature Cohesion in Industrial Fluidization

Currently, the most important aspect of high temperature cohesion in industrial fluid-particle systems is avoiding it. Difficulties caused by high temperature cohesion include particle deposition in high temperature cyclones (Jen and Tsao,1980), fouling of transport lines (Blake and Liss, 1985), agglomerate formation at distributor plates and other fluidized bed surfaces (Kwauk,1984), poor heat transfer and fluidization quality (Benson et al. 1982), and catastrophic defluidization (Squires, 1969). Futhermore, during the course of this research program, contact with many people from industry yielded reports

of operating limitations (sometimes severe) due to high temperature particle cohesion. But since most companies are reticent to reveal their particular problems, these situations are almost never reported in the literature. If anything, one good reason for this study is that the high temperature cohesion encountered in industry is almost never anticipated.

A few technologies have been developed to exploit high temperature cohesion in fluidized beds as a method of increasing particle size. The most familiar of these is the ash-agglomerating coal gasifier. In this process, coal is gasified at high temperatures in a fluidized bed which consists of a central oxidizing jet surrounded by auxillary air jets. The conditions are made such that the mineral content (ash) of the coal melts and coalesces into large bodies which then separate from the smaller and less dense coal particles by classification.

Comprehensive reviews of ash-agglomerating coal gasification have been written by Blake and Liss(1985), and Exxon(1984). Even though the development of this process precipitated the initiation of a number of research projects to study high temperature agglomeration phenomena, it really involves much more than high temperature solid sintering. The mechansim of ash agglomeration and bonding includes a number of steps starting with the melting of mineral matter in the coal particle. While exact mechanisms have not been formulated it is assumed that the melted ash migrates to the surface where it forms beads of liquid (coal is not wetted by the molten ash). Upon particle collisions, these beads coalesce. It is not clear if growth occurs by droplet coalescence only

or if ash solidifies and then bonds by sintering. (For a discussion of the ash agglomerating mechanism in gasifiers, see Harvey et al., 1975).

Discriptions of the few other applications of high temperature agglomeration can be found in Siegell(1976), Tardos et al.(1985a) or Huang(1985). Perhaps as the mechanisms of high temperature particle bonding and agglomeration become better understood, new applications will evolve.

An important difference between sintering in powder metallurgical applications and sintering in fluidized beds, is that the particles are not mechanically pressed prior to heat treatment in the fluidized bed. In metallurgical applications the powders are compacted prior to heat treatment and the theories and experiments relate only to this process. In a high temperature fluidized bed the particles first come into contact at the high temperature and the only compressive force acting between particles in addition to the capillary force of the particle-particle interface is the force due to collision.

1.4 Literature Review of High Temperature Agglomeration

1.4.1 Note on terminology

There is no established terminology for describing particle size enlargement in fluidized beds. In the fluidization literature the terms clustering, agglomeration, granulation, aggregation, and sometimes agglutination are used almost interchangeably and sometimes arbitrarily to label the process of size enlargement. Thus to avoid confusion, the term "agglomerate" will be used throughout to denote any secondary

structure of primary particles which forms in fluidized beds. Also, the particular form of the secondary structures will be referred to as the "state of agglomeration".

Similarly, "sintering" will be used to denote any high temperature physical process that results in interpaticle bonding, but no particlar mechanism of bonding is implied by this term.

As Adamson (1982) states: "The term high temperature is clearly a relative one". Surface mobility of refractory materials requires thousands of degrees while ice particles will form bond necks at $-10^{o}C$. As will be shown in Chapter 2, particles become cohesive at temperatures as low as 45%, while others show no cohesion at temperatures as high as 95% of their absolute melting point. Therefore, the high temperature range of a particle system starts at the temperature at which the particles first become cohesive and ends at the melting point of the solid. The temperature of incipient particle cohesion has been referred to in the literature as the "minimum sintering temperature", "minimum softening temperature", or the "initial sticky temperature". In this work, "minimum sintering temperature" will be used throughout, again with no particular mechanism of particle bonding implied.

1.4.2 High temperature fluidization in Bubbling Beds

Gluckman, Yerushalmi, and Squires (1976) and Siegell (1976, 1984) were the first to make a systematic study of the effect of thermally induced particle cohesion on fluidization. Siegell was also the first to use dilatometry for predicting particle cohesion in fluidized beds.

Siegell fluidized a variety of metallic, polymeric and glassy materials in a 2 inch diameter bed, and coal ash particles in a 6 inch bed. He measured the excess gas velocity ($U-U_{mf}$) needed to keep a bed fluidized at a number of different temperatures (i.e. a number of cohesion levels). Dilatometry was used to find the temperature at which the particles became cohesive as shown in Figure 1.2. The temperature at which contraction (shrinkage) of the material first occurred was assumed to be the temperature at which the particles first become cohesive, and the term "initial sticky temperature" was coined. (It is now more common to refer to the "initial sticky temperature" as the "minimum sintering temperature" which is denoted by T_s.)

Siegell organized his data by plotting the excess gas velocity versus the excess temperature ($T-T_s$) as shown in Figure 1.3a for copper particles. Linear regression was used to correlate the data from each individual run. In many of the runs, linear regression seemed to fit the data quite well, however in a number of cases, such as the one shown in Figure 1.3b, the straight line did not go through the origin. This means that either the data can not be modeled linearly or the initial sintering temperature as measured by dilatometry was not accurate. The inaccuracy of the dilatometry results was attributed to the difference in compressive forces between the dilatometer and the fluidized bed environment.

Siegell observed defluidization to occur very quickly. In his words: "the bed would be fluidized one minute and dead the next". Inspection of the fused bed material showed that the particles had not lost their integrity and that agglomerates were quite weak. From this it

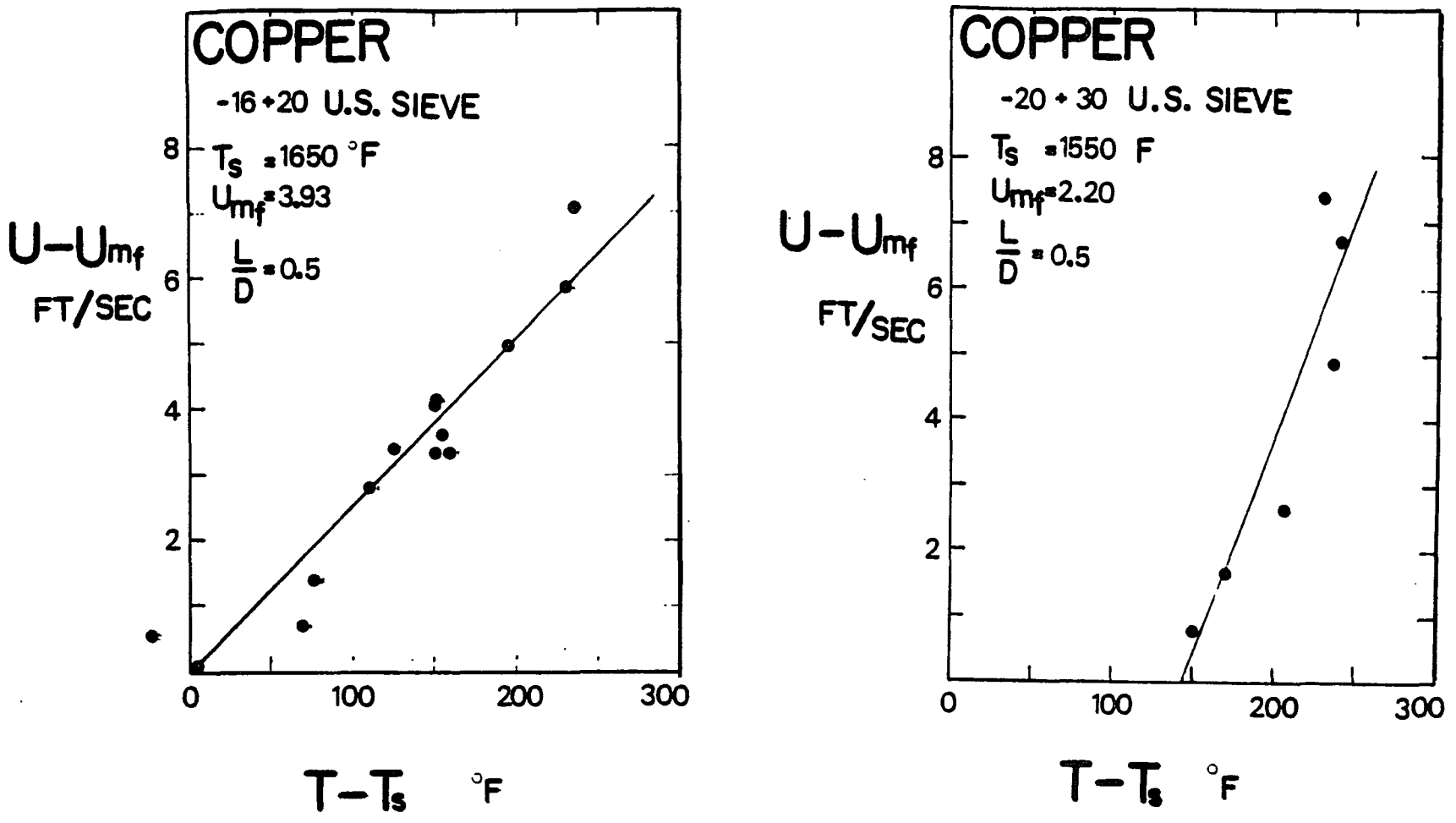

Figure 1.3. Siegell's (1976) defluidization data for copper shot.

was concluded that "neither melting nor substantial softening takes place".

Of particular interest, agglomeration in the fluidized state was observed directly using a high speed camera. This film shows quite clearly the simultaneous formation and disintergration of agglomerates. Agglomerates comprised on the order of three to six primary particles were common as the defluidization velocity was approached, and as defluidization occurred secondary structures formed which looked to be about one half the size of the column. These large structures lasted only seconds before defluidization occurred.

Following the pioneering work of Squires and Siegell, there have been only a few experimental studies of high temperature, bubbling bed fluidization. Basu (1982), and Basu and Sarka (1983) used dilatometry and a 10cm diameter fluidized bed to study coal ash agglomeration. Figure 1.4 shows Basu's dilatometry curve for an unidentified coal ash; the shape of the curve is much like those reported by Siegell. Tardos et al. (1985b) measured the defluidization charateristics of polyethene and polypropylene particles. Few of the results from these two studies conflicted with Siegell's conclusions except that Tardos and co-workers did not see a linear relationship between excess velocity and excess temperature in a log-log plot (see Figure 1.5). Both Basu (1982) and Tardos et al.(1985a) presented models of agglomeration, which are discussed in the next section.

Lau (1981), and Lau and Wally (1980) studied high temperature defluidization of caking coals in a 10cm fluidized bed. Sintering is not

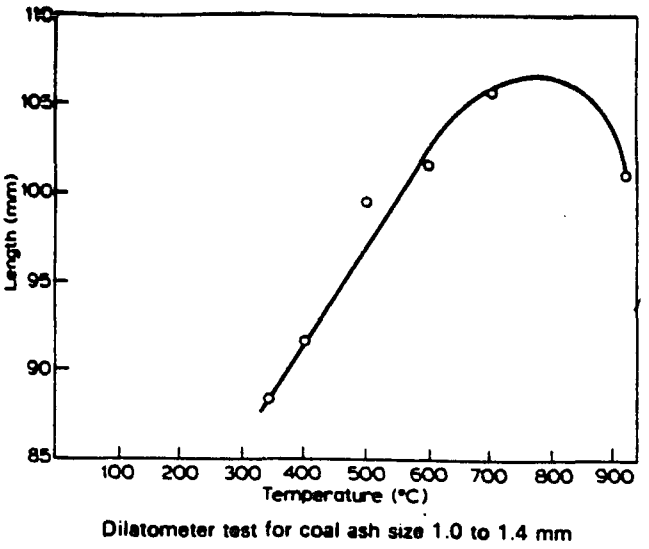

Figure 1.4. Basu and Sarka's (1983) dilatometry data for coal ash (ash not identified).

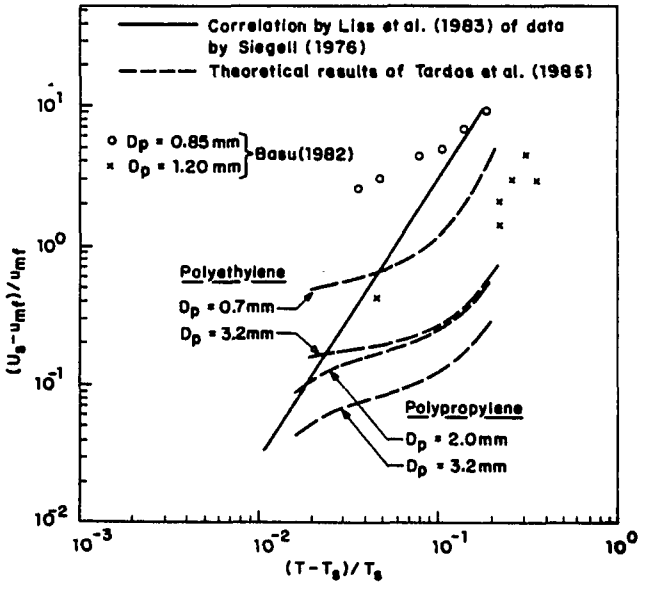

Figure 1.5. Defluidization results from Tardos et al. (1985b).

the mechanism of binding for coal powders (Exxon, 1984) but the observations of changing fluidization quality are interesting. These authors found that there was a possible transition of bubbling to slugging behavior as the temperature was increased.

Work of Huang, Arastoopour, and Weil

High temperature agglomeration was studied both theoretically and experimentally by Huang, Arastoopour and Weil. The experimental results can be found in Huang (1985) and Arastoopour et al.(1988). The model is presented in Huang (1985) and Rehmat et al.(1988). Again, discussion of the model is given in the next section.

The equipment in Huang et al's study was a six inch column with either a porous gas distributor or a porous distributor containing a central hot gas jet (hotter than the bubbling region). Only the incoming gas was heated. Both batch and continuous experiments were performed using polyethyene granules and polymer coated silica sand. The degree of agglomeration was defined as the number of agglomerates formed having a diameter larger than some predetermined value, usually 850μm. Initial particle sizes ranged from about 150μm to just under 850μm. The number of agglomerates was determined by sampling using small buckets.

The authors found that the percentage of agglomerates formed increased linearly with residence time, bed temperature, and fluidizing gas velocity. It is not clear however whether the temperature of the particles was known. The jet was much hotter than the surrounding phase but the time spent by a particle in each of the two phases was not determined. A particle temperature calculation was made in Rehmat et

al.(1988) but was based on the heat transfer to a single sphere in an infinite fluid (e.g. Bird, Stewart and Lightfoot, 1960). Increasing the jet velocity may have also increased the temperature of the particles. Consequently, the effect of temperature and jet velocity may not have been measured independently. Additional conclusions from this work were that larger primary particle sizes resulted in a smaller number of agglomerates and that agglomeration was dependent on the configuration of the entrance region of the jet.

It is interesting to note that Huang et al's initial experimental setup consisted of a porous distributor only. The reason for changing over to a jet arrangement was apparently because of the formation of large agglomerates (they called them "sinters") which invariably segregated and covered the plate. In the studies noted above, the beds were heated through the walls. Huang attributed the problem to a zone of higher temperature directly above the plate.

In their discussion of the interparticle bonding mechanism, Huang et al. followed the discription of sintering as put forth by Hirschhorn (1976). They state however that the powder metallurical theories do not directly apply to sintering in fluidized beds because (1) fluidized particles are only in contact for short durations, (2) temperatures are not uniform in fluidized beds, and (3) "powder metallurgy machines exert constant loads on particles while in fluidized beds the kinetic energy of colliding particles changes the interparticle force upon contact." These arguments conflict with the conclusions of Siegell (1976), Tardos et al. (1985b), and Basu(1982) in the sense that the later authors found dilatometry results to apply.

Studies on the effect of temperature on minimum fluidization

In addition to the studies on sintering particles there is a large body of literature concerning the effect of elevated temperature on the minimum fluidization velocities of non-cohesive particles (See for example, Hartman and Svoboda,1986; Yang et al,1985 and Botterill et al.,1982). Sometimes this literature is confused with the literature on cohesive materials, but these reports contain only a modification of the relationship between the drag coefficient and the Reynolds number as the temperature and pressure are increased in a fluidized bed. The aim of these studies is to account for the hydrodynamic factors needed to predict the minimum fluidization velocity for a wide variety of particle types and gas properties. The results show that the Ergun correlation (see Kunii and Levenspiel, 1969) is quite adequate for predicting the pressure drop through fixed and incipiently fluidized beds if the voidage and shape factor of the particles are known. However, none of these theories or correlations apply to fluidization of cohesive powders because interparticle forces are completely neglected.

1.4.3 Models of Fluidized bed Agglomeration

Two Body Models

To date, the most detailed models of fluidized bed agglomeration are the two body models as put forth by Huang et al.(1985) at IIT (also published in Rehmat et al.(1988)); Moseley and O'Brien(1986) at Morgantown; Scharff et al.(1980) at JAYCOR; and Jen and Tsao(1980). Though there are differences between these four models, the main premise

is that the state of agglomeration of a system can be characterized by the probablistic success or failure of individual two-body collisions. In addition, collisions are assumed to be successful if the kinetic energy of impact can be dissipated by some process, for example, viscous flow of molten material on the particle surface.

Huang(1985) proposed the following theory of two-body interactions: The particles are treated as viscoelastic bodies. When two particles collide their velocities change and the compressive force causes deformation of the contact area. He writes

> "Due to the change in the velocities of the particles (i.e., the deceleration of the particles), the viscous molten material on the surfaces of the particles, outside the contact area, moves towards the contact area to help the formation of bonding. The compression force between the particles may also squeeze some of the molten material out of the contact area...This viscous flow inevitably causes kinetic energy dissipation."

In this theory the bond between particles is not characterized by a bond strength. Agglomerates were modeled as spheres which are equal in volume to the number of primary particles of which they are comprised. All agglomerates are therefore equal in density. Also the potential for energy dissipation is related to the creeping flow of a molten layer over the spherical particles.

Bubbling Bed Models

The second type of model to be considered are those in which the effect of cohesion on the mimimum fluidization velocity of a bubbling bed system is taken into account (See Appendix A).

Baerns(1966), Basu(1982), and Liss et al.(1983) modeled the effect of cohesion on the minimum fluidization velocity of the system. Their approach was to modify the force balance on the solids at minimum fluidization

$$\Delta P_b \cdot A_b = W_b \qquad (1.1)$$

where ΔP_b is the pressure drop over the bed, A_b the bed cross sectional area, and W_b the bed weight, by the inclusion of a cohesive term, C

$$\Delta P_b \cdot A_b = W_b + C \qquad (1.2)$$

where C accounts for the effect of the interparticle force. This approach would appear to be incorrect. In the fluidized state the pressure drop over the bed can not exceed the weight of the bed, regardless of the state of agglomeration. Baern's theory differed in that the force balance was taken over a single particle, but the same criticism applies once the individual forces are summed to give the total pressure drop.

Chaoki et al.(1985) presented a model of agglomerate formation in which the weight of an agglomerate in the fluidized state is related to the force balance on the solids in the fixed bed state. These authors state that the drag force acting on an agglomerate in the fixed bed must

equal the weight of the agglomerate, W_{agg}, and must equal the interagglomerate cohesive force, F_{agg}

$$F_{agg} = W_{agg} \qquad (1.3)$$

This approach disregards the fact that the forces acting on particles in the fixed bed state are different from forces acting in the fluidized state: one is a static situation and the other is dynamic. Collisions between particles are completely ignored in this formulation.

The model proposed by Yamazaki et al. (1986) is somewhat similar to the model by Chaoki et al.(1985) but the force balance is not derived from the fixed bed state. In this theory the interparticle force, F_{ad}, is assumed (for reasons which are unclear) to be proportional to the weight of the agglomerate

$$F_{ad} = k \cdot W_{agg} \qquad (1.4)$$

where k is a constant of proportionality. Unfortunately there is still no inclusion of dynamic forces and so the result is similar to the force balance derived from the fixed bed state in Chaoki et al.'s theory (see Equation 1.3).

Tardos et al.(1985a) took a different approach to modeling the minimum fluidization velocity of cohesive systems. They assumed the defluidization velocity as that needed to fracture the largest possible agglomerate in the bed, that is, an agglomerate equal in size to the diameter of the bed. They felt that if an agglomerate of this size could

be prevented from forming the bed would remain fluidized. The strength of the agglomerate was related to the dynamic forces acting on it using fracture theory. Also, they stressed the importance of a dynamic equilibrium between agglomerate formation and breakage. Though the assumption of such a large agglomerate may be unrealistic, the concept of finding a limiting state of defluidization rather than solving for agglomerate sizes seems to be consistant with the needs of industry to avoid agglomeration.

Siegell(1976) also took into consideration the dynamic forces in the bed and proposed that the rate of agglomeration should be proportional to the interparticle force times the surface area, and inversely proportional to the particle momentum. He assumed that the particle momentum is proportional to the excess fluidization velocity and that the high temperature interparticle force is proportional to the excess temperature above the minimum sintering temperature and arrived at a correlation of the form

$$R_{agg} \sim \alpha * (1/d_p \rho_s T_s) * (T-T_s/U-U_{mf}) \qquad (1.5)$$

where R_{agg} is the agglomeration rate, α is a constant, and ρ_s is the particle density. This model did not appear to correlate his own data very well.

1.5 Objectives

The primary objective of this work is to refine and broaden the dilatometric technique for predicting incipient cohesion in gas-solid fluidized beds. This means not only determining the high temperature behavior of materials which have not been previously investigated, such as inorganic salts, but also a number of industrially important materials as well. Except for those presented by Siegell (1976), very few dilatometry results have been tested in high temperature fluidized beds. Much more data is needed.

The success of the dilatometric technique depends on a more fundamental understanding of both the agglomeration process in the fluidized bed, and the particle-particle bonding process. To date, the mechanism of high temperature bonding in fluidized beds has usually been assumed to follow powder metallurgical theories, where the particles are contacted (cold pressed) before high temperatures are reached. In the high temperature fluidized bed particles collide at the high sintering temperatures and are not cold pressed. Any bond neck formation must occur after collision.

Because the main concern with regard to high temperature cohesion is avoidance, further understanding of the minimum sintering temperature is needed. Siegell (1976) reported a small amount of data on the effect of particle size on minimum sintering temperatures, but to date no relationship has been established between the minimum sintering temperature and particle composition.

The actual choice of experimental materials used in this work was sometimes guided by industry. During the course of this research project we were contacted by people from industry who had questions regarding the high temperature behavior of a number of specific materials. Studying these materials ensured applicability to real issues. The results of these experiments are presented in Section 2.3. Glass beads, sodium chloride, and calcium chloride were used as model study materials and the rationale for choosing these is described in detail in Section 2.2.1.

EXPERIMENTAL RESULTS

2.1 Design and Operation of Equipment

2.1.1 High temperature fluidized bed

Fluidization experiments were performed using a 7.62 cm (3 inch) diameter fluidized bed. Referring to the schematic in Figure 2.1, fluidizing air from a Roots positive displacement rotary pump is passed through an Adams Poro-Stone centrifugal air filter which eliminates oil and water from the air stream. The compressed air stream is sent through a regulator and then a bank of rotameters. Air temperature and pressure are measured at the rotameter exit in order to correct for density changes.

Prior to entering the fluidized bed section through a porous (sintered) distributor plate, the air is preheated in a fixed bed packed with ~40 mesh sand. The tubes are heated by surrounding electrical resistance elements. The fluidized bed is also heated using electric resistance wall units which extend from the distributor plate to above the height of the fluidized particles. Even with this arrangement it was difficult to obtain uniform temperature beds. Temperature gradients were sometimes dependent on flow rates, particle size and the degree of agglomeration. In general however, it was possible to limit temperature differences to about 10-15^{o}C. Attempts to heat from the walls only were unsuccessful.

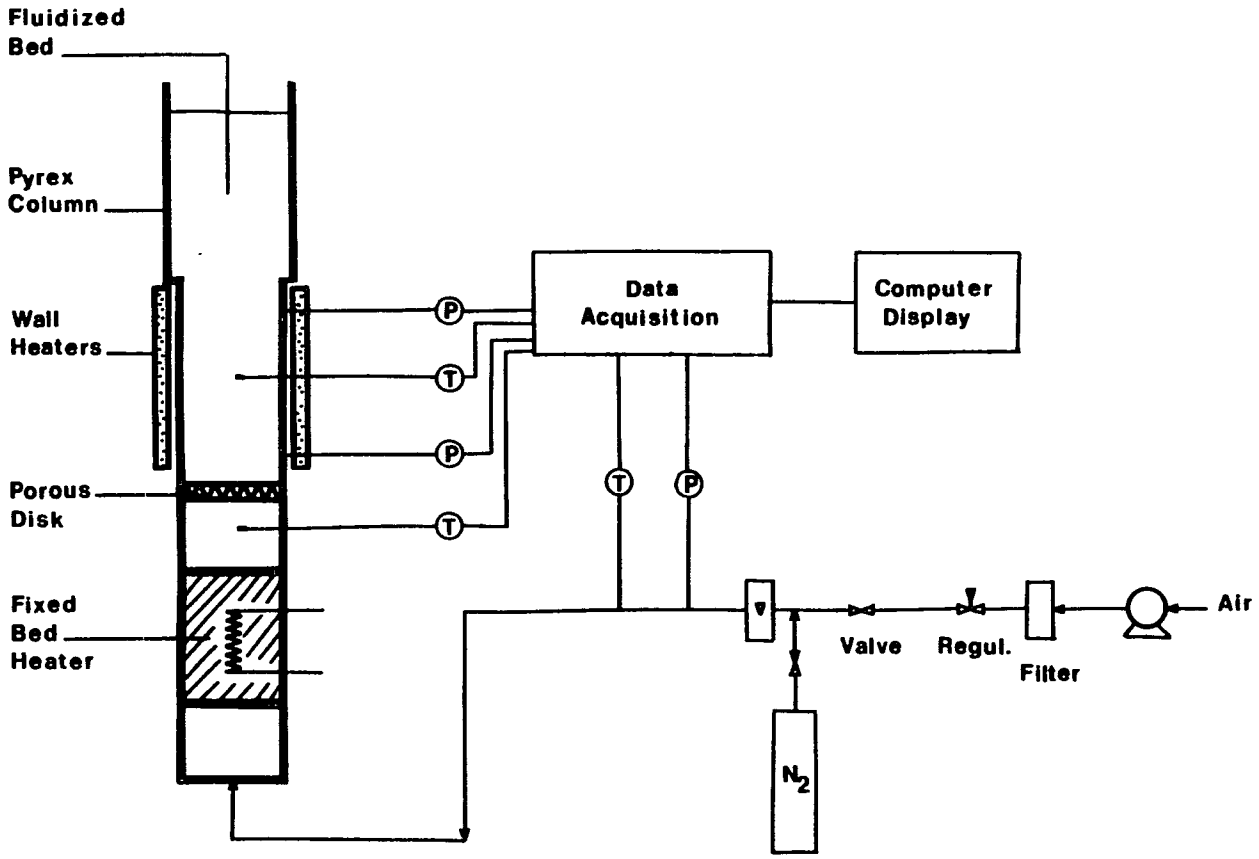

Figure 2.1. Schematic of three inch fluidized bed.

The fluidized bed section and the preheater are made of stainless steel when temperatures below 850°C are required and quartz for temperatures between 850 and 1200°C. Above the heated section of the bed is a pyrex column which allows for some visual observation of the fluid particles when relatively low temperatures were employed. At temperatures above 700°C when the particles glowed red, the upper surface of the bed was observable by placing a mirror above the column opening.

The pressure in the bed was measured directly above the distributor plate and at intervals along the bed wall, using open, 1/16th inch ID stainless (or quartz) tubes connected to diaphram pressure transducers (Validyne, Model Dp-15). These transducers are interfaced with an IBM-XT computer through a Data Translation A/D board (Model DT-1205). The pressure tap directly above the plate is placed with the tube opening centered in the column, while the the other taps were flush with the column wall. Superficial gas velocities were corrected by the ideal gas law using the pressure measured directly above the plate.

Temperature measurements are made (1) directly below the distributor plate, (2) 2-3cm above the distributor and (3) at about half the distance to the surface of the fluidized particles using 1/8 inch, exposed junction, type K thermocouples. The thermocouples extended one inch into the bed.

When gases other than air were used, dry gas was supplied from a high pressure tank and introduced directly upstream from the rotameters (see Figure 2.1).

2.1.2 Dilatometer

The dilatometer used in this work consists of two sections: a sample holder which is enclosed in a temperature controlled furnace and a sensor which detects the movement of the sample. The dilatometer was purchased from Theta Industries (Port Washington, N.Y.) and is a modified version of the Dilatronic Model. A schematic is shown in Figure 2.2.

The powder is placed in a small specimen tube, about 2cm long, with an internal diameter ranging from 4 to 6mm depending on the diameter of the particles. A piston is placed on top of the sample, which fits smoothly into the tube, but not so loose as to allow particles to migrate into the annular space. It was found that the height of the piston is best made about equal to its diameter. This size is found to be large enough to keep the surface of the particle sample compact in a horizontal position but not so large as to result in excessive friction on the tube wall.

Once the piston is in place, the specimen tube is lightly tapped which eliminates irregular packing and removes any particles which had lodged between the piston and tube wall. It is important to remove these particles so that the piston slides freely through the specimen tube.

The measuring head assembly consists of an adjustable mount for the position sensor, which is an LVDT (linear variable displacement transducer) mounted to a vertical height adjuster. Connected to the core of the LVDT is a pushrod which rests on the piston covering the sample and which moves along with this piston. The weight of the pushrod compressing the sample is referred to as the load. By the use of a

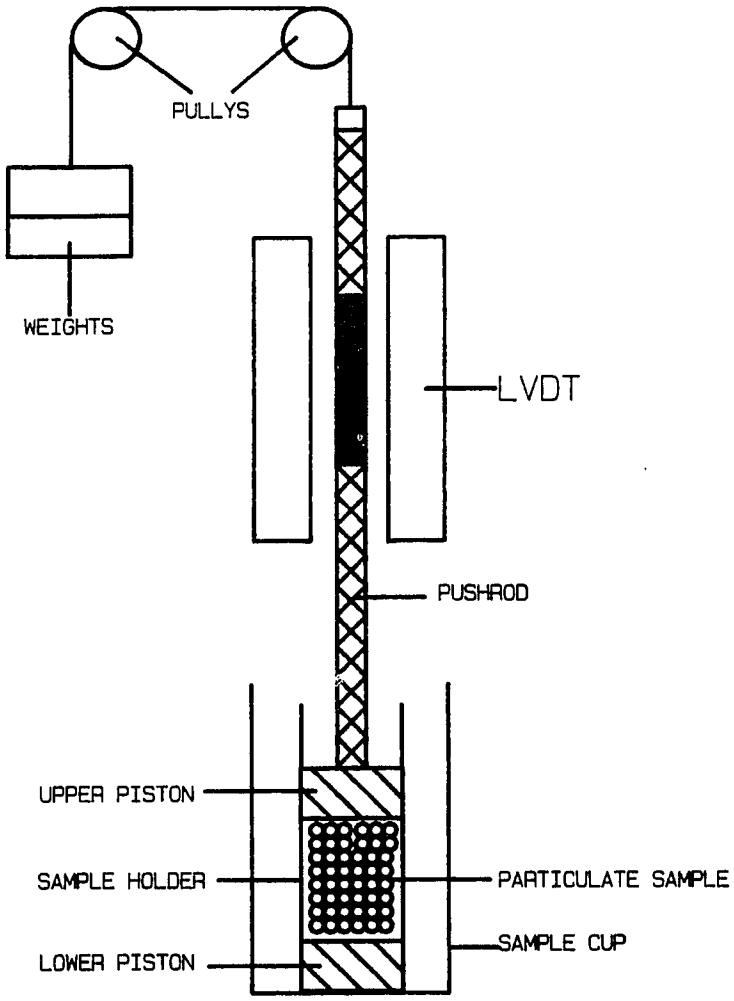

Figure 2.2. Schematic of dilatometer.

weights and pulley system the load may be varied from approximately 10 to 130 grams force. If loads less than about 10 grams are used, frictional forces become a problem.

The temperature of the sample was measured using a bare thermocouple placed into the sample holder from above and positioned such that the junction rests on the specimen tube. Type K thermocouples were used for measurements below 1100^{o}C and type S thermocouples were used for measurements between 1100^{o}C and 1500^{o}C. The signals from the LVDT and the thermocouple are sent to an IBM-XT microcomputer via a Data Translation A/D interface (model DT-2801) which has cold junction compensation circuitry and 12 bit resolution. The output of the LVDT is calibrated to 0.0254cm/volt, which coupled with a 2.44MV resolution on the A/D board results in a measurement resolution of 6.2 x 10^{-4}cm.

Two different furnaces were used for heating: a standard nichrome wire furnace at temperatures Below 1100^{o}C, and a silicon carbide element furnace at temperatures above 1100^{o}C. The maximum heating rate was approximately 25 to 35^{o}C/min. Heating is programmed as either a steady ramp (cooling or heating) or an isothermal soak for a specified length of time.

Samples were tested under controlled atmospheres using a vacuum tight protection tube mounted onto the measuring head. An atmosphere control module permits the use of vacuum and gases supplied from high pressure tanks.

All parts of the system which are enclosed in the furnace must be made of either quartz or sintered alumina. These materials exhibit fairly low thermal expansion in the temperature range needed and are

resistant to contamination and thermal shock. The temperature limit for the use of quartz (fused silica), which is less expensive and easier to fabricate, is about 1000°C.

2.1.3 Constant heating rate and isothermal dilatometry

Two different experiments are performed using the dilatometer: isothermal dilatometry and constant heating rate dilatometry (CHR). Isothermal dilatometry involves raising the temperature to the desired level as a step change and then recording sample length changes as a function of time. Unfortunately, true step changes cannot be obtained. Step changes in temperature are at best fast ramps; heating rates of 25 to 35°C/min are the maximum available at temperatures below ~800°C while at higher temperatures heating rates are as slow as 5-15°C/min.

CHR dilatometry is performed by heating the sample at some prescribed rate from ambient to the end of the temperature range of interest and then back down again if so desired. The heating rate is in general limited by the heat transfer to the powder. In order to keep the temperature uniform and at the same value as the prescribed setting, heating rates are kept at around 200°C/hr. In some cases where the effect of heating rate is to be studied, rates up to 600-700°C/hr may be used, but results from these runs must be considered qualitative only in view of the heat transfer limitations mentioned above.

2.2 Experimental Results on Model Materials

2.2.1 Rationale for choice of model materials: Glass beads, Sodium Chloride, and Calcium Chloride

The choice of model particles to be used in high temperature studies represents a compromise of a number of factors. The particles must become cohesive at temperatures which are not too high because of equipment constraints. However materials which sinter at low temperatures are difficult to find and are generally of less interest in industry. Also the material must be available in reasonable amounts at reasonable prices.

To satisfy these requirements glass beads, sodium chloride crystals (NaCl), and calcium chloride crystals ($CaCl_2$) were chosen as model materials. Figure 2.3a-c show micrographs of the particles. The soda-lime glass beads used were 95% true spheres. Glass is clean and inert to atmospheric conditions and softens at temperatures below 600^{o}C, which poses few equipment constraints. Sodium chloride is interesting because it is available as almost perfect cubes, a particle morphology which has not been investigated to date. The calcium chloride was obtained as the dihydrate ($CaCl_2.2H_2O$) which is a common commercial form. When heated above 135^{o}C the lattice water is lost leaving a porous structure. In contrast to the glass spheres and cubical sodium chloride particles, the dried calcium chloride particles are irregular and jagged. The relatively low melting points of sodium chloride (802^{o}C) and calcium chloride (772^{o}C) also pose no difficulties with respect to materials of construction for the fluidized bed and dilatomter. Finally,

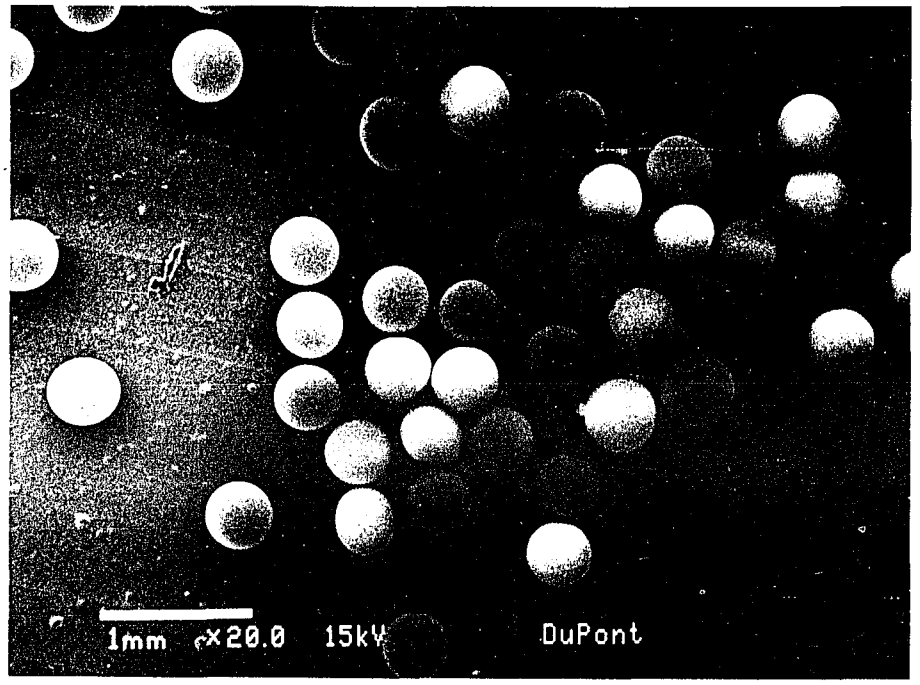

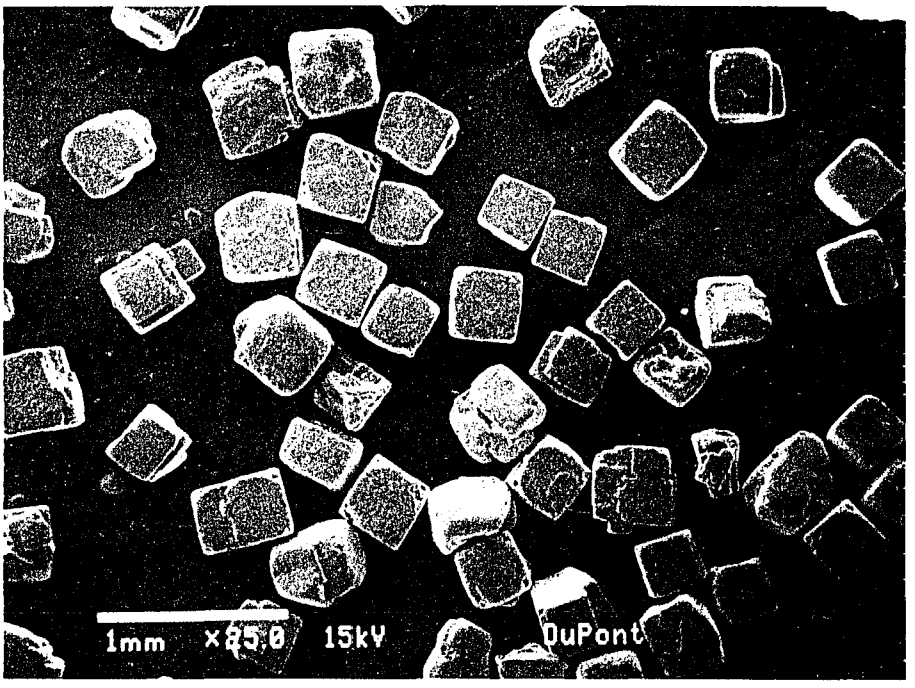

Figure 2.3. Micrographs of starting materials.
(a) glass beads (b) NaCl crystals.

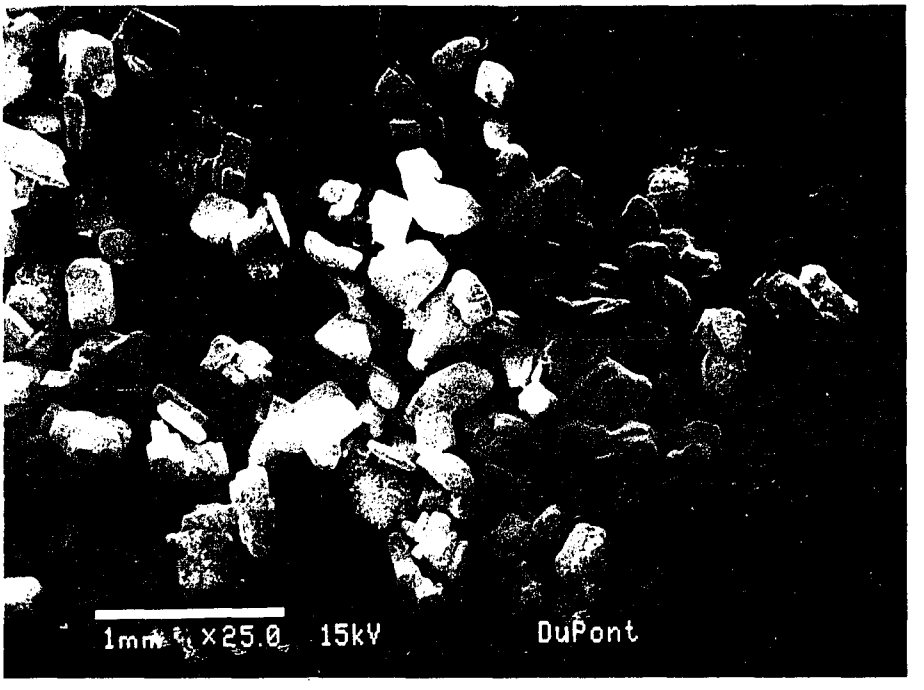

Figure 2.3c. Photomicrograph of $CaCl_2.2H_2O$ starting material.

as pointed out in section 1.5, none of the studies of high temperature cohesion in the literature include salts and so these are a class of materials which need investigation.

Some properties of the glass, NaCl, and $CaCl_2$ particles are shown in Table 2.1. Particle sizes reported were obtained by averaging U.S. standard sieve results.

2.2.2 Fluidization behavior at high temperatures

A number of runs were performed to measure the minimum fluidization velocities of the glass, NaCl, and $CaCl_2$ at temperatures at which the materials were non-cohesive. The conventional method of pressure drop versus gas velocity was used. A typical result for sodium chloride is shown in Figure 2.4. The data for all the runs are listed in Appendix B.

At high temperatures the fluidization procedure used is basically similar to the approach taken by Siegell(1976) and Tardos(1985a). The particles are first fluidized at ambient temperature at a gas velocity,U, higher than the minimum fluidization, U_{mfo}. Then, as the temperature is raised slowly (approximately 100-150^{o}C/hr) the gas velocity is kept constant by adjusting the flow rate through the rotometer. During the course of the experiment, the pressure in the bed is measured 1cm above the distributor plate and at about one half the height of the bed at rest. The reported pressure values are averages of 100 readings taken over 10 seconds.

Figure 2.5a shows the result of this "constant velocity procedure" for NaCl at a relative gas velocity (U/U_{mfo}) of 1.6. The value P_1 is the

Table 2.1. Properties of glass, NaCl, and $CaCl_2$ particles.

Material	d_p(μm)	ρ_s(g/cm)	Φ_p(-)[4]
Glass[1]	720	2.47	0.95
Glass[2]	50-720	2.4	0.95
NaCl[3]	300-720	2.16	0.80
$CaCl_2$[3]	~500[5]	-	0.63

[1] soda lime glass obtained from the Bahl Glass Co., New Jersey (now out of business)
[2] soda lime glass obtained from Potters Ind., New Jersey
[3] obtained from Spectrum Chemical Co., Calif.
[4] approximate
[5] broad size distribution

Table 2.2 Conditions of constant velocity experiments for NaCl.

RUN #	d_p(mesh)	d_p(μm)	W_b(g)	U/U_{mfo}
1	30-40	595-420	1200	1.6
2	30-50	595-300	1200	3.6
3	30-40	595-420	1200	3.7
4	40-50	420-300	1750	4.6
5	30-50	595-300	1200	5.25

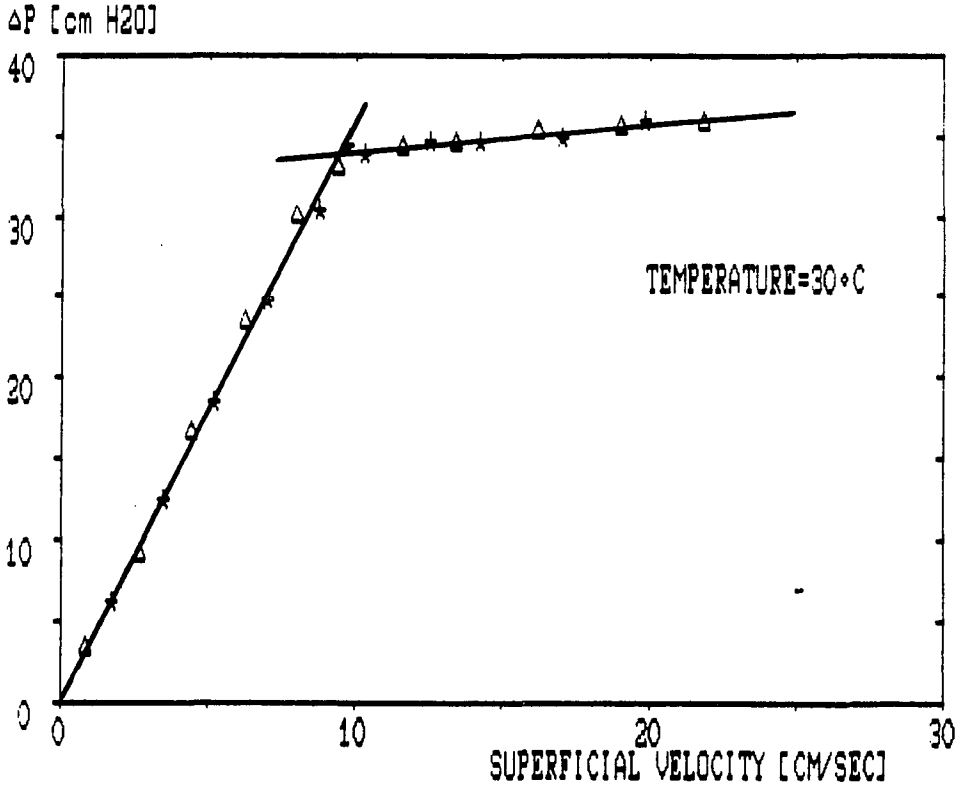

Figure 2.4. Minimum fluidization velocity determination for NaCl (d_p=0.36mm)

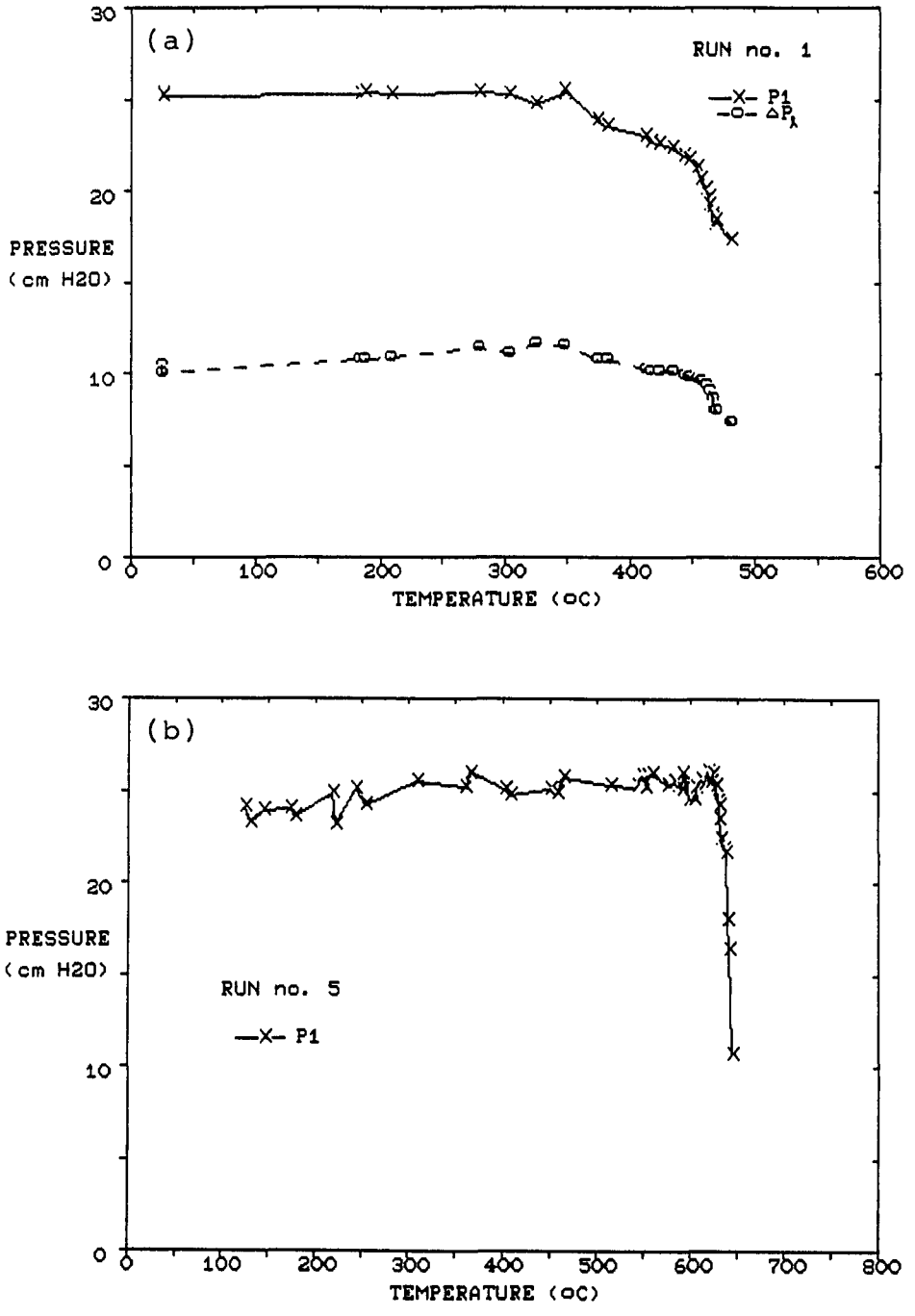

Figure 2.5. Constant velocity defluidization procedure for NaCl. (a) Run #1 (b) Run #5. (see Table 2.2 for experimental details).

gage pressure measured 1cm above the distributor plate and ΔP_{ℓ} is the difference between P_1 and the pressure measured 10cm above the distributor. Up to about 325°C P_1 is relatively constant, but then begins to decrease slowly. At 450°C, the bed was observed to defluidize completely, with the formation of channels which accounts for the drastic decrease in pressure. In the range between 325°C and 450°C the bed was observed to be well fluidized suggesting that partial segregation of agglomerated material had occurred due to cohesion and hence the decrease in the value of P_1 mentioned above.

The constant velocity procedure was repeated at a number of gas velocities. The conditions for the runs are shown in Table 2.2 in which W_b is the weight of the bed. In run #5, where the ratio $U/U_{mfo} = 5.25$ was high, the pressure remained constant until defluidization took place - no partial segregation was observed. The values obtained for ΔP_{ℓ} were used to calculate the voidage at minimum fluidization, ε_{mf}, according to the equation

$$\varepsilon_{mf} = 1 - (\Delta P_{\ell} / \rho_s \cdot \ell) \qquad (2.1)$$

where ℓ is the distance between the two pressure taps and ρ_s is the density of the solids. At low temperatures the voidage was measured at U_{mf} while at high temperatures the voidage was measured just prior to defluidization. For example, in Run #1 (Figure 2.5a), ΔP_{ℓ} was taken to be 10.2cm H_2O just prior to complete defluidization. A plot of ε_{mf} versus temperature is shown in Figure 2.6.

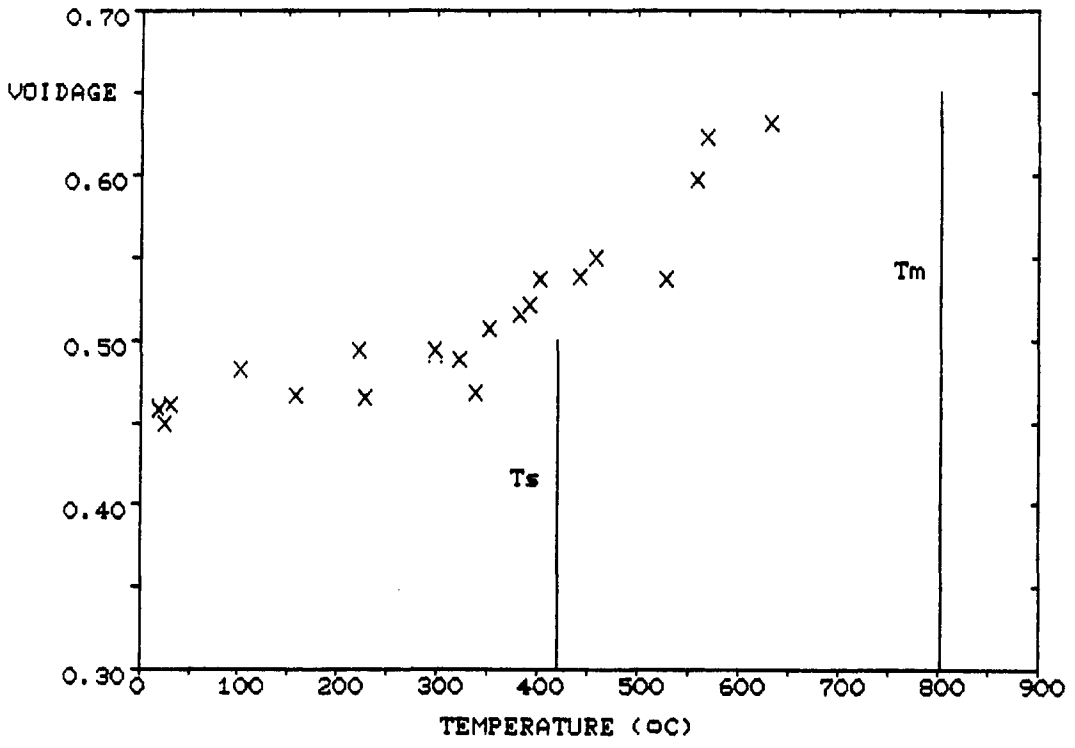

Figure 2.6. Voidage at defluidization for NaCl calculated using Equation 2.1

Similar experiments at low and high temperatures were performed using the glass beads and calcium chloride. Figure 2.7 shows the results of the constant velocity procedure for glass (d_p= 720μm) at two different relative velocities. At the lower velocity the pressure drop at complete defluidization actually increased suggesting the formation of a fixed bed without channeling. The pressure at defluidization also increased in the second run with sodium chloride. A result of pressure drop versus velocity for calcium chloride (U/U_{mf}= 2.2, W_b= 500g) is shown in Figure 2.8; again, the gradual loss of pressure from about 350°C until complete defluidization at 607°C indicates segregation due to cohesion. These results conflict somewhat with Siegell's (1976) observations. He reported that defluidization occurred instantaneously and that segregation did not occur. He also reported that the pressure drop always decreased at defluidization.

Using the above results, a plot of the velocities at which complete defluidization occurred as a function of temperature could be constructed. The results for sodium chloride, calcium chloride, and glass are shown as Figures 2.9a, b, and c respectively. In these figures the gas velocities U are normalized by the minimum fluidization velocity measured at ambient temperature, U_{mfo}. The line labeled "Ergun Correlation" is the value of U_{mf} predicted by the Ergun correlation (Kunii and Levenspiel, 1969) using the single particle properties only (see Equations A-1 through A-3 in Appendix A). Two sets of defluidization points are shown for glass; these correspond to experimental results with 720μm and 275μm diameter particles respectively.

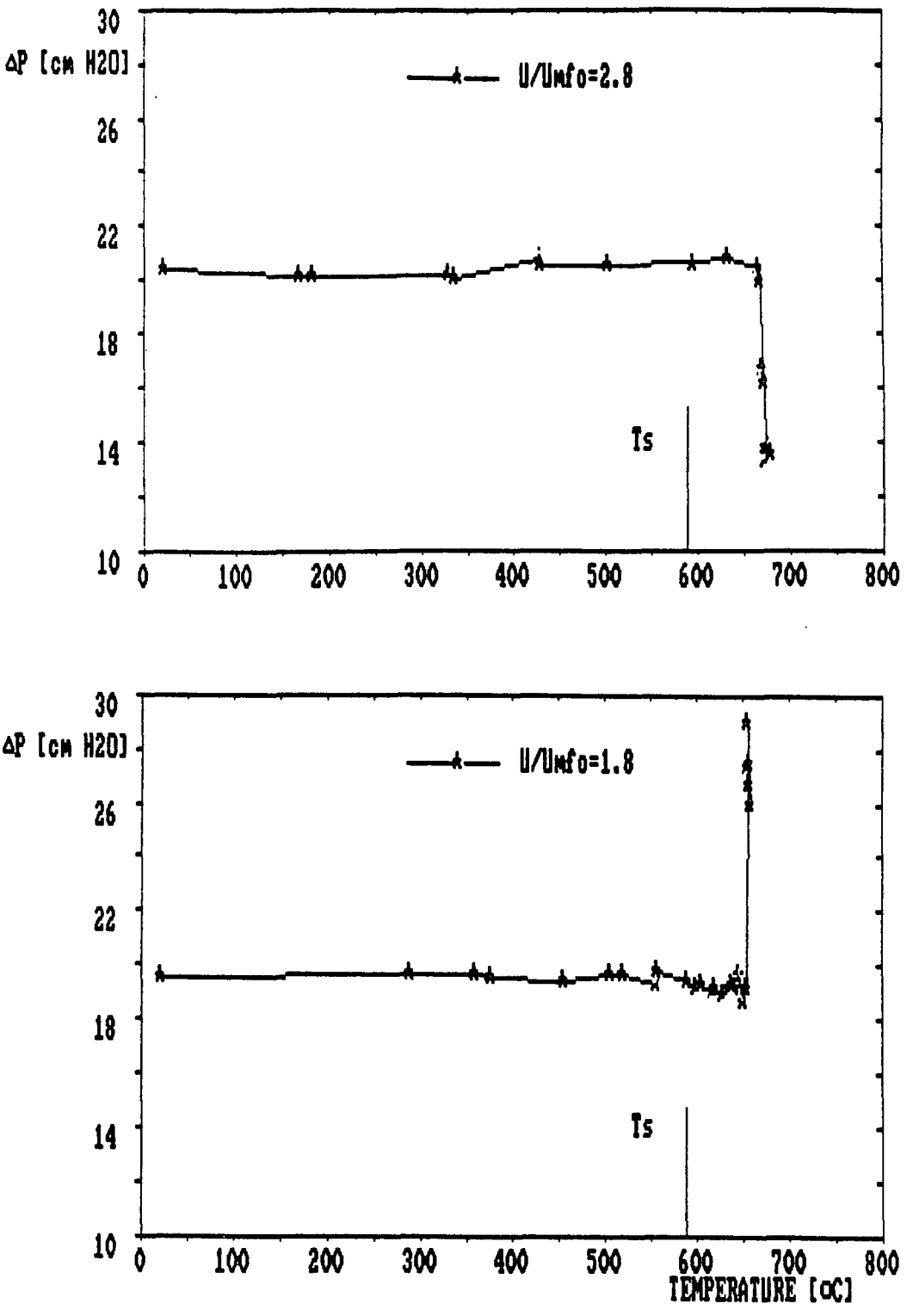

Figure 2.7. Constant velocity defluidization procedure for glass beads at two different relative gas velocities. d_p=0.72mm.

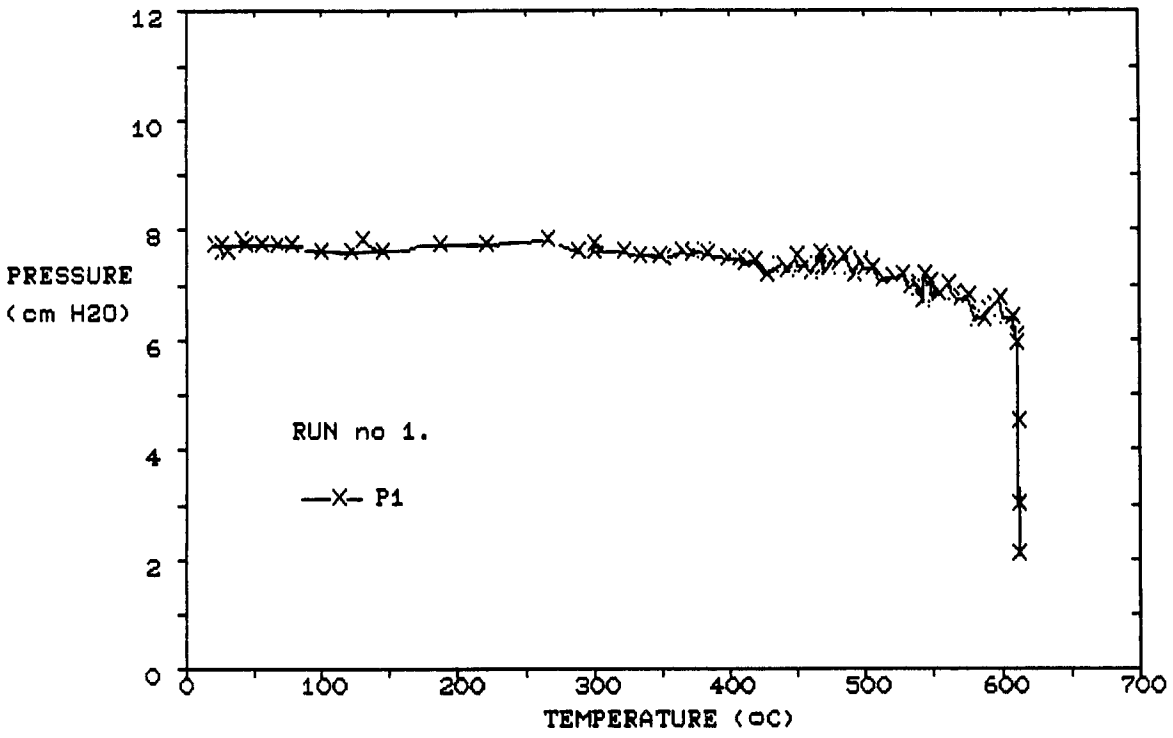

Figure 2.8. Constant velocity defluidization procedure for $CaCl_2$, U/U_{mfo}=2.2, W_b=500g.

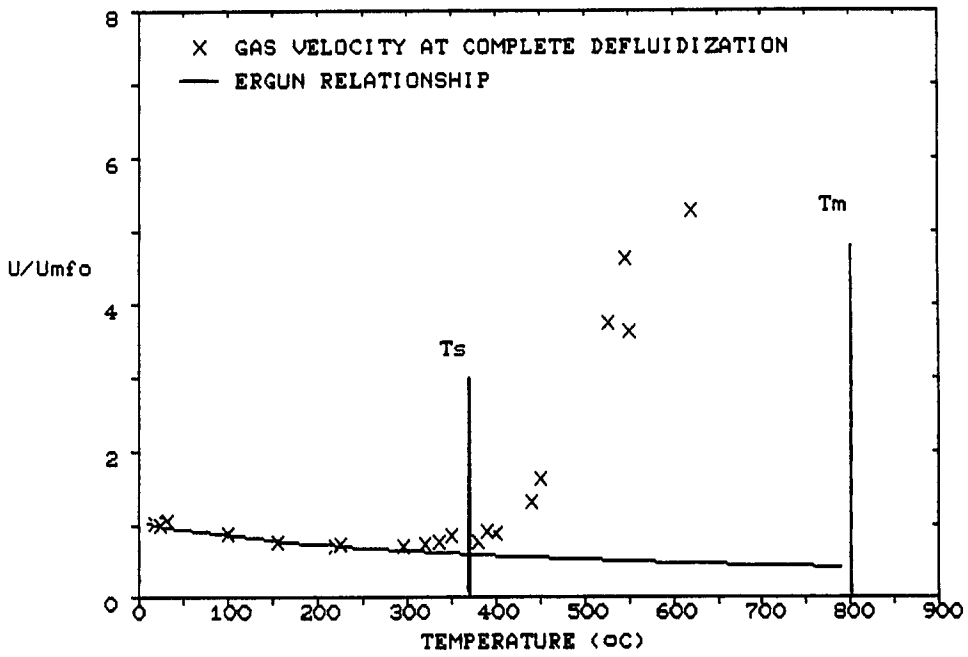

Figure 2.9a. Gas velocity at complete defluidization versus temperature for NaCl.

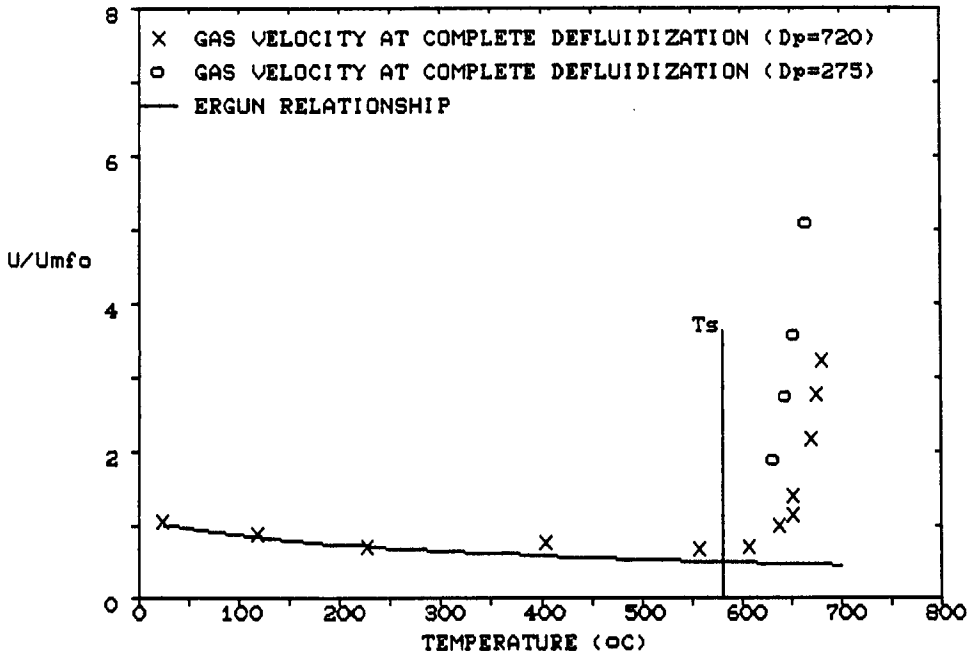

Figure 2.9b. Gas velocity at complete defluidization versus temperature for two different particle sizes of glass beads.

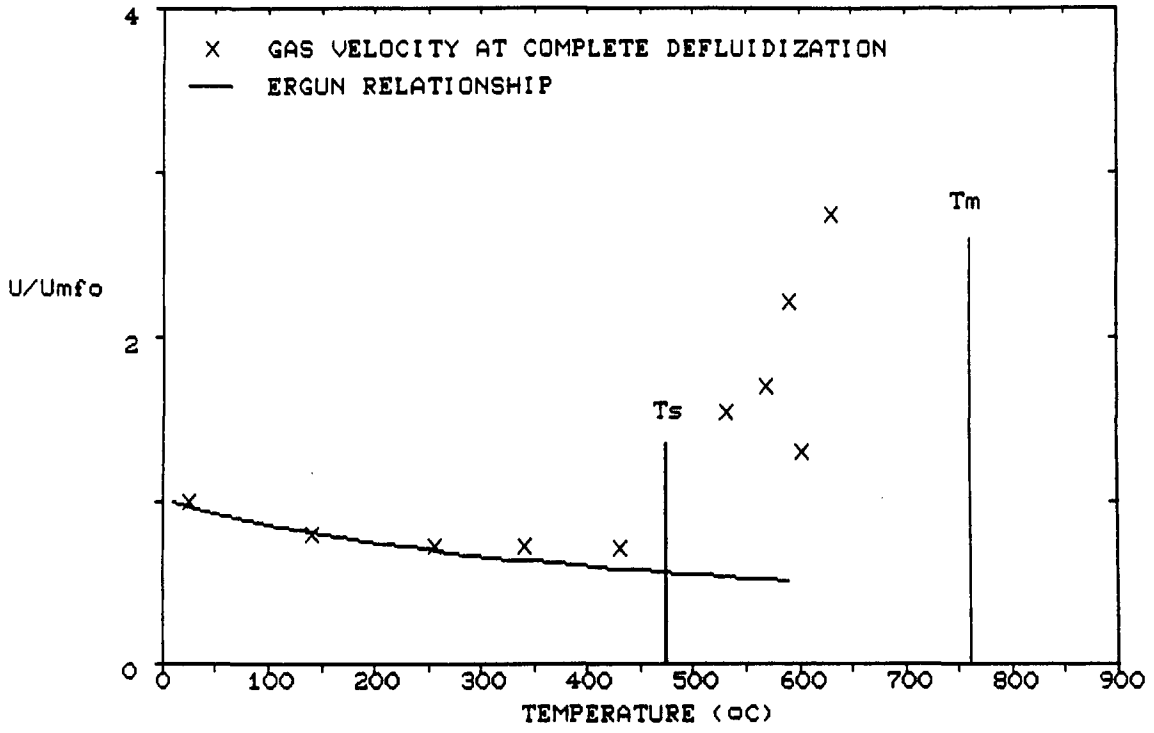

Figure 2.9c. Gas velocity at complete defluidization versus temperature for $CaCl_2$.

In addition to the data presented above, two important observations were made during the constant velocity experiments:

(1) Inspection of material which was sampled from the bed during the runs did not usually reveal the presence of agglomerates. Sometimes, a small number of dimers (an agglomerate comprised of two primary particles) and trimers were found, but in general, the bed consisted of primary particles only. This observation must be qualified: the term agglomerate must be defined as those structures which survive the sampling process. Surprisingly, the particles removed from the bed at these temperatures would fuse quite readily in the sampling container. The resulting structures could easily be broken, but nevertheless, it was clear that the particles had the potential to form agglomerates. It also appeared that more agglomerates were present in the experiments at high relative gas velocities. Figure 2.10 shows sampled material from NaCl Run #5 (U/U_{mfo}=5.25).

(2) Unlike the results of some of the cohesive fluidization studies reviewed in Chapter 1. where interparticle adhesion was sometimes found to stabilize the bed, no type A fluidization was observed in these high temperature experiments. The bubbling behavior continued right up to the point of defluidization. Defluidization was usually accompanied by severe channeling, indicative of type C fluidization.

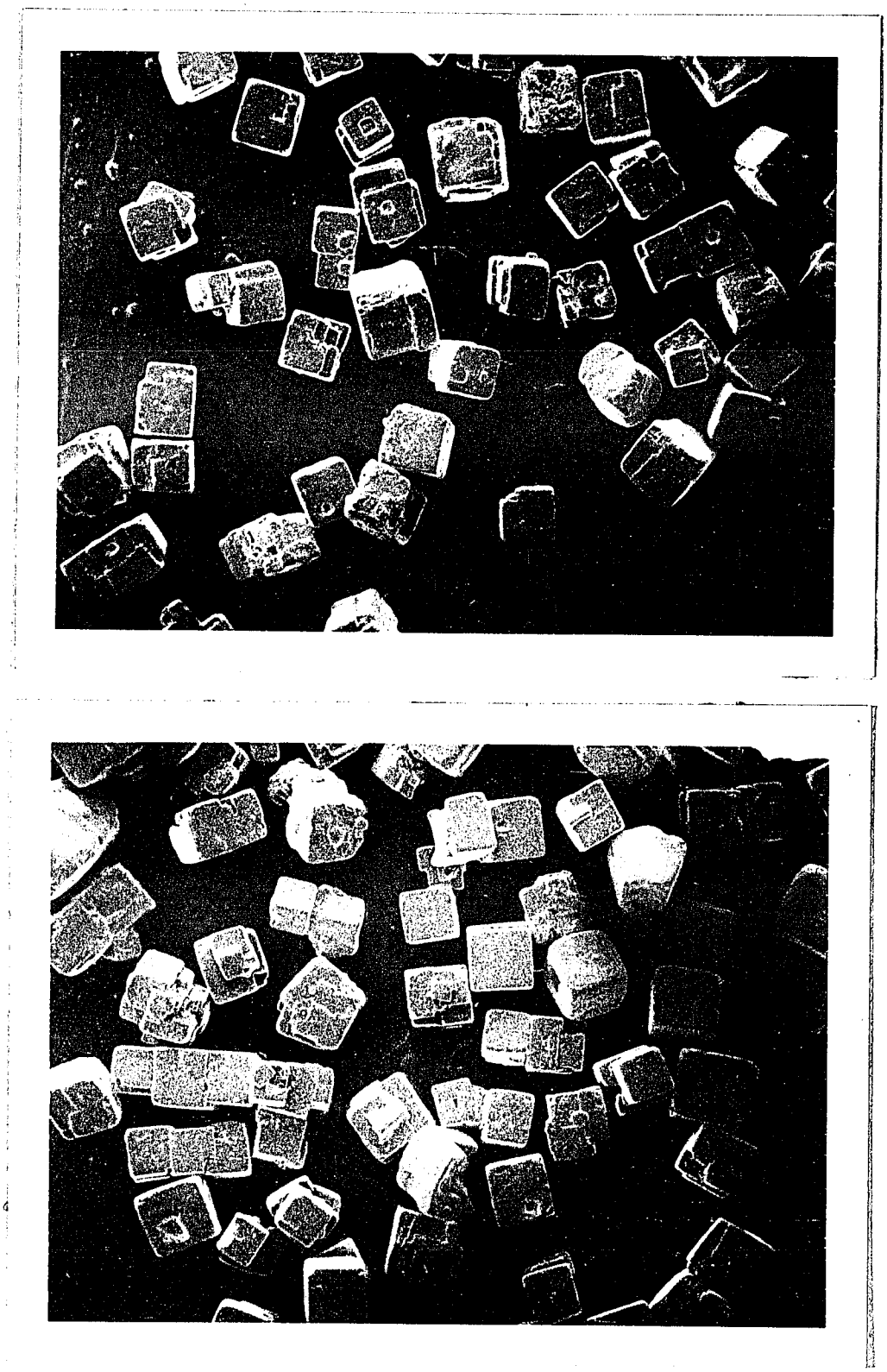

Figure 2.10. Photo micrographs of used bed material from NaCl defluidization Run #5 (see Table 2.2.)

2.2.3 Dilatometry

Figure 2.11 shows a constant heating rate (CHR) dilatometry curve for glass beads. The length of the sample remains fairly constant until the large contraction beginning at about 580°C. Siegell's (1976) and Basu's CHR dilatometry curves showed much broader regions of change (see Section 1.4.2). The curve in Figure 2.11 suggests that the minimum sintering temperature is the temperature at which the large contraction begins (580°C). Drawing a line at 580°C on the defluidization curve for glass (Figure 2.9c) supports this assumption. Below 580°C the glass beads do not appear to be cohesive. This raises the question whether contraction in the CHR dilatometry curve necessarily indicates interparticle cohesion. In the case of the weak contraction starting at 300°C the answer appears to be no, while the strong shrinkage at 580°C is due to bondneck growth and contraction of the sample.

Tardos et al.(1984) showed that the dimensionless bondneck diameter, D_p/b, can be related to the dimensionless change in length, $\Delta L/L_o$, of a randomly packed powder compact by

$$b/D_p = 1-[1-(\Delta L/L_o)3\beta/2]^2 \qquad (2.2)$$

where β is a packing factor given as

$$\beta = 2/3\ [\pi/3\ 2(1-\varepsilon)]^{1/3} \qquad (2.3)$$

Equation 2.3 is plotted in Figure 2.12 for three values of the voidage, ε, demonstrating a weak dependency on voidage. Assuming that at the

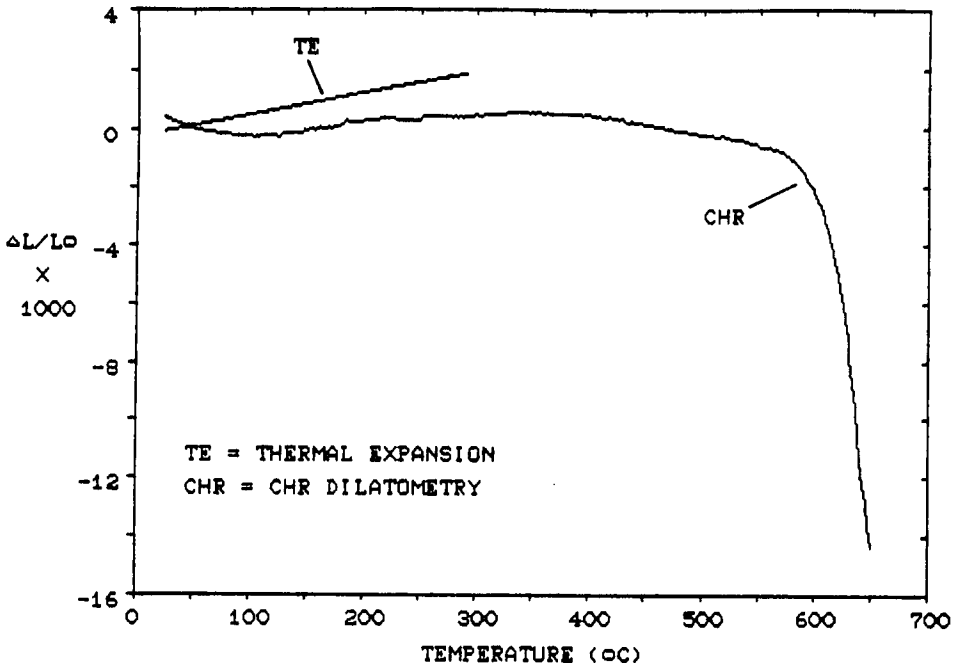

Figure 2.11. CHR dilatometry for glass beads. d_p=0.51mm, heating rate=200°C/hr, load=18g, Lo=1.5cm.

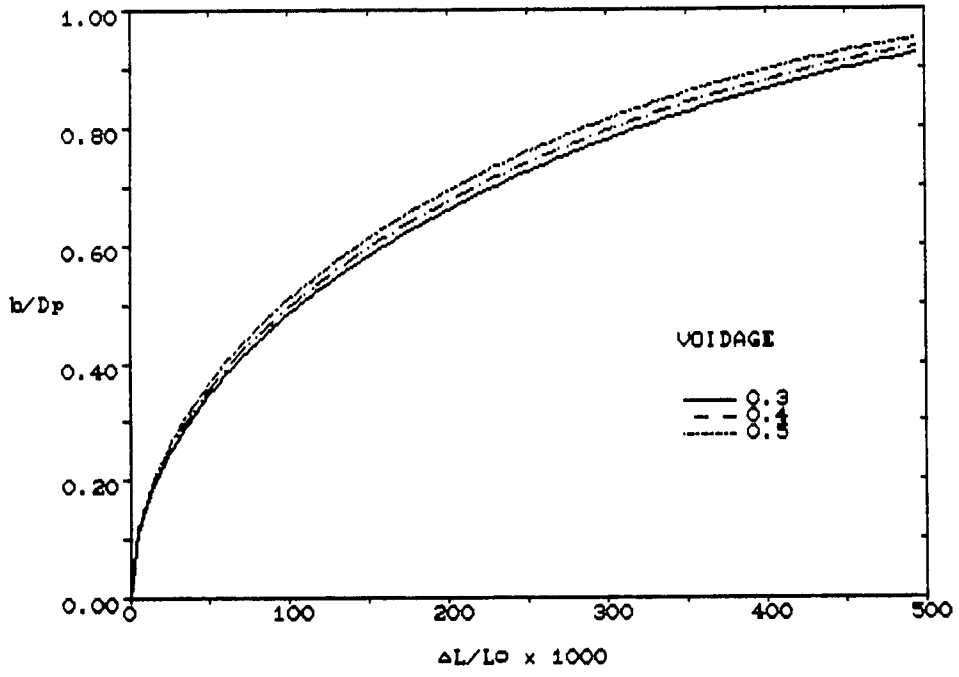

Figure 2.12. Dimensionless bond neck diameter versus dimensionless sample length. Calculated from Equation 2.2.

minimum sintering temperature, the bond neck diameter is zero (b=0), a value of 0.19 is obtained for the dimensionless bond-neck diameter at 650°C; this is in agreement with values reported for glass beads by Rumpf (1977).

The interpretation of the CHR curve in the temperature range below T_s is not as clear. If bond-neck growth is not taking place, the sample should dilate due to the thermal expansion of the material. However relating the thermal expansion of a solid to the thermal expansion of a powder compact of the same material is not straight forward. In randomly packed beds, the particles do not lie directly on top of each other and so the thermal expansion of the particle bed should be lower than the bulk value. As a rough approximation it is assumed that the expansion of the powder is about 75% of the bulk solid. The coefficient of expansion for the glass beads was reported by the manufacturer (Potters Ind., Carlstadt, New Jersey) to be 8.5 x 10^{-6}(cm/cm/°C) in the temperature range 20°C to 300°C. Plotting the expansion, TE, given by

$$TE \sim 0.75 \cdot \alpha \cdot (T-T_o) \qquad (2.4)$$

in Figure 2.11 shows that the CHR curve below 300°C does not correspond to Equation 2.4 at first, but then at about 130°C the upward slope seems to fit Equation 2.4 better. Barringer et al.(1984) explain that this type of behavior is not unusual in constant heating rate dilatometric studies in powder metallurgy. Particles rearrange in the compact because of stresses caused by thermal expansion and sintering.

Though data was not available, the glass manufacturer suggested that in the temperature range between 300°C and the sintering temperature glass expands at even greater rates than shown above. In contrast, the CHR curve has a negative slope after 300°C. As shown in Figure 2.9c, fluidization experiments do not indicate the presence of interparticle cohesion at temperatures between 300°C and 580°C. This discrepancy may be explained by particle rearrangement.

The CHR curve obtained for calcium chloride (Figure 2.13) contains a contraction beginning at about 130°C obviously resulting from the removal of lattice water from the hydrated crystal ($CaCl_2 \cdot 2H_2O$). Following this contraction, the length of the compact remains almost constant until the slope begins to change very gradually at about 475°C. Again, by plotting a line at 475°C on the defluidization curve for calcium chloride (Figure 2.9b) the assumption that the temperature at which large contractions begin is the minimum sintering temperature seems to be reasonable, but not exact.

An important aspect of the calcium chloride dilatometry result is that using Equation 2.2, the bond-neck diameter calculated at 650°C is nearly 60% of the diameter of the particles. Inspection of the sample removed from the dilatometer after reaching 650°C did not reveal this kind of bonding and the compact was found to be friable and easily crushed. It is believed that this result is due to the loss of water when the material is initially dried. This leaves a porous, open structure which compacts at high temperatures. It might also be reasoned that with such a particle structure there is both internal and external surface which has the potential to reduce surface energy.

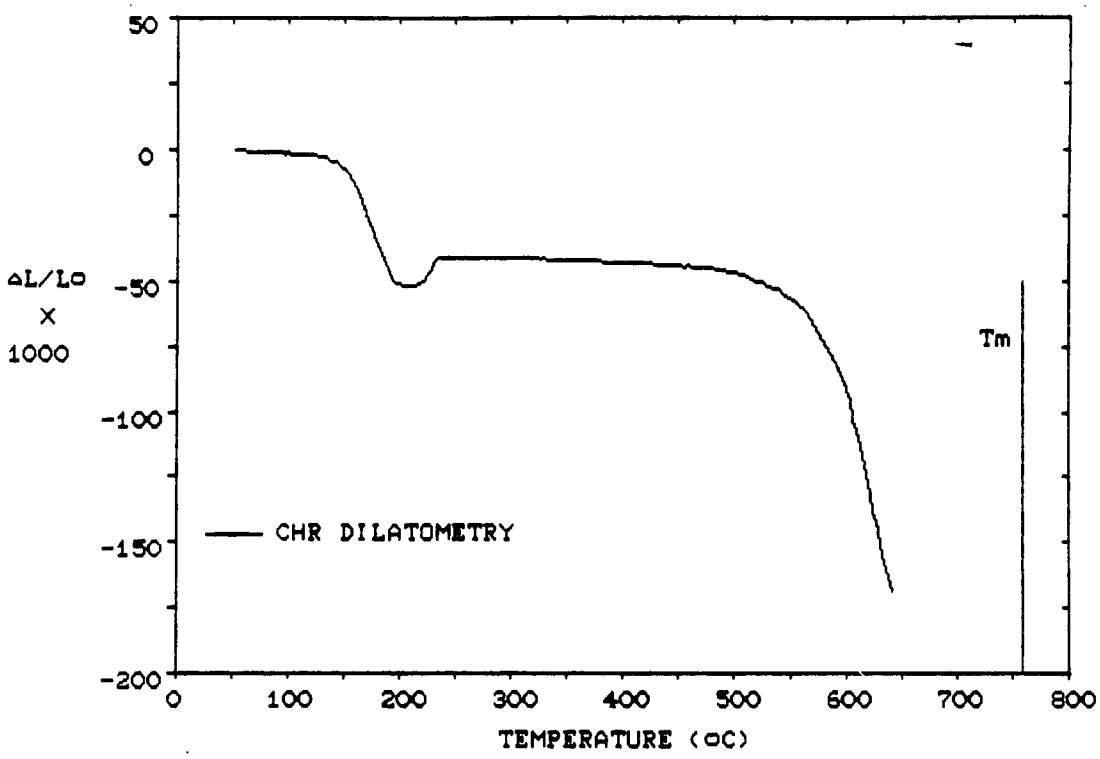

Figure 2.13. CHR dilatometry for $CaCl_2$. d_p=0.36mm, heating rate=200°C/hr, load=33g, Lo=0.48cm.

The calcium chloride particles were also tested using isothermal dilatometry. Figure 2.14 shows the results of measurements at five different temperatures. As the temperature increases, the rate of shrinkage, as well as the ultimate shrinkage of the compact increases. In Figure 2.15 the isothermal and CHR dilatometry results are compared. The individual data points represent the isothermal value at a particular temperature and time. Note that the CHR curve has been shifted up so that at 400°C the isothermal and CHR values coincide. This seems reasonable as below 400°C there was no contraction in the CHR result (except when the water was lost). Also, cohesion was not detected in the fluidization experiments below 400°C. The result shows that after 30min the isothermal values correspond well to the CHR curve.

The CHR dilatometry curve for sodium chloride (Figure 2.16a) is completely different from any other data reported to date. Up to about 370°C the NaCl crystals expand according to the thermal expansion coefficient of the bulk material (Touloribian et al., 1977); but then the slope increases. There is actually no contraction until close to the bulk melting point (802°C). The temperature at which the CHR curve begins to deviate from the thermal expansion curve correlates quite well with the initial cohesion temperature measured in the fluidized bed (see T_s= 370°C drawn into Figure 2.9a). The effect of applied load on the CHR behavior of sodium chloride is shown in Figure 2.16b. Increasing the load decreases the minimum sintering temperature.

To investigate this phenomena further, sodium bromide (NaBr) was tested under identical conditions. It would be expected that sodium

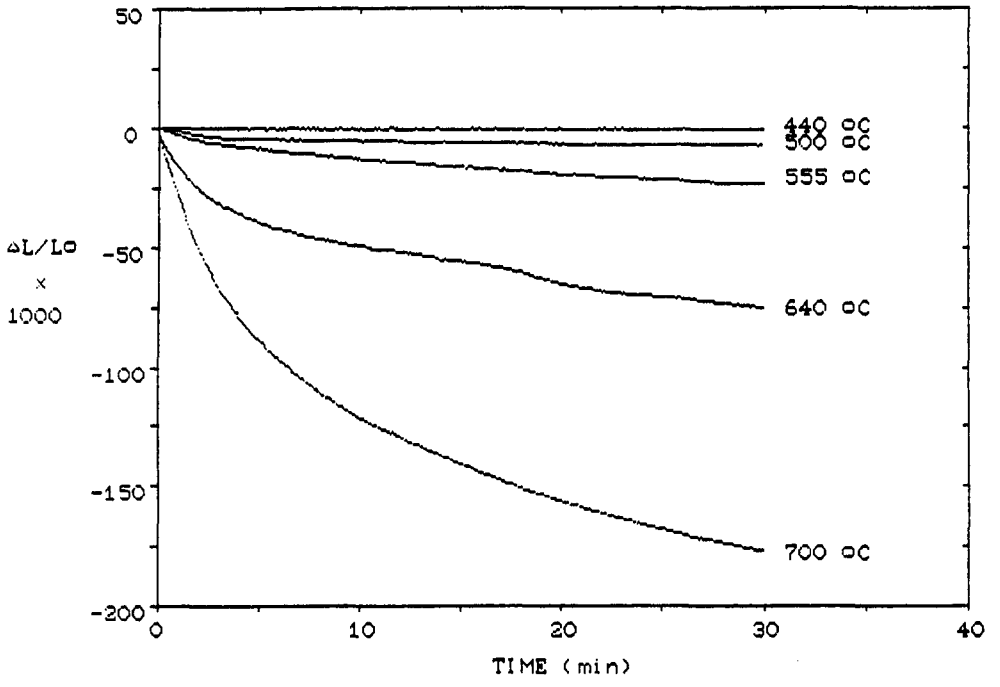

Figure 2.14. Isothermal dilatometry of $CaCl_2$. (d_p=0.36mm, Lo=4.8mm, load=33g)

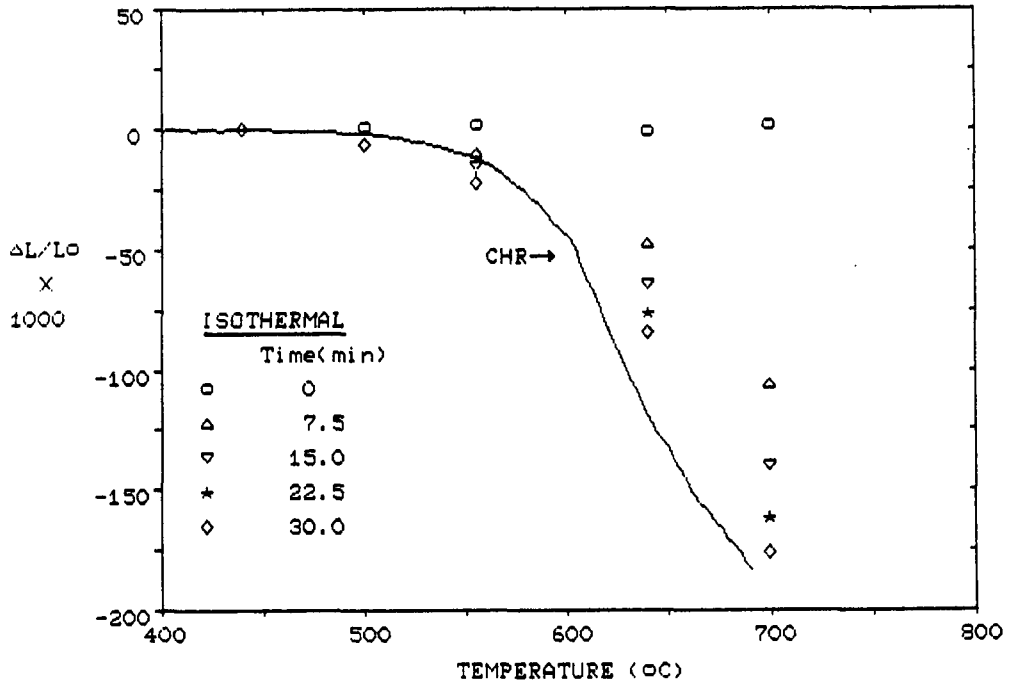

Figure 2.15. Comparison of isothermal and CHR dilatometry for $CaCl_2$.

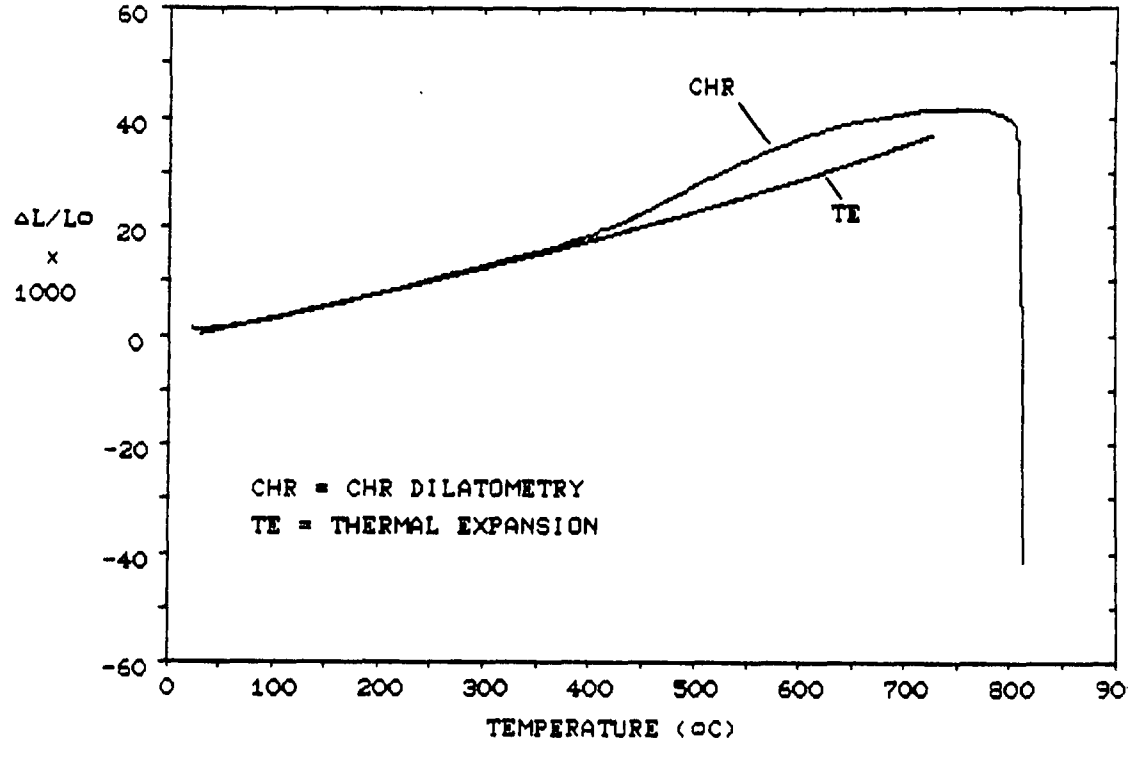

Figure 2.16a CHR dilatometry for NaCl. (d_p=0.36mm, load 23g, heating rate=200°C/hr, Lo=5.2mm).

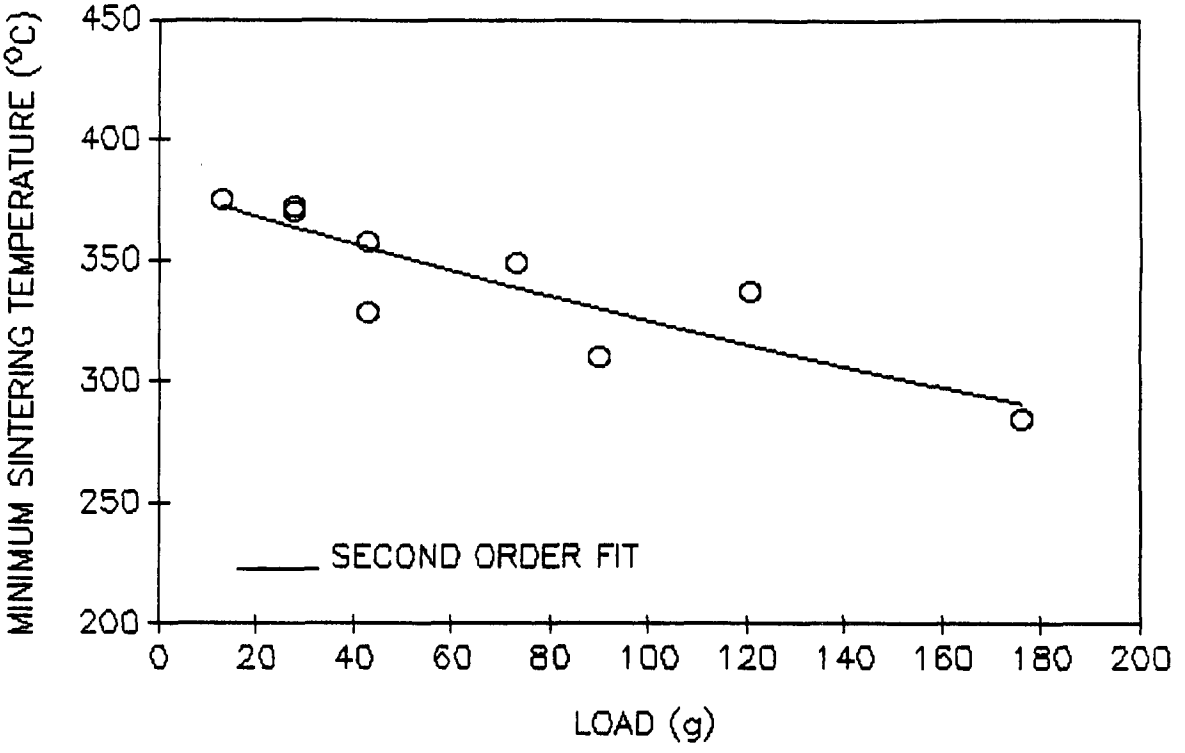

Figure 2.16b. Effect of load on the minimum sintering temperature of NaCl. (d_p=0.36mm, heating rate=200°C/hr).

chloride and sodium bromide would behave similarly. The result (Figure 2.17) is similar though the effect is not as pronounced. Sodium Citrate ($Na_3C_6H_5O_7.H_2O$) particles also showed an increase in slope on heating. This result, given in Figure 2.18a shows a small contraction at 170°C but then the expansion begins again and at a greater rate. Finally the sample contracts drastically very close to the reported bulk degredation value of 310°C. A constant velocity fluidization run was performed using the sodium citrate as shown in Figure 2.18b. The loss of pressure at about 150°C is caused by loss of lattice water. Defluidization occurs at about 240°C, a temperature at which the CHR dilatometry of the salt shows expansion.

2.2.4 Summary

The following is a summary of the experimental findings from high temperature fluidization and dilatometric studies of glass beads, sodium chloride, and calcium chloride crystals.

The fluidization characteristics of these model materials at high temperature were studied using a procedure where the relative gas velocity (U/U_{mfo}) was kept constant as the temperature was increased. Different types of defluidization behavior were found to occur: usually beds defluidized with the formation of channels (rat holes) as indicated by drastic loss of pressure drop over the bed. In some cases, channels did not form at defluidization and the resulting fixed bed caused an increase in pressure drop at defluidization (because velocities greater than U_{mf} were possible without fluidization). In other experiments, some of the fluidized material would segregate out of the bed prior to

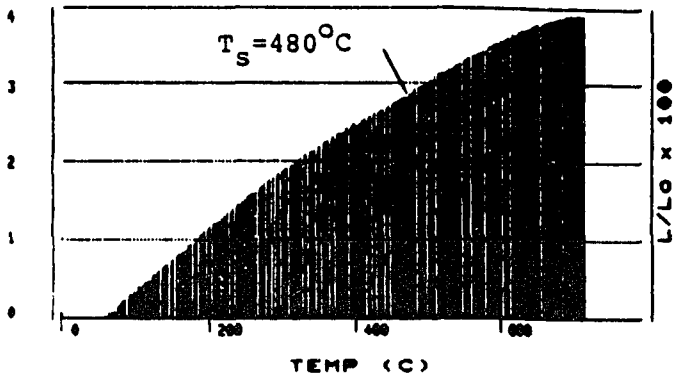

Figure 2.17. CHR dilatometry of NaBr. (d_p = 0.36mm, heating rate=200°C/hr, load=43g, Lo=4.2mm).

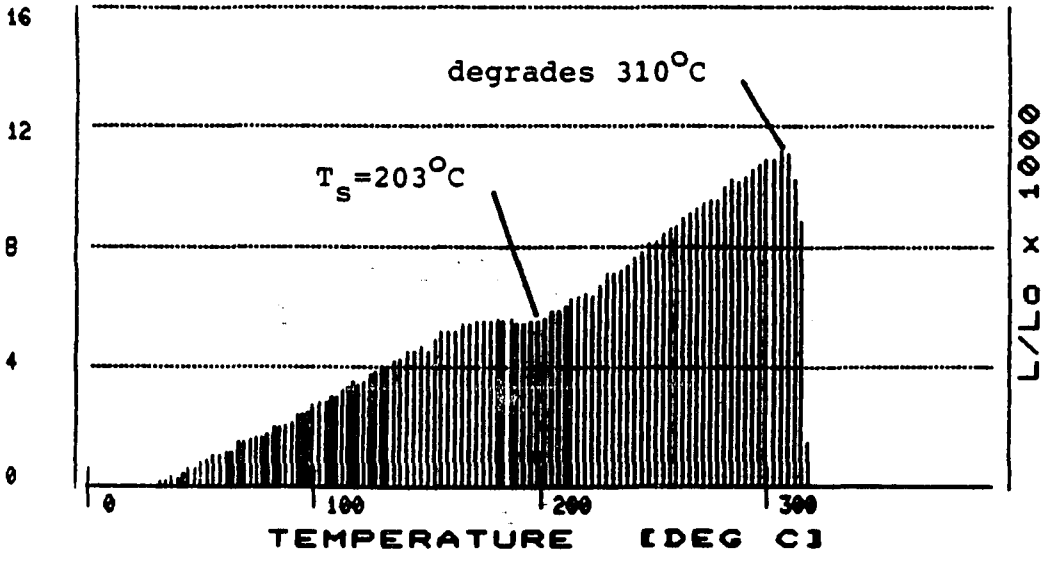

Figure 2.18a. CHR dilatometry of sodium citrate. (d_p=0.36mm, heating rate=200°C/hr, load=28g, Lo=5.3mm).

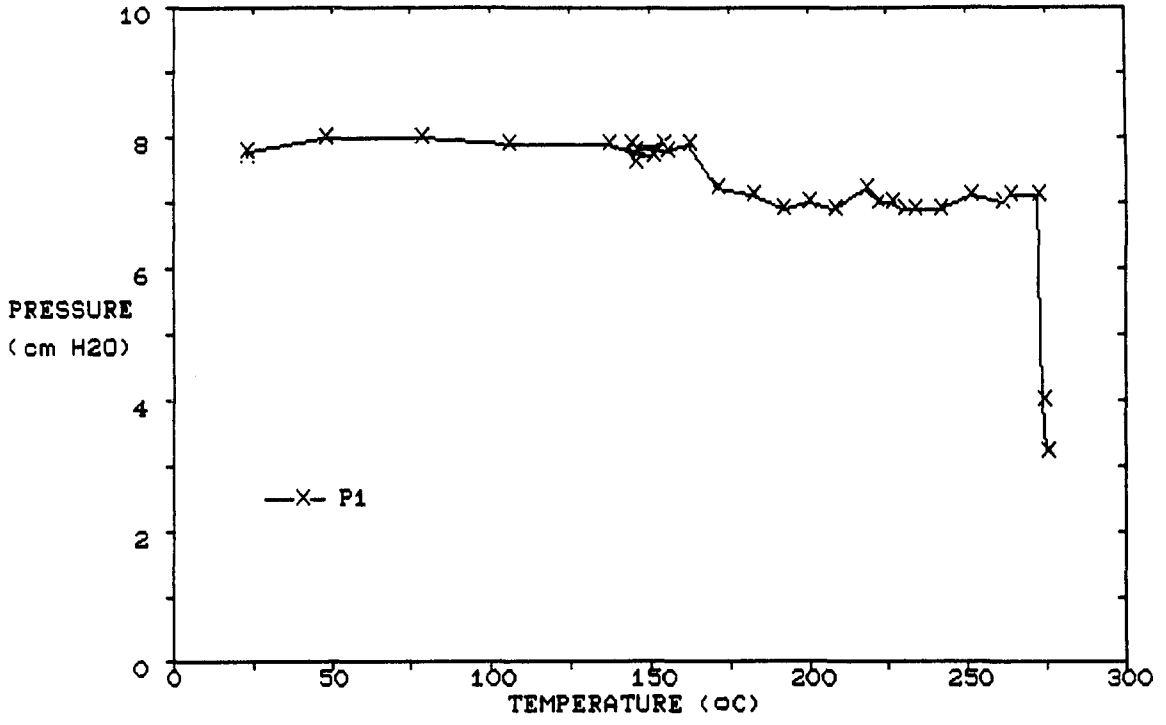

Figure 2.18b. Constant velocity defluidization procedure for sodium citrate. (broad particle size distribution, U/U_{mfo}=4.1).

defluidization as indicated by the gradual loss of pressure drop over the bed. Sampling of the beds however did not show that the bed material was strongly agglomerated, in fact only a small number of dimers and trimers were observed and then only when the relative gas velocity was high.

Changes in the volumetric properties of particle compacts as measured by CHR dilatometry appear to correlate well with the onset of particle cohesion as detected by pressure drop changes and defluidization. However CHR dilatometry results must be interpreted with caution: compact shrinkage does not necessarily indicate surface softening (glass at 300^{o}C) and some particle compacts actually demonstrate increased rates of dilatation when the particles become cohesive (sodium chloride, sodium bromide, and sodium citrate). Also, volumetric changes due to bulk particle properties such as the removal of lattice water, and rearrangement of the particle compact can cause compact shrinkage when particle cohesion is not present.

The minimum sintering temperature was found to decrease with decreased particle diameter and also with increased load in the dilatometer.

2.3 Cohesive Properties of Industrial Materials

2.3.1 FCC Catalyst

FCC catalysts are used in high temperature fluidized beds in the fluid catalytic cracking of petroleum. These systems consist of two fluidized beds. The first is a riser where heavy hydrocarbons are cracked into lower molecular weight compounds, carbon deposition results in catalyst deactivation. The second unit is the regenerator in which the catalyst is reactivated by carbon burnoff. Generally, the riser operates at temperatures in the 480 to 550°C range while the regenerator runs at higher temperatures between 560 and 700°C.

The high temperature sintering characteristics of five catalysts taken from an industrial FCC unit were studied. Five catalyst types were obtained in one of three conditions: fresh (unused), spent (deactivated) and equilibrium (regenerated). The five catalysts are labeled A through E. Sample A was obtained in both the fresh and equilibrium condition, B is fresh, C is equilibrium and D is a spent catalyst. Sample E is an equilibrium catalyst which was later ground to an average diameter less than 20μm.

CHR DILATOMETRY

Table 2.3 lists the experimental conditions and results of CHR dilatometry. Changes in slope were found to occur at four characteristic temperatures which are labeled T_1 through T_4. Here a temperature value given in parenthesis means the effect was weak or that

Table 2.3. Results and conditions of CHR dilatometry for FCC Catalysts. (T1 through T4 are the temperatures at which the four characteristic deformations of the catalyst samples begin).

Sample (condition)	Ave. d_p (μm)	T1 (°C)	T2 (°C)	T3 (°C)	T4 (°C)	Figure #
A (fresh):	34.5	315	498	561	881	2.19a
A (equil.):	34.5	339	-	(600)	847	2.19b
B (fresh):	34.5	~250	496	552	922	2.19c
C (equil.):	34.5	~250	-	630	932	2.19d
D (spent):	34.5	324	(523)	-	895	2.19e
E (equil.):	<20	270	(510)	682	924	2.19f

conditions:
1. Heating rate = 200°C/hr.
2. Load = 28 grams.
3. Sample holder = 5mm.

Table 2.4 Results and conditions of Isothermal dilatometry of FCC Catalysts.

Sample (condition)	ave. d_p (μm)	Time of soak (min)	Time for max. deformation (min)	Temp. of soak (°C)
A (equil.):	<25	200	63	750
C (equil.):	34.5	345	106	800
C (equil.):	34.5	70	35	1000

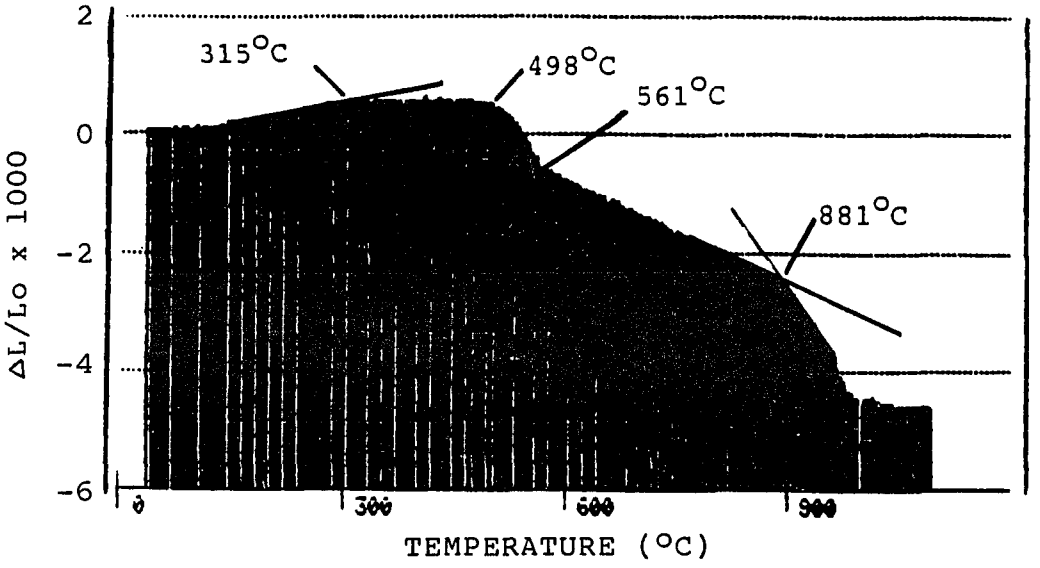

Figure 2.19a. CHR dilatometry for FCC catalyst A (fresh).

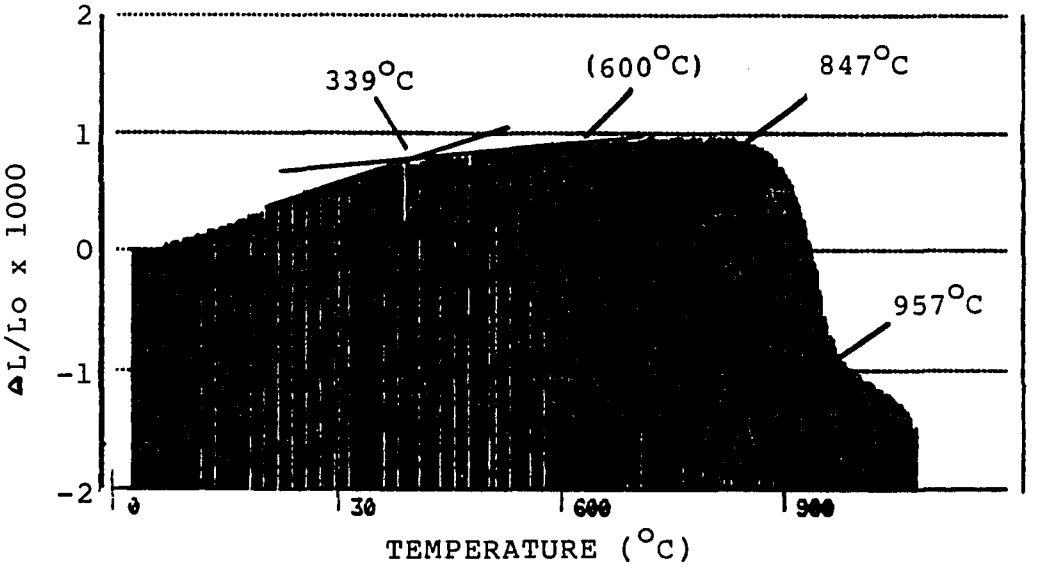

Figure 2.19b. CHR dilatometry of FCC catalyst A (equilibrium).

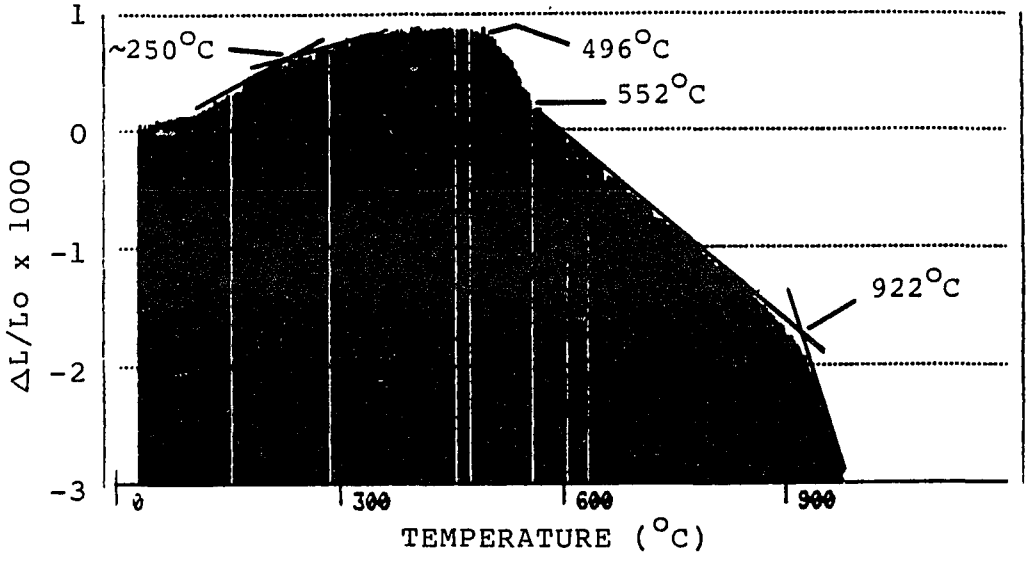

Figure 2.19c. CHR dilatometry for FCC catalyst B (fresh).

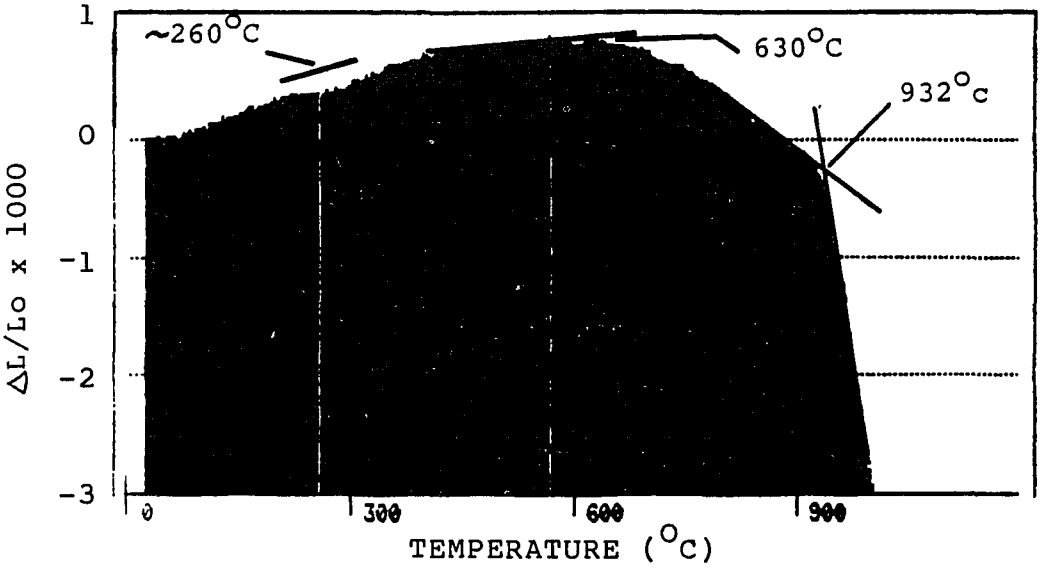

Figure 2.19d. CHR dilatometry for FCC catalyst C (equilibrium).

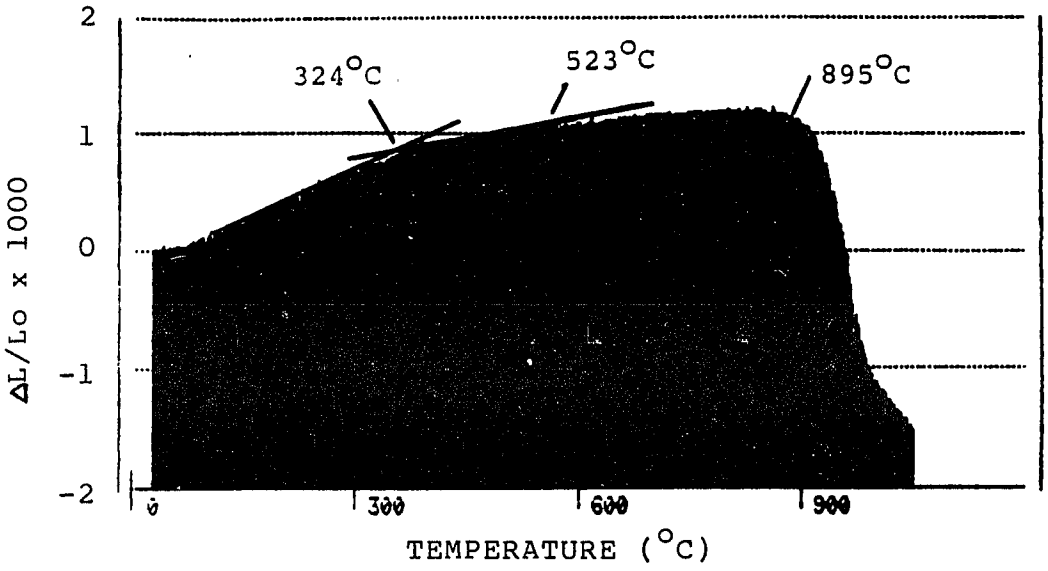

Figure 2.19e. CHR dilatometry for catalyst D (spent).

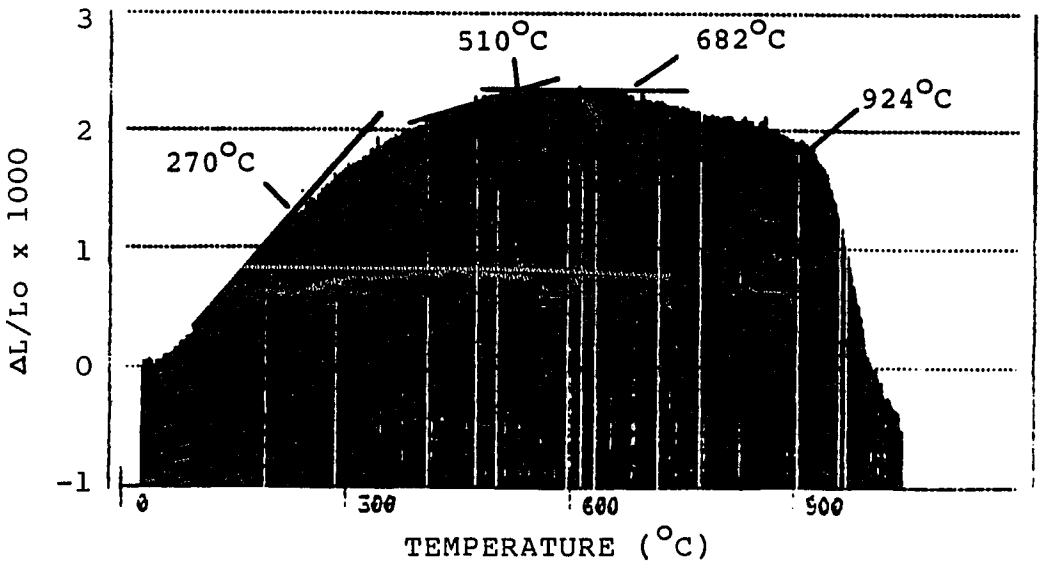

Figure 2.19f. CHR dilatometry for catalyst E (equilibrium fines).

its identification was difficult. The CHR dilatometer runs are shown in Figures 2.19a through 2.19d.

All samples exhibited a slight decrease in thermal expansion in the 250 to 340°C range initiating at T_1. Since the effect is found in both fresh catalysts it is not due to surface deposits. The effect is not eliminated by heating or catalyst use because it is found in all samples. Differential Scanning Calorimetry of fresh catayst (sample B) shown in Figure 2.20 confirms a weak thermal effect at 291°C. This effect was interpreted as a phase change of a minor constitutent of the catalyst such as a metal. This interpretation was confirmed by the manufacturer who is aware of physical changes in the fresh catalyst occurring in this temperature range.

The large contraction which appears in the temperature range of 860 to 940°C (T4) is also present in all samples and is probably the sintering of the catalyst structure. This temperature (T4) is approximately 70% of the fresh catalyst melting point (1260°C).

The contraction occurring at T_2 is only found in the two fresh catalysts (498°C for sample A, 496°C for sample B) and possibly in spent D and equilibrium E samples. The contraction of the fresh catalysts at this temperature is moderately strong while the change in the spent at 523°C and the equilibrium at 510°C is weak and of a different character. It is probably correct to assume that the T_2 deformation present in fresh catalysts is eliminated after use of the catalyst either because of surface annealing or because of mechanical abrasion (grinding and polishing) which reduces the presence of high energy surface asperities. Another possibility is that adsorbed deposits on equilibrium and spent

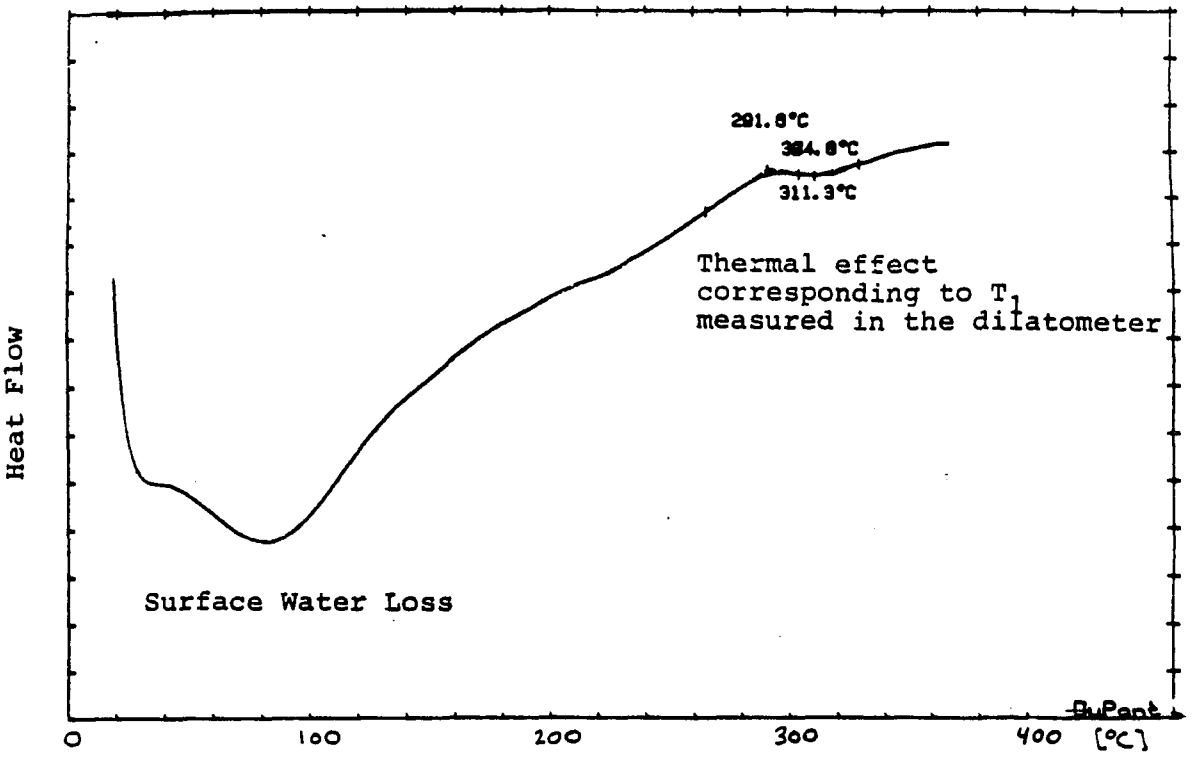

Figure 2.20. Differential Scanning Calorimetry scan of fresh FCC catalyst (sample A) showing a small thermal change at 291°C. (See Table 2.3 for identification of samples).

catalysts stabilize the surface at this temperature thereby reducing the driving force for the surface to rearrange to a lower energy state. This might explain why the equilibrium E sample shows a change at T_2 while the other two equilibrium catalysts do not. Sample E was not taken from the regenerator as fines, but were ground from a larger particle size equilibrium catalyst. The result of grinding is to produce fresh catalyst surfaces which could then behave as the pure fresh catalysts do.

The remaining characteristic temperature range starting at T_3 is the least regular among the six samples tested. In the fresh catalysts a change in slope at 550°C seems to be a modification of the deformation starting at T_2 (500°C). The three equilibrium catalysts show varying degrees of change at temperatures ranging from 600 to 682°C and the spent catalyst shows no changes at all from T_2(523°C) to T_4(895°C). The divergent behavior of the samples in the the region around T_3 suggests that the changes are due to surface deposits.

DEFLUIDIZATION OF EQUILIBRIUM CATALYST A

Defluidization tests were performed using equilibrium sample A at three different gas velocities: two, four, and eight times the minimum bubbling velocity. Otherwise the experimental conditions for the tests were identical. The minimum bubbling velocity was found to be about 0.4 cm/sec. The minimum bubbling velocity was used as a reference point because the catalyts are type "A" particles and do not bubble at the minimum fluidization velocity. The particles were tested "as is" without sieving and about 1.5 Kg of the material was used giving an at rest

height to diameter ratio of 4.25. The pressure drop versus temperature curves are shown in Figure 2.21. (Note that this graph is really three separate plots, one for each relative gas velocity.) All three pressure drop curves are normalized by the weight of the bed divided by the cross sectional area of the bed.

The fluidization results show that even at a gas velocity of only twice the bubbling velocity, the material fluidizes with out deviation from the theoretical pressure drop up to 600°C. This indicates that the changes in slope of the CHR dilatometery curves at T_1 and T_2 (both below 600°C) are not due to particle bonding. In the region around T_3(~600°C) there is apparently a development of weak interparticle cohesion: it is sufficient to defluidize the bed at the lowest fluidization velocity as shown by the irreversible drop in pressure in the experiment performed at two times minimum bubbling velocity.

At four times the minimum velocity a region of over pressure develops at T_3, suggesting a fixed bed region right above the distributor plate through which the gas is forced to pass through. After forming, the agglomerate must have developed a channel through which the gas could pass indicated by the drop in pressure below theoretical. The remainder of the bed remained fluidized until about 870°C, thirty or so degrees higher than the major deformation occuring in the dilatometry curve. The complete defluidization occurring at 870°C lends support to the interpretation of catalyst sintering at T_4. During this run it was also observed that a change of color from dark grey to yellowish white occurred between ~600 and ~700°C. This may suggest that some type of reaction or carbon burn-off occurs in this temperature range which

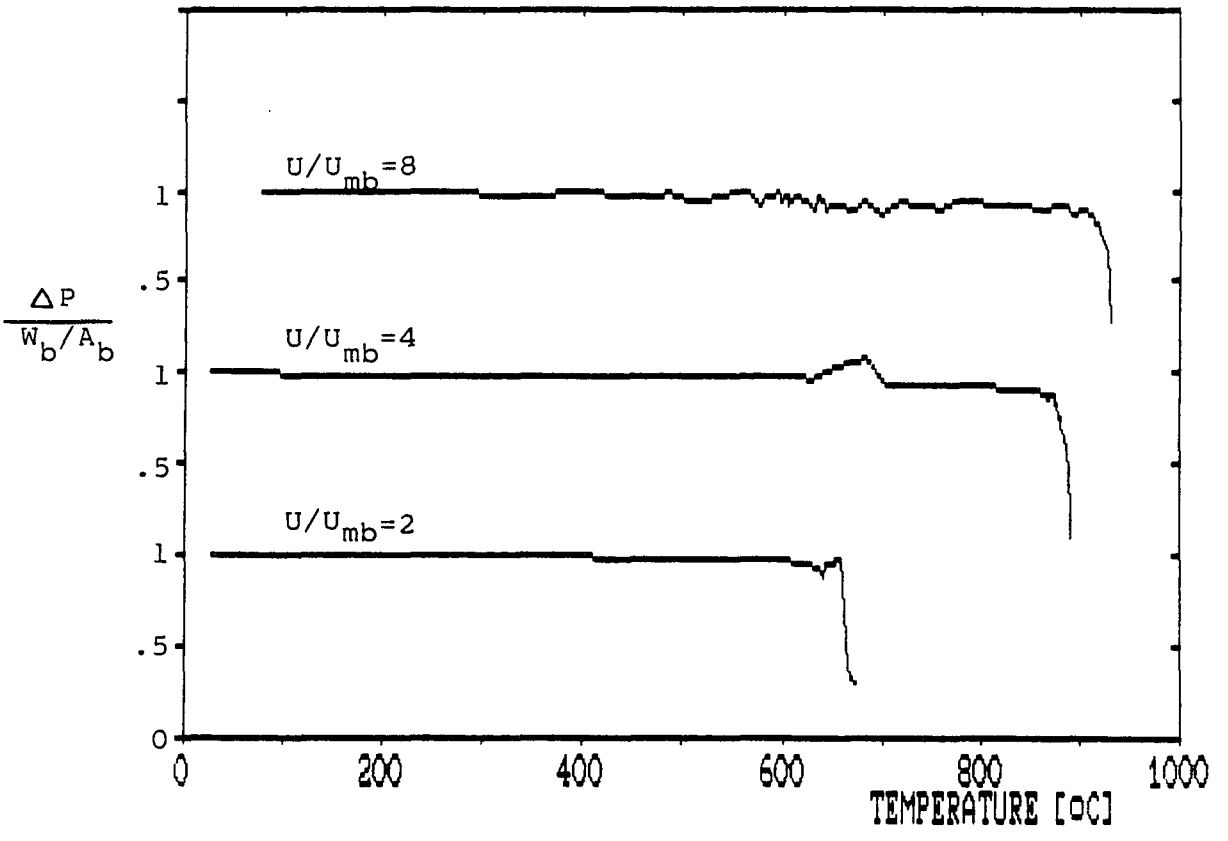

Figure 2.21. Constant velocity defluidization procedure for equilibrium catalyst (sample A). U_{mb}=0.4cm/sec. Defluidzation curves for three gas velocities are shown.

alters the surface. Since the gas surrounding the particles in the dilatometer is fairly stagnant this reaction may have been inhibited in the dilatometer. This could explain why the change at T_3 was not always clear in the dilatometer but was obvious in the fluidized bed.

In the run with the highest gas velocity ($U/U_{mb}=8$), the cohesion developed in the T_3 range (600°C) seems to have some effect as indicated by the fluctuations of pressure, but no overpressure developed. Defluidization did not occur until 900°, 50° higher than the catalyst sintering temperature (T_4).

ISOTHERMAL DILATOMETRY

Equilibrium catalysts A and C were tested isothermally (see Table 2.4 for experimental conditions and results). Indicated in the table are the length of time of the soak and the time at which maximum deformation has occurred. It is clear that for temperatures ranging from 750 to 1000°C deformation is essentially complete after about 100 minutes or less.

SUMMARY OF FCC CATALYST RESULTS

The dilatometry and fluidization results of the FCC catalysts are interpreted as follows: (1) the changes in slope occurring at T_1(~300°C) and T_2(~500°C) in the CHR dilatometry curves do not indicate surface bonding and T_1 is due to a change in the bulk structure of the material as confirmed by the manufacturer. (2) some interparticle bonding occurs at T_3 which is due to a chemical process on the surface. The sample changes color in this temperature range, and the effect is not picked up

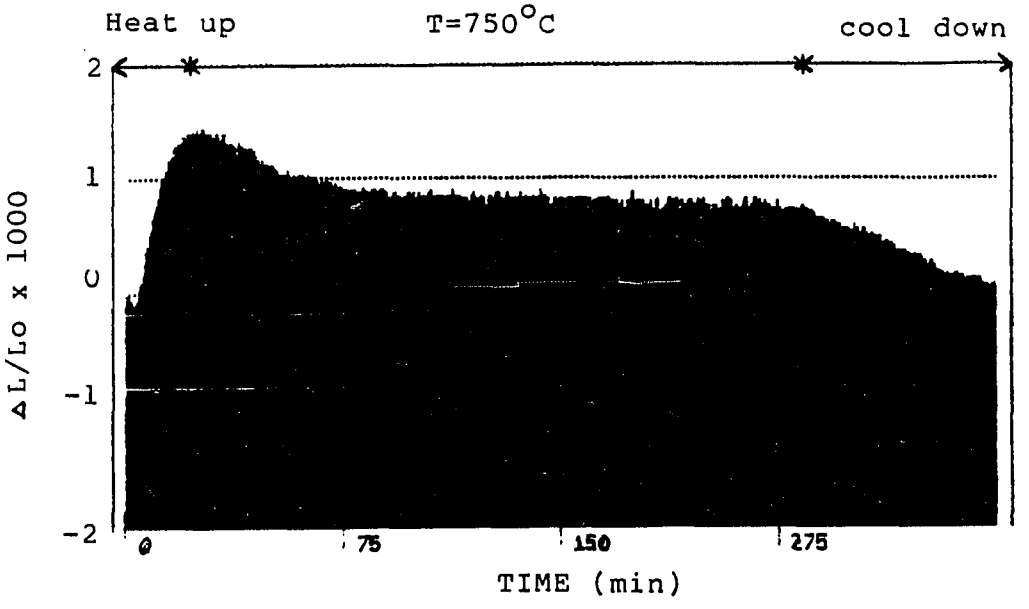

Figure 2.21a. Isothermal dilatometry for catalyst A (equilibrium). Temperature=750°C.

very well in the dilatometer presumably because the surfaces are not softening. This chemical cohesion is of sufficient magnitude to agglomerate these particles at the lower gas velocities. Perhaps the very slight change in the dilatometer is in accordance with such a weak cohesion development. (3) The contractions at T_4(~900°C) are due to the sintering of the catalyst structure itself and results in strong interparticle bonding as demonstrated by the complete defluidization of the samples in this temperature range.

2.3.2 Granular Polyethylene

A set of nine polyethylene samples were supplied by a company which had found certain of the nine to agglomerate in a fluidized bed process at temperatures around 90°C. All of the nine have crystalline melting points greater than 124°C and except for one sample, no melting point is higher than 128.5°C. They had assumed that materials with similar melting points would exhibit similar minimum sintering temperatures, and were quite surprised that any of the nine would agglomerate. The agglomeration was a problem in their fluidized bed process and so a number of experiments were performed to identify the minimum sintering temperatures of the nine different polyethylenes.

Table 2.5 lists the crystalline melting point, the Vicat softening point and the mean sphericity of each polymer which are labeled A though I. The particle densities of these samples, as measured by pycnometry, ranged from 0.923 to 0.960 g/cm^3. CHR dilatometry was performed using the following experimental conditions:

Table 2.5. Physical properties of granular polyethylene samples.

Sample	Crystalline Melting Point (°C)	Vicat softening Point (°C)	Mean* Spher-icity	Dilatometry T_1 (°C)	Dilatometry T_2 (°C)
A	125.9	98	64.1	91.9	-
B	127.3	86	60.2	93.6	-
C	133.3	127	70.1	127.3	-
D	124.8	100	62.5	97.1	-
E	128.5	100	63.0	98.6	67.6
F	127.7	104	57.6	88.7	75.8
G	125	90	65.3	90.9	60.5
H	124.7	97	55.1	89.5	66
I	126.4	98	61.7	91	54

*mean sphericity = (area/perimeter^2) x 1256.64

Table 2.6. Conditions for defluidization experiments using granular polyethylene.

SAMPLE	AVE. d_p (μm)	U_{mfo} (cm/s)	GAS VEL. (U/U_{mfo})	DEFLUIDIZATION TEMPERATURE (°C)
C	~610	~18	2.0	127-132
F	~600	~16	1.3	101
G	510	~12	1.3	104

Ave. particle size:	359 μm (40-50 mesh)
Load:	23 grams
Initial sample length:	2-3mm
Sample holder diameter:	6mm
Heating rate:	ambient to 60°C = step change
	60°C to melting point = 1°C/min

Each sample was tested at least twice. The average value of the results obtained for each sample is listed in Table 2.5.

The CHR results show that there are two types of behavior depending on the number of characteristic changes that appear in the curves. Those of the first group, including polymers A (Figure 2.22a), B, C (Figure 2.22b) and D, exhibit the simplest behavior. Initial heating results in either no change in length or some thermal expansion (C and D); then at the temperature labeled T_1 the sample contracts sharply; T_1 was greater than 90°C in all cases.

The second group, consisting of polymers E (Figure 2.22c), F, G, H, and I (Figure 2.22d) show two characteristic temperatures. The first, labeled T_2, is the temperature at which a slight, somewhat linear contraction begins. This change, which occurs at considerably lower temperatures in the 60 to 75°C range, is then followed by the sharp contraction found in the polymers of the first group; this temperature is again labeled as T_1.

To see if the weak contraction at T_2 was due to interparticle bonding, samples C, F, and G were tested in the fluidized bed. The powders were fluidized at low gas flow rates ranging from 1.3 to 2 times

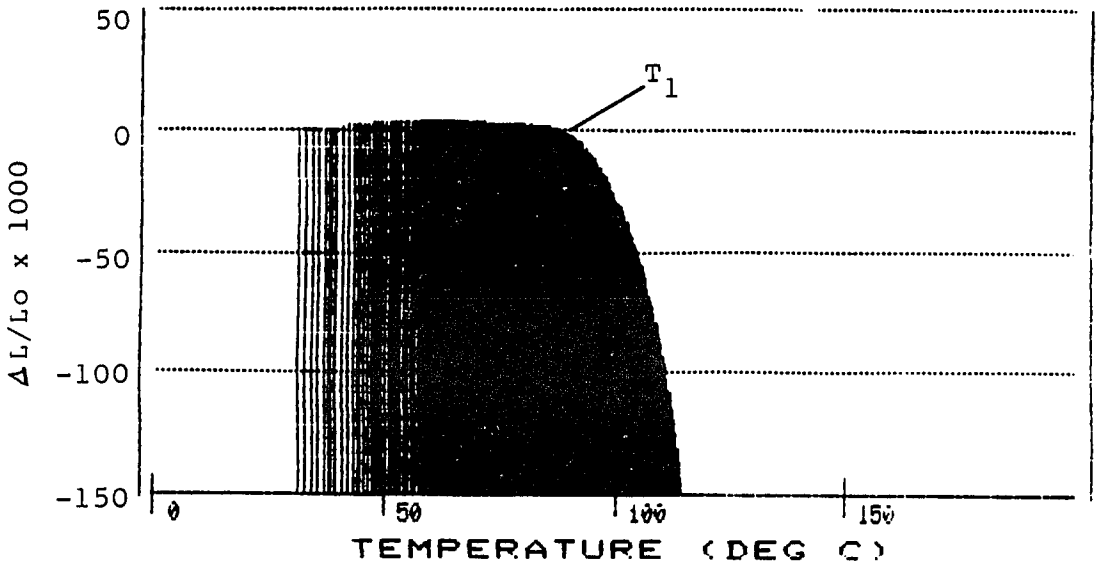

Figure 2.22a. CHR dilatometry for polyethylene sample A.

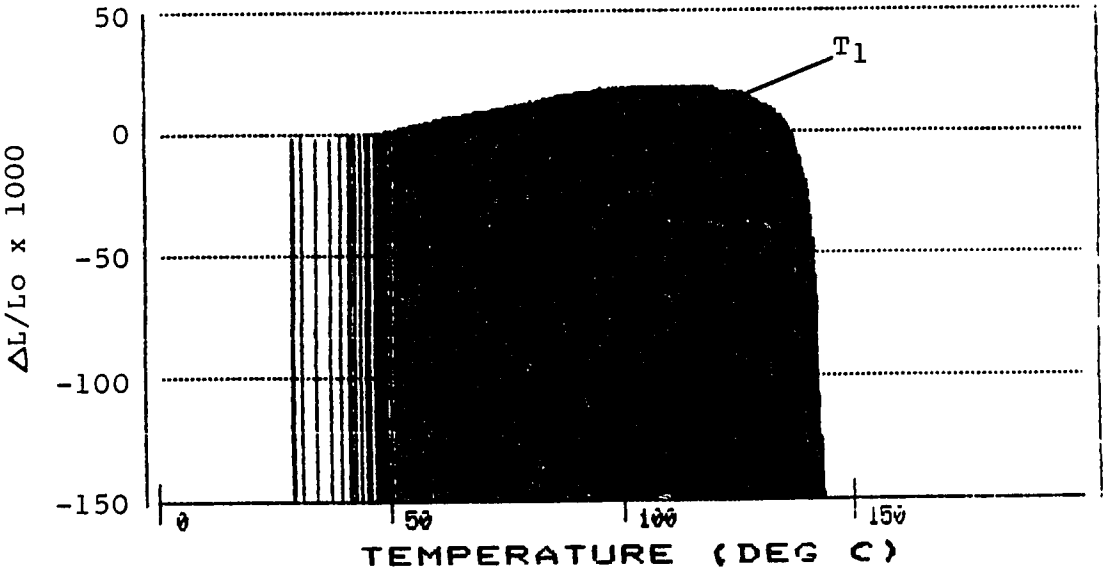

Figure 2.22b CHR dilatometry for polyethlene sample C.

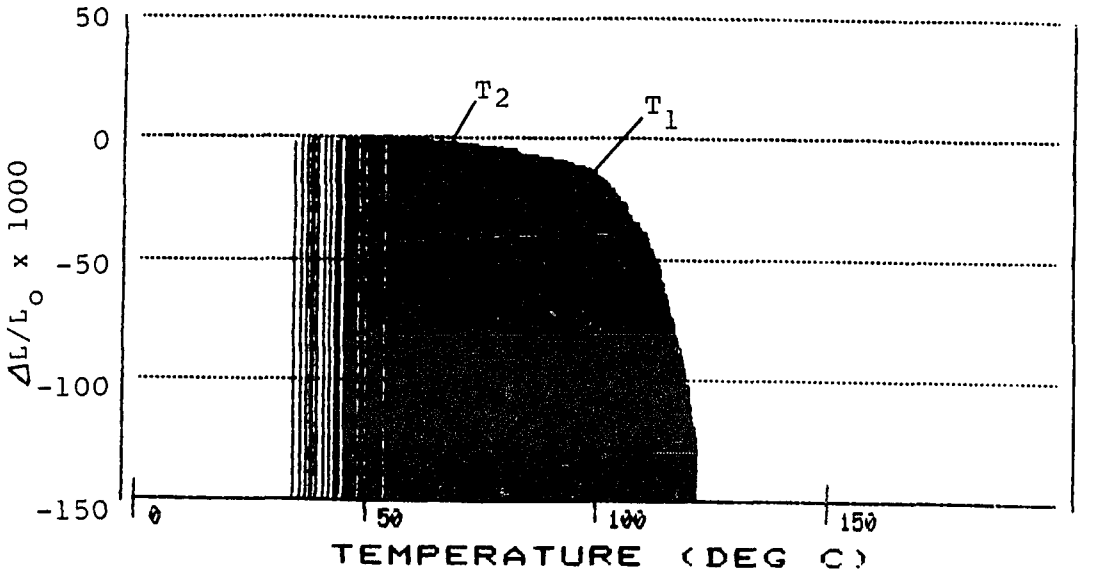

Figure 2.22c. Constant heating rate dilatometry for polyethylene sample E.

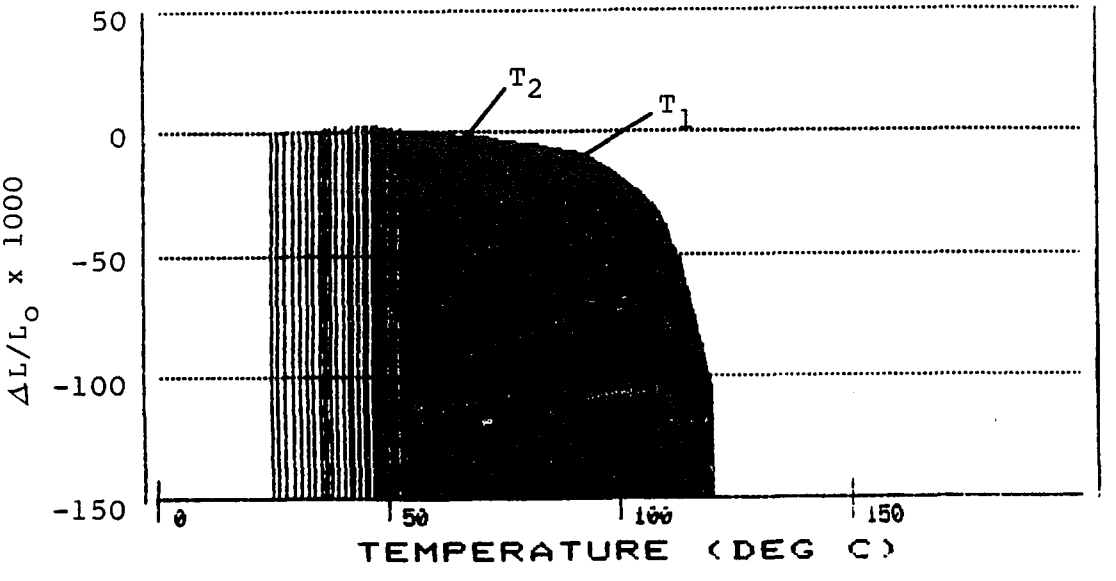

Figure 2.22d. Constant heating rate dilatometry for polyethylene sample I.

the ambient minimum fluidization velocity. Table 2.6 gives the experimental conditions for these runs.

The pressure drop data for the run using sample F is shown in Figure 2.23. In this run the bed started to defluidize at about 101°C, 12°C higher than the measured value of T_1. Sample G defluidized at 104°C, 13°C higher than T_1. Cohesion in the temperature range between T_1 and T_2 was not detected; this was unexpected because the suppliers of the material had said that agglomeration occurs in the 90°C range.

In order to clarify this situation a number of simple isothermal experiments were performed. Samples were poured into crucibles, lightly packed, and then placed in a hot oven for about 20 minutes after which the samples were removed. Inspection of the samples showed that some agglomeration does occur between T_2 and T_1 but that it is not strong. For example, polymer H showed weak agglomeration after being soaked for 20 minutes at 69°C but agglomerated strongly after a 20 minute soak at 91°C. Polymer F also demonstrated weak agglomeration after a test at 77°C which is only two degrees higher than T_2.

After completion of this study, discussions with the supplier of the polyethylene revealed that it was those samples exhibiting the weak contraction at T_2 which had indeed agglomerated in their fluidized bed. They were able to account for the differences in minimum sintering temperatures in terms of molecular weight characteristics. The CHR appears to be an excellent tool for the prediction of this phenomena, much better than defluidization tests and better than a correlation of bulk properties. A plot of the Vicat softening point and the crystalline melting point against the measured minimum sintering temperature (Figure

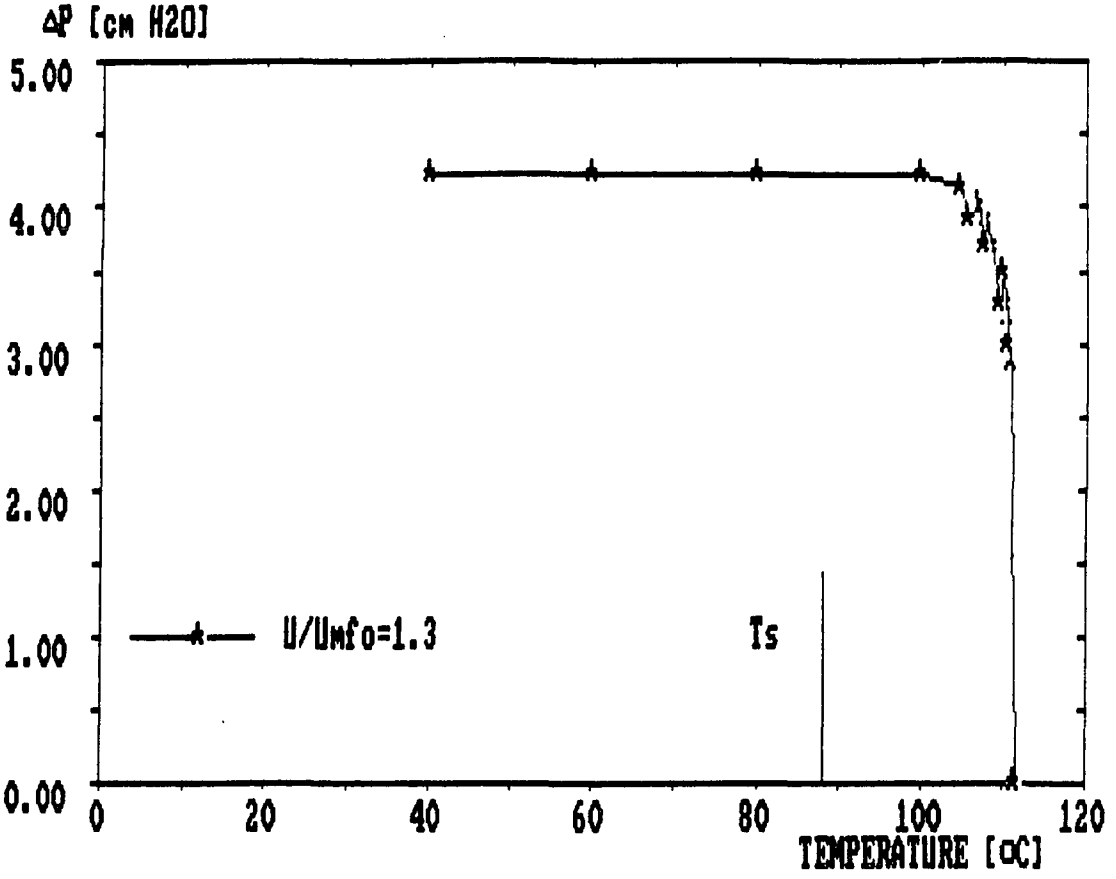

Figure 2.23. Constant velocity defluidization procedure for granular polyethylene (sample F).

2.24) shows practically no correlation of these bulk properties with minimum sintering temperature. The only exception being sample C which has a very high Vicat softening point (127°C) and a high minimum sintering temperature (127.3°C). This sample also defluidized at a much higher temperature (about 130°C) than the other samples.

2.3.3 Coal Ash powders

As discussed in the introduction, Section 1.3, coal ash agglomeration in coal gasification is a complex process in which the behavior of cohesive particles may or may not be involved. On the other hand, coal ash agglomeration in coal fired boilers does involve cohesion of particulate solids. Schobert et al. (1987) state that "the deposition of slag on boiler walls and ash on superheater tubes is the most significant technical problem encountered in the utilization of lignites in the United States". A number of studies on the properties of these coal ashes have been reported in which various techniques have been proposed for measuring sintering characteristics. In this section the sintering characteristics of coal ashes as measured by the dilatometric technique are compared to previously reported results.

Five coal ash samples were prepared by combustion of ground coals at 700°C as described in Ledesma et al.(1987). Table 2.7 identifies the samples along with the rank and total mineral content of each coal used. Table 2.8 shows the elemental analysis of each of the ashes. CHR dilatometry was performed in air. The powdery ashes were compressed with a load of 23 grams and heated at a rate of 10°C/min.

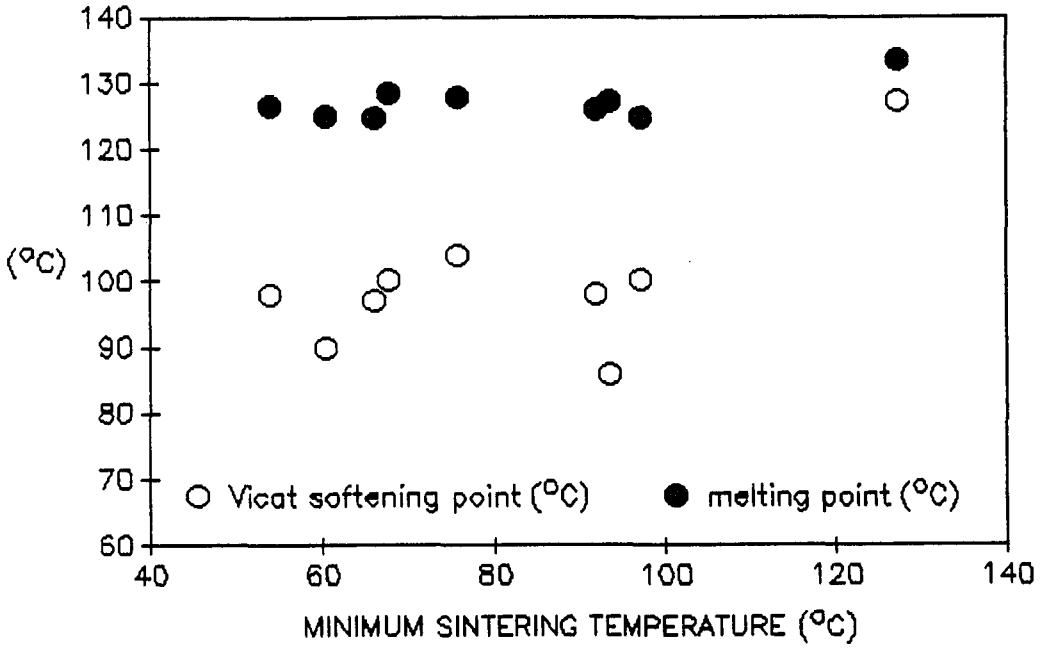

Figure 2.24. Vicat softening temperature and crystalline melting temperature versus the minimum sintering temperature for the granular polyethylene samples listed in Table 2.5.

Table 2.7. Identification of coals used in coal ash Experiments.

Derivative Coal	PSU Number	Total Mineral Content (wt. % dry)
North Dakota Lignite	PSOC-246	10.99
Wyoming Sub-bituminous B	PSOC-241	8.13
Virginia HVA	PSOC-265	17.98
Illinois #6 HVB	PSOC-282	11.78
Illinois #6	PSOC-022	11.88

Table 2.8. Elemental analysis of coal ashes used in dilatometry studies as obtained by ICP (Inductively Coupled Plasma). Data reported is percentage of major elements (>0.1% conc.).

COAL	Ca	Mg	Na	Al	Fe	Si	Ti
North Dakota Lignite	10.1	1.67	1.54	0.36	2.72	10.2	0.26
Wyoming Sub-bituminous B	6.44	2.14	2.73	6.93	8.58	9.18	0.49
Virginia HVA	0.58	0.56	0.14	11.5	3.88	22.19	1.01
Illinois #6 HVB	0.47	0.43	0.72	10.21	7.63	18.99	0.51
Illinois #6	0.95	0.41	0.15	6.1	7.0	17.7	0.55

The results of these experiments (Figure 2.25) show that the overall shape of the CHR curve is similar for all five ashes. There are differences in sintering temperatures however: the North Dakota lignite ash appears to sinter at a temperature well below the others and the Virginia HVA ash sinters at a somewhat higher temperature. The slopes of the shrinkage curves appear to be almost parallel. This might mean that the ashes sinter by similar mechanisms. Inspection of the cooled samples showed that weak, easily broken agglomerates had formed.

Raask (1982) developed a method of simultaneous shrinkage and electrical conductance measurements to study coal ash sintering. Unlike the present study, no commercial dilatometer was employed. However the instrument constructed by Raask is similar to a dilatometer in most respects. Raask found that the resistance to electric current flow through compacts of glass particles and certain coal ashes increased sharply at the temperature at which shrinkage occurred and attributed this behavior to the increased area for electrical fluxing due to bond neck growth. Conn and Austin (1984) confirmed this result using an apparatus based on Raask's design. Figure 2.26a shows the data of Conn and Austin for glass shot, while the shrinkage data is shown in Figure 2.26b. The large hysteresis effect obtained supports the interpretation that bond neck growth (which is not a reversible process) enhances current flow. In a short communication, Cummings and Sanyal (1980) reported preliminary results of electrical resistance measurements to determine sintering behavior of coal ash, but found a lesser degree of hysteresis to occur.

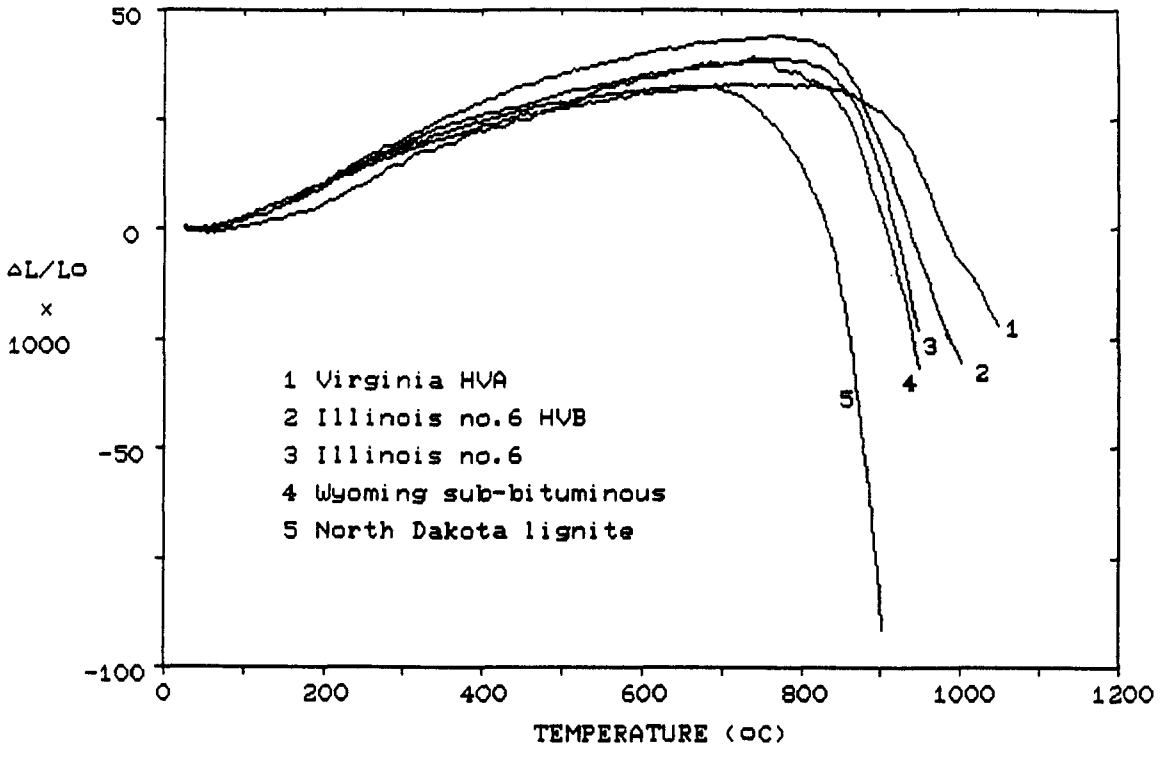

Figure 2.25. Constant heating rate dilatometry for five coal ash powders. Load=23g, heating rate=10°C/min, Lo=2.0-2.5mm, air atmoshpere.

Raask (1982), and Conn and Austin (1984) also found that for ashes produced from certain low rank coals such as North Dakota lignite, the electrical sinterpoint could be as much as 200°C lower than the sinterpoint obtained from shrinkage data (see Figure 2.27). This would imply that bond neck formation had occurred without change of the center to center distance between particles. These authors attributed this result in part to the presence of low melting fluxing agents, particularly sodium and calcium, which are in high concentration in lignite coal ashes.

A procedure which does not involve the measurement of sample deformations is the agglomerate sieving test developed by Stallman and Neavel (1980). Coal ashes were agglomerated at various temperatures in crucibles. After cooling, the agglomerates were screened for 20 minutes and the weight percent retained on a particular screen versus temperature was plotted (Figure 2.28). Ashes from lignite coals were not found to sinter at lower temperatures than non-lignite coal ashes. In all these studies it was concluded that the ASTM cone deformation test (Am. Soc. Test. Mat., 1978) consistently overpredicts minimum sintering temperatures for coal ashes.

The dilatometry results obtained in the present work agree in general with the results obtained by Raask, and Conn and Austin though the initial shrinkage points measured by CHR dilatometry are lower. Illinois #6 ash begins to shrink at 793°C and the North Dakota lignite at 692°C (these two curves are plotted seperately in Figure 2.29 for clarity). Conn and Austin report the initial shrinkage temperatures for Illinois #6 and North Dakota lignite to be 850°C and 750°C respectively.

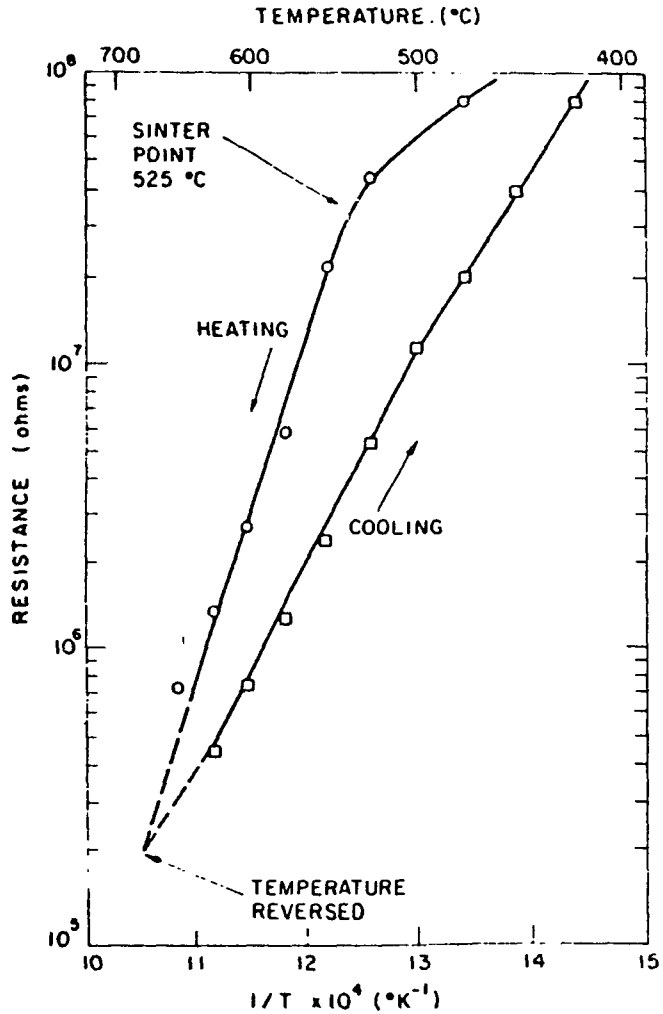

Heating (O) and cooling (□) cycle for soda glass. Ground soda glass, 90μm, heating and cooling rate: 6°C/min

Figure 2.26a. Electrical conductance data for glass from Conn and Austin (1985).

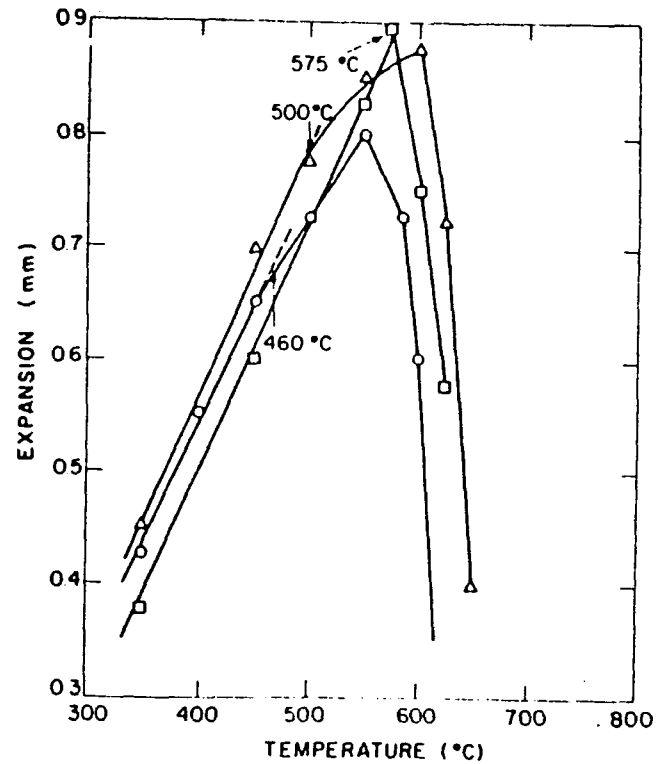

Effect of particle size on the sinter point of soda glass as determined by shrinkage measurements. Ground soda glass, bulk density 1100 kg m⁻³: O, < 10 μm; Δ, 38–45 μm; □, 75–90 μm

Figure 2.26b. Shrinkage data for glass from Conn and Austin (1985).

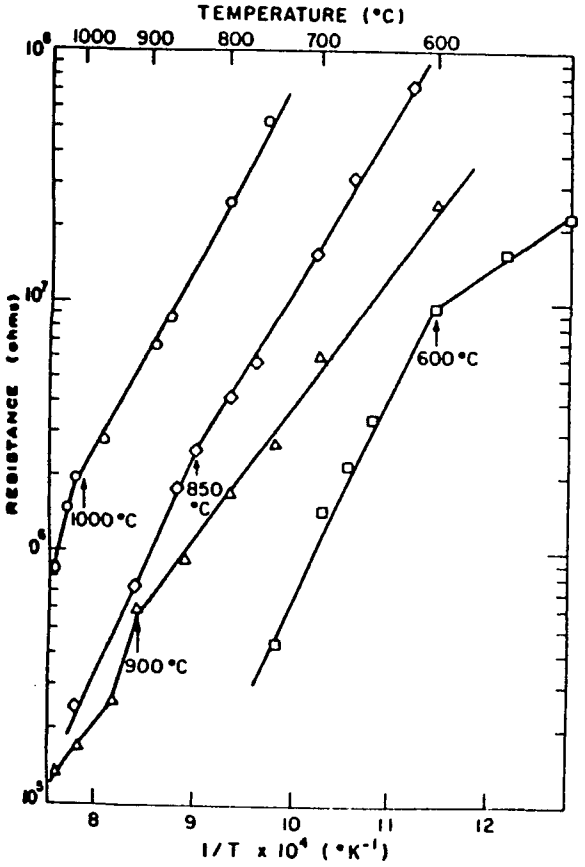

Comparison of sinter points for ASTM ashes as determined by electrical resistance measurements ○, Keystone; ▲, Texas lignite; □, N. Dakota lignite; ◇, Illinois No. 6; all coals, <75μm

Figure 2.27. Electrical conductance data for coal ashes from Conn and Austin (1985).

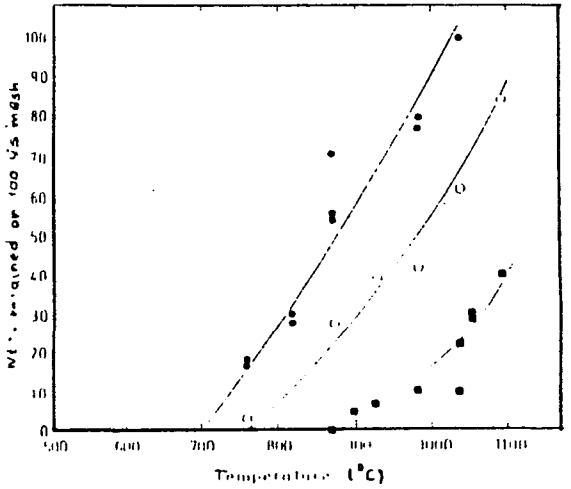

Figure 1. Agglomeration of Gulf Coast lignite ashes. ●, Texas sample 1; ○, Arkansas sample; ■, Texas sample 2

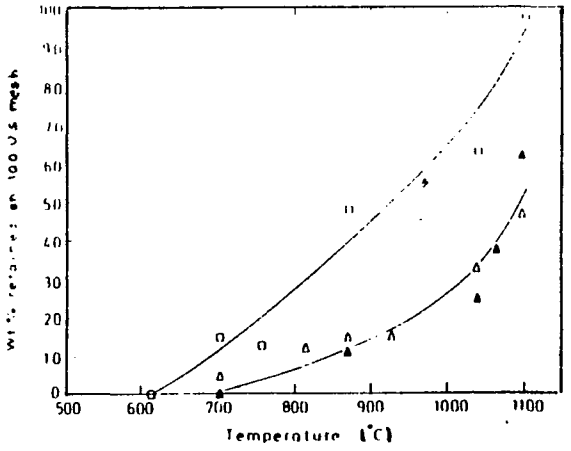

Agglomeration of Illinois and Wyoming coal ashes □, Illinois sample; ▲, Wyoming sample 1; △, Wyoming sample 2

Figure 2.28. Sieve technique from Stallman and Neavel (1980).

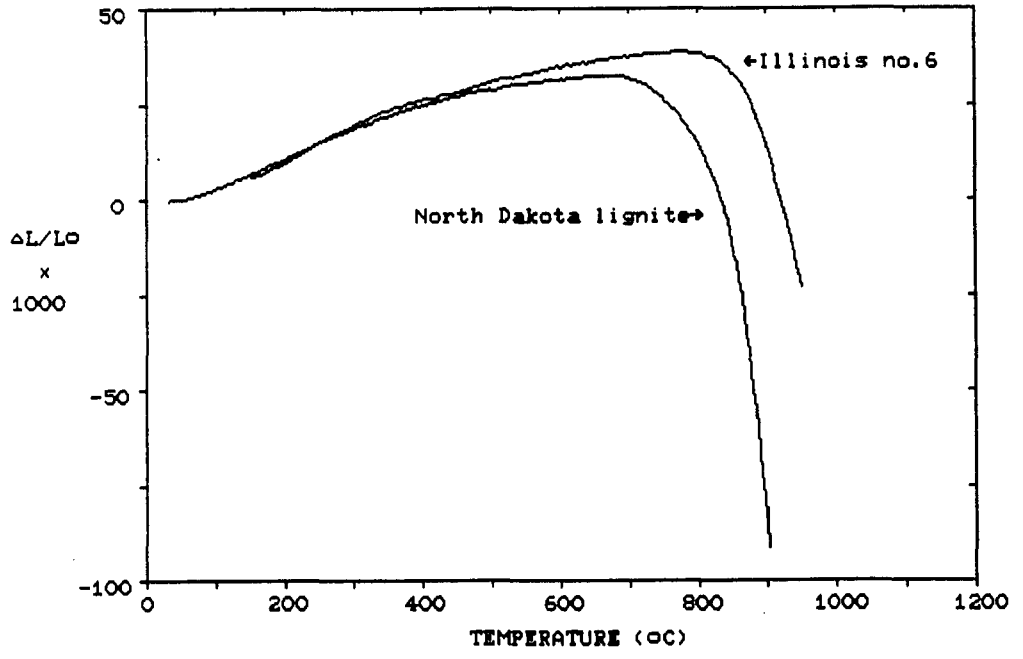

Figure 2.29. Constant heating rate dilatometry for Illinois #6 and North Dakota lignite coal ashes.

While the dilatometer measured initial temperatures about 60°C lower in both cases, the difference (about 100°C) is almost identical. It could be said that the slope of the North Dakota lignite CHR curve begins to decrease at a lower temperature than the Illinois #6 curve (at about 500-550°C) but the effect is not strong. Stallman and Neavel (1980) found Illinois #6 to agglomerate beginning at about 620°C (Figure 2.28), a result not predicted by any of these measurements.

The effect of composition was investigated by plotting in Figure 2.30 the minimum sintering temperatures, defined as the temperatures at which each of the five coal ashes first exhibited a negative slope, against the percentages of various elements. As Raask, and Conn and Austin showed, the higher the concentrations of sodium and calcium, the lower the minimum sintering temperature. The linear regression on the semi-log plot seems to fit the calcium better. Also the greater the concentrations of titanium and silicon the higher the minimum sintering temperature. No significant correlation was found between minimum sintering temperature and the concentrations of magnesium, aluminum or iron.

2.3.4 Ferrous chloride powder

A company asked the author to investigate the high temperature fluidizability of a ferrous chloride ($FeCl_2$) powder. A commercially available (Morton Thiokol, Inc) ferrous chloride powder was tested by dilatometry and then fluidized using nitrogen atmosphere. In the CHR dilatometry experiment the heating rate was 5°C/min and the load on the sample was 18 grams. The powder, which was supplied in a wide size

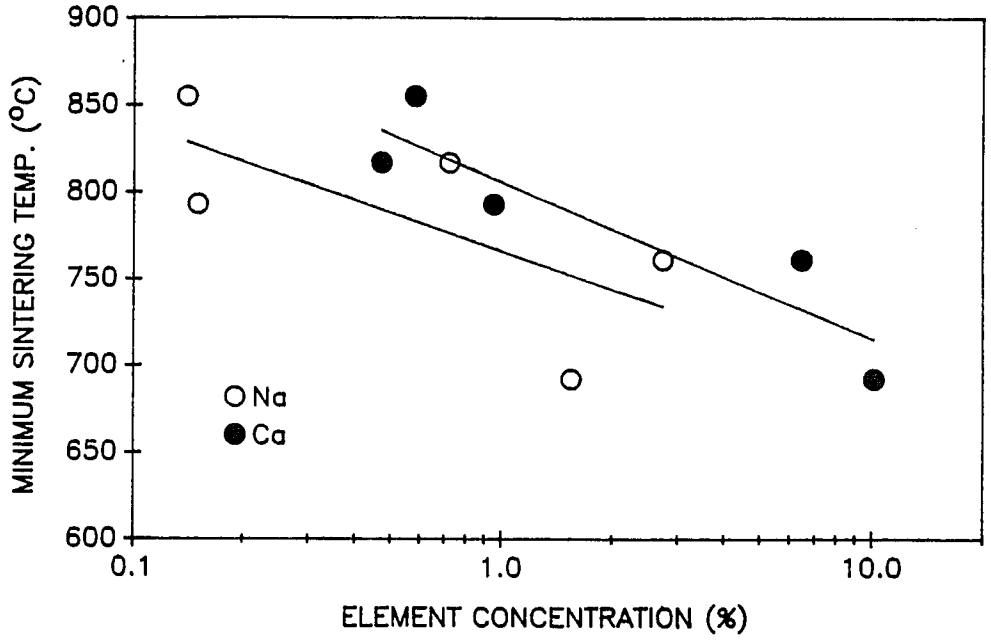

(a)

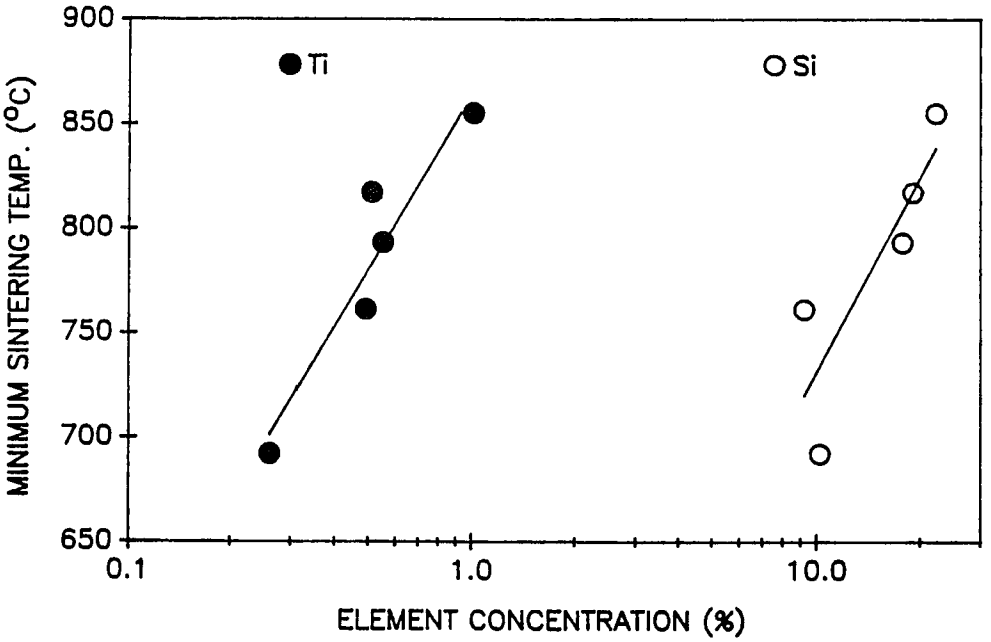

(b)

Figure 2.30. Correlation of minimum sintering temperature with the concentration of various elements in coal ashes. (a) sodium and calcium (b) titanium and silicon.

distribution, ranging from about 20 to about 600μm, was sieved to remove all particles larger than 300μm. The particles were quite fine and difficult to fluidize at room temperature.

The CHR dilatometry curve (Figure 2.31) shows two regions of shrinkage. The first begins at 217°C and continues at a gradual slope until about 550°C where the sample begins to contract more quickly with temperature. It was found that in the temperature range between 217°C and 535°C the original light brown sample turned dark blue and red in some regions. Mellor (1935) shows that ferrous chloride can react with oxygen and water. The experiments using the ferrous chloride powder were performed before the equipment for a controlled atmosphere was perfected and its possible that some air leaked into the sample chamber during the run. Even under these conditions however, it was found that the shrinkage of the powder at 217° could be eliminated by preheating the sample in the fluidized bed at 235°C using a pure nitrogen atmosphere. The curve labeled "preheated" in Figure 2.31 is the CHR result for the pretreated sample tested under otherwise identical conditions. Preheating the sample emphasizes the temperature of strong shrinkage which is seen to occur at 536°C.

The untreated ferrous chloride powder was fluidized in nitrogen using the constant velocity procedure. The gas rate was kept at twice the minimum fluidization velocity (which could only be approximated owing to the naturally cohesive nature of the material; probably due to the small particle size distribution). The powder was again sieved to remove particles of diameter greater than 300μm. The pressure drop vs. temperature curve obtained from this run is shown in Figure 2.32. As the

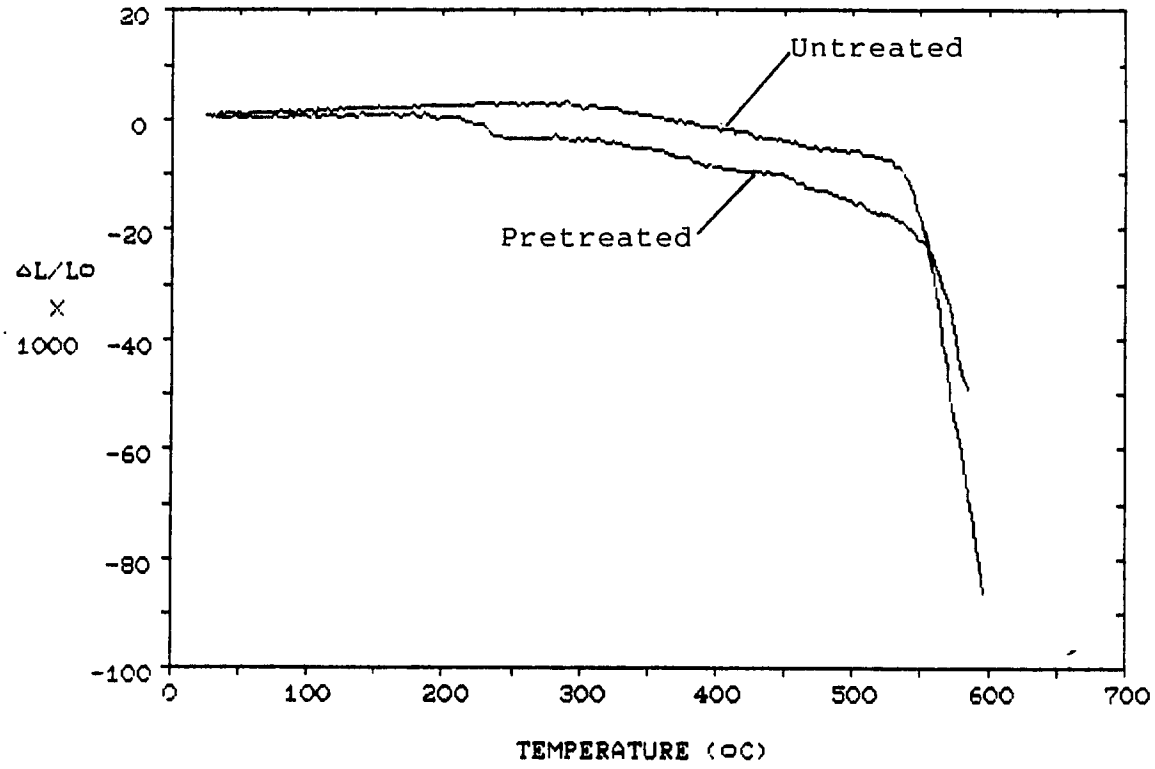

Figure 2.31. Contant heating rate dilatometry of a ferrous chloride powder. Heating rate = 300°C/hr, load=18g, Lo=3.7mm.

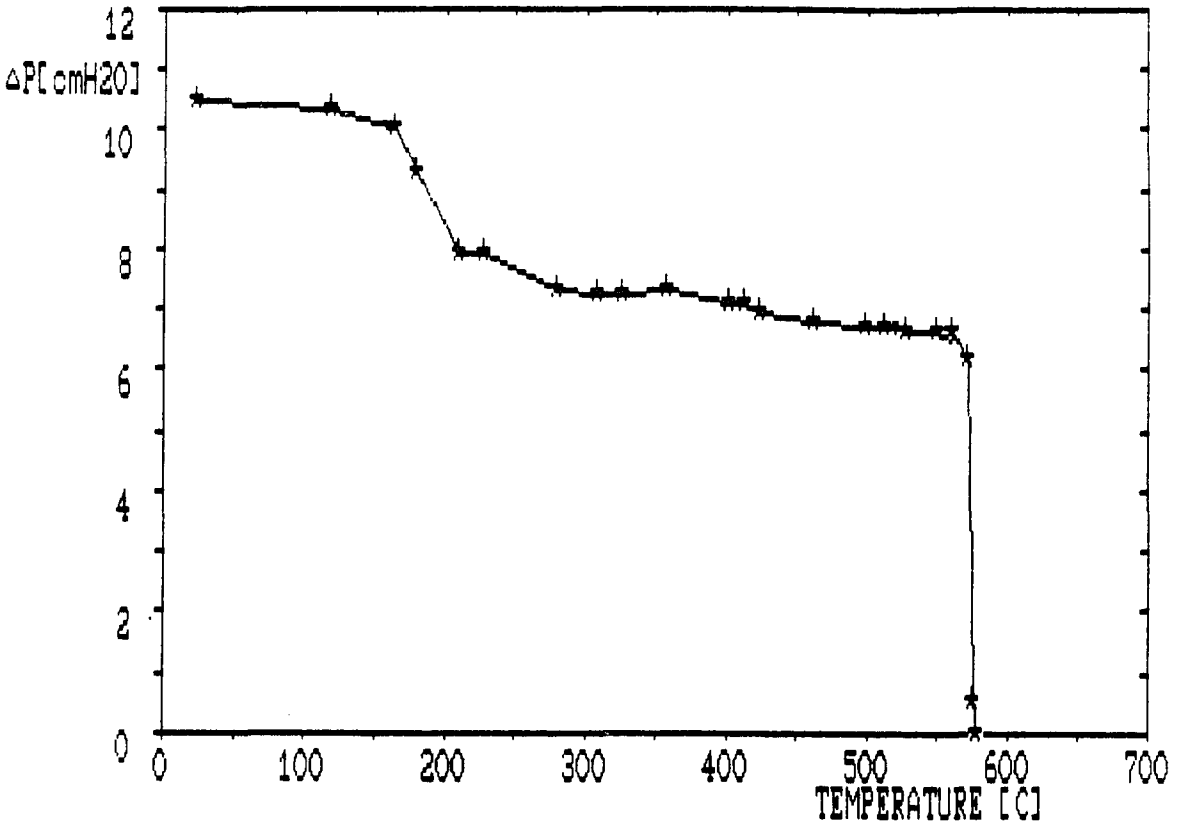

Figure 2.32. Constant velocity defluidization procedure for a ferrous chloride powder. U/U_{mfo}=2.1, nitrogen atmosphere.

temperature was increased the fluidization became better. The reduction of pressure in the 150°C to 200°C range corresponds roughly to the weak shrinkage measured in the dilatometer initiating at 217°C, and represents a weight loss of approximately 20% of the fluidized powder. After this initial drop in pressure the sample fluidized well until the bed defluidized completely at 565°C as indicated by the complete loss of pressure through the bed. The loss of pressure between 200 and 565°C was attributable in part to fines sticking on the upper column walls.

These results again demonstrate the importance of distinguishing between shrinkage in the dilatometer due to sintering and that due to bulk property changes. The loss of pressure in the fluidized bed at 150-200°C results from the same process which gave low temperature shrinkage in the dilatometer but not from agglomeration. Even though the starting material was anhydrous, the bulk process was most likely the loss of water which had contaminated the sample. The fact that preheating did not eliminate the low temperature shrinkage between 217 and 535°C indicates the filling in of void spaces created by water loss. A similar process was found to occur with the dihydrate calcium chloride sample (Section 2.2.3). Some color change of the fluidized sample was also noted in this temperature range, perhaps some of the loss of pressure was due to chemical changes. It follows then that the minimum sintering temperature of the ferrous chloride powder tested here is 535°C; that the sample defluidized at a temperature only 30 or so degrees centigrade higher supports this conclusion.

2.3.5 Beneficiated ilmenite ore

Ores are a class of fluidizable materials which are of industrial interest. Like the coal ashes tested in section 2.3.3, ores are in general nonhomogenous in composition. The aim of the experiments presented here using a benificiated ilmenite ore, is primarily to see if the correlation between the shrinkage, as measured by CHR dilatometry, and cohesion in the fluidized bed holds for such a complex material.

Table 2.9 lists the composition and a sieve analysis of the particles; the bulk density is 2.460 g/cm^3. CHR dilatometry was performed using nitrogen gas atmosphere, an applied load of 23 grams, a heating rate of 200°C/hr and a 5 mm diameter sample holder. The sample was fluidized in nitrogen at a gas velocity of 1.7 times the minimum (~15cm/s).

The CHR result shown in Figure 2.33 indicates strong shrinkage at about 980°C. Defluidization (Figure 2.34) occurred at 1120°C. From 975 to 1120°C however there was a decrease in pressure over the bed indicating some agglomeration and segregation. The minimum sintering temperature is therefore the same in the dilatometer and the fluidized bed. The fact that changes in fluidization and dilatometry behavior occur over a fairly broad temperature range could be due to the non-homogenous nature of the material. Nevertheless, no deviations from normal fluidization were noted to occur below 975°C, which is the temperature where strong shrinkage begins in the dilatometer.

Table 2.9. Composition (A) and Particle Size Distribution (B) of Beneficiated Ilmenite Ore particles. Composition Determined by XRF.

(A) Composition (wt. %)

TiO_2	65.3
Fe_2O_3	30.4
MnO	1.3
Al_2O_3	0.9
CaO	0.2
P_2O_5	0.2

(B) Sieve Analysis

mesh	wt. %
+70	0.5
+100	9.1
+140	66.2
+170	22.4
+200	1.5

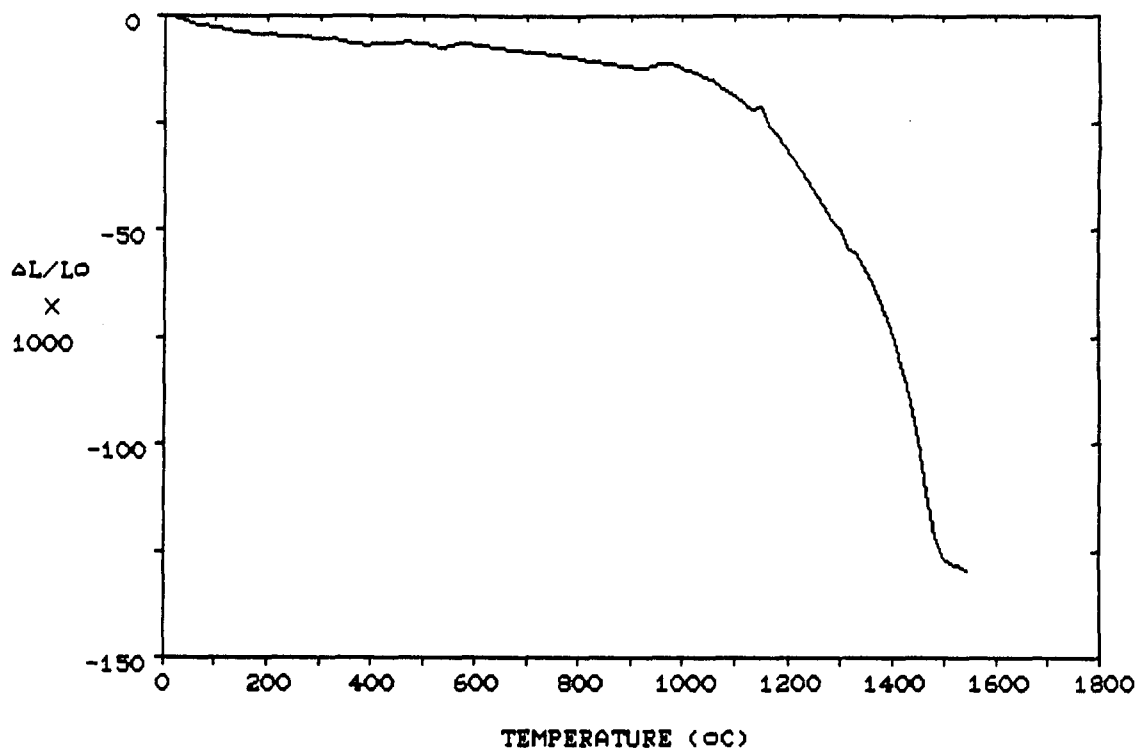

Figure 2.33. Constant heating rate dilatometry for a beneficiated ilmenite ore. Heating rate= 200°C/hr, Lo=3.8mm, load=28g, nitrogen atmosphere. (See Table 2.9 for particle properties.)

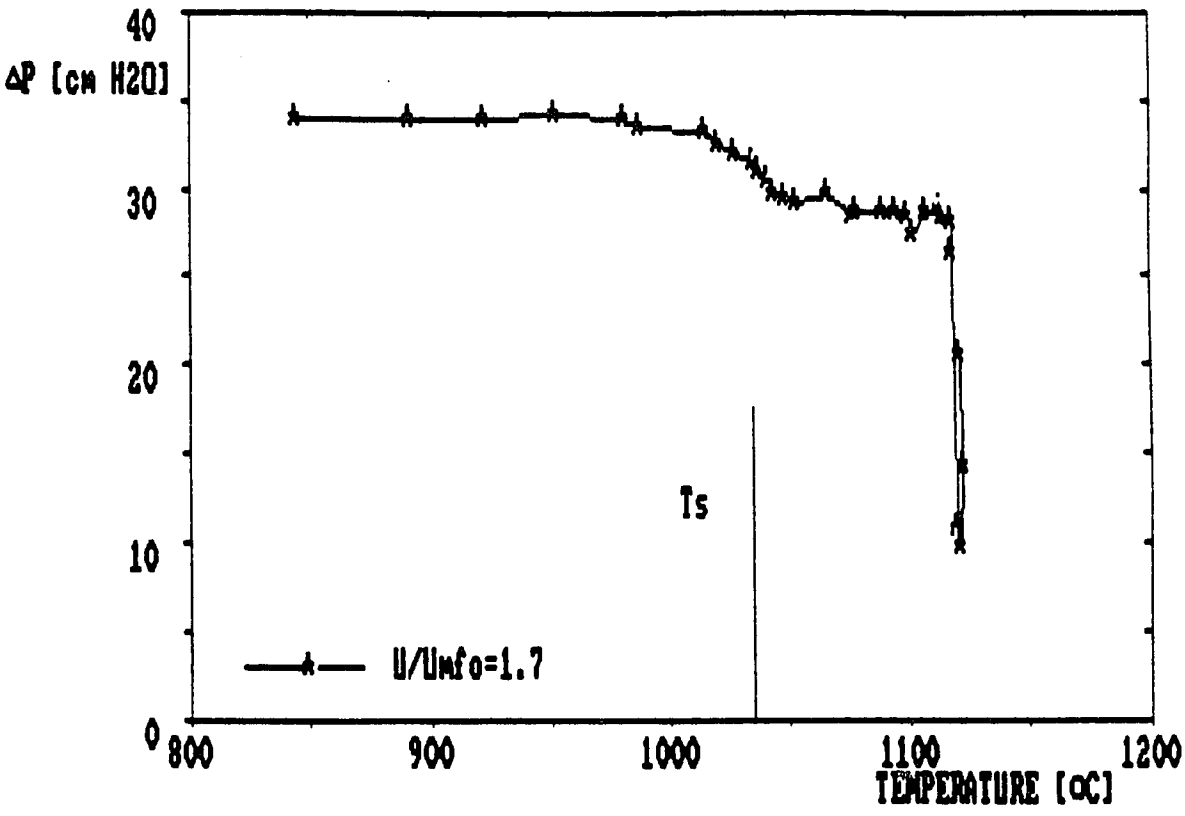

Figure 2.34. Constant velocity defluidization procedure for a beneficiated ilmenite ore. Nitrogen atmosphere. (See Table 2.9 for particle properties).

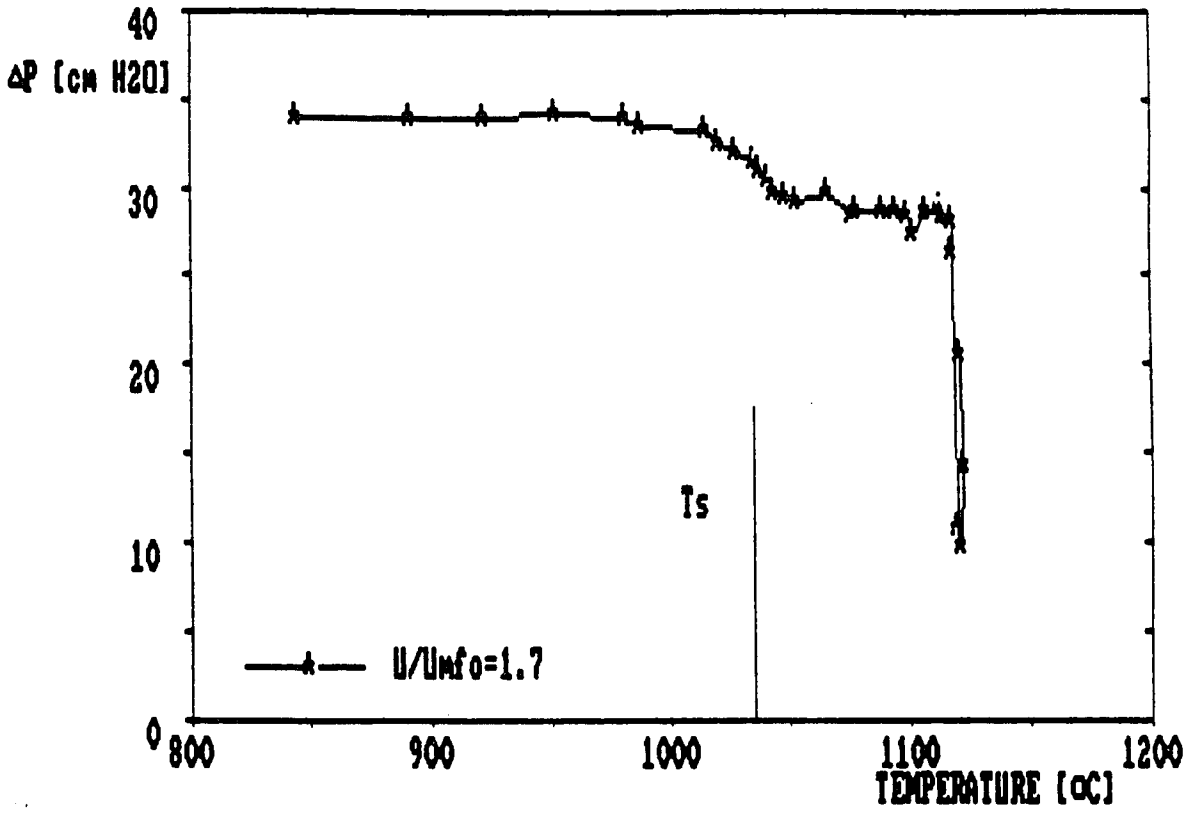

Figure 2.34. Constant velocity defluidization procedure for a beneficiated ilmenite ore. Nitrogen atmosphere. (See Table 2.9 for particle properties).

2.3.6 Summary

The high temperature fluidization and dilatometric behavior of FCC catalyst, granular polyethylene, coal ash powders, ferrous chloride powder, and a benificiated ilmenite ore have been investigated. These materials were chosen because of their industrial importance. In general, the methods and interpretations presented in Section 2.2 for the model materials hold here as well. In particlar, shrinkage in the dilatometer usually corresponds to interparticle bonding and cohesive behavior of the particles in the fluidized bed. In the case of FCC catalyst however, chemical changes on the surface also resulted in some particle cohesion.

A study of a set of nine granular polyethylenes demonstrated that the minimum sintering temperature does not correlate with the crystalline melting point of the material. These polyethylene samples demonstrated two different temperature sintering regimes. The sintering characteristics of five different coal ashes showed the importance of composition as it effects the minimum sintering temperature. The results of coal ash sintering are used to compare the dilatometric method to other methods of sintering detection. The dilatometric and high temperature fluidization behavior of a beneficiated ilmenite ore show that the methods used also apply to materials comprised of more than one chemical species.

3. DISCUSSION

3.1 Fluidized Bed Agglomeration

The discussion which follows is restricted to systems where (1) cohesive particles exist in a dynamic environment, (2) the level of interparticle attraction is such that collisions have a finite probability of agglomeration success (3) the primary particles do not degrade, that is, the only mechanism by which particle sizes can change is by the formation and breakage of agglomerates of primary particles, (4) motion in the system is due only to the movement of a fluid and the transfer of momentum from the fluid to the solids, and (5) the system is closed with respect to the solids. All of these conditions are met in the fluidization experiments presented in Chapter Two.

3.1.1 Mechanism of agglomeration

The forces acting on particles in fluidized beds may be classified either as attractive (giving rise to particle cohesion) or breaking forces. Attractive forces are the Van der Waals, electrostatic, capillary, material bridges etc; breaking forces are the result of the dynamic interactions between the gas, particles and vessel walls. In particular, breaking forces occur if a dynamic process results in a force having a component which acts opposite to the attractive forces,

or if a dynamic process results in the stressing of a particle-particle bond.

Particles constantly collide in a fluidized bed. If sufficient attractive forces are present agglomeration will occur. The simplest agglomerate is a dimer. If however, the primaries are not perfect spheres, there will be a number of ways in which two particles can combine to form a dimer. For example, two cubes (like sodium chloride) can combine in different configurations as shown in Figure 3.1. This figure also shows that quasi-spherical particles can form dimers of different configurations. Only with perfect spheres is there only one distinguishable dimer configuration.

A dimer which has formed may collide with a primary particle to form a trimer. Figure 3.2 shows that there are more possible trimer configurations than dimer configurations. A trimer of perfect spheres may also have different configurations. A trimer may collide with a primary to form a tetramer, and again there are many more possible tetramers than trimers, and so on. A tetramer however may also form from the collision of two dimers. For that matter, a trimer or tetramer might even result from the simultaneous collision of three or four primaries.

This reasoning can be extended to larger agglomerates. A primary particle may collide with a large agglomerate in different ways: it could attach to only one particle of the agglomerate or it could attach to many particles at a time. Also, a primary particle could attach to a large agglomerate in such a way that its final position is either closer or further away from the center of mass of the agglomerate. These alternatives are shown in Figure 3.3. In general, it is assumed that

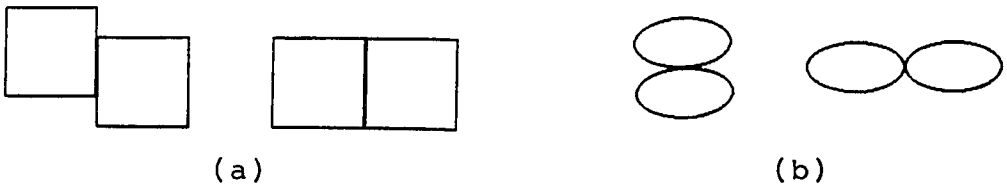

Figure 3.1. Different dimer configurations for (a) cubes (b) quasispherical particles.

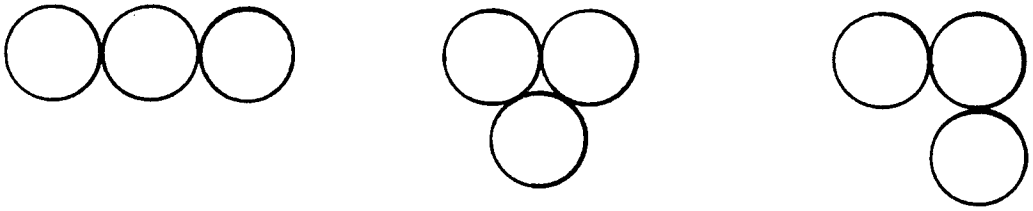

Figure 3.2. Different trimer configurations for perfect spheres.

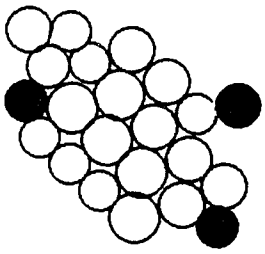

Figure 3.3. Various ways in which a primary particle can attach to an agglomerate.

(1) as the number of primaries comprising an agglomerate increases, the number of possible configurations increases; (2) particle collisions are random and result in the formation of a wide variety of configurations; and (3) the probability of formation of a given configuration increases with the concentrations of the precursor colliding species.

In the high temperature experiments reported in Chapter Two, agglomerates were found to exist only in a limited number of cases. When agglomerates did exist, only a certain type was found: the close packed, quasi-spherical structure (see Figure 2.10). The question then arises: why didn't open, non-spherical structures form? For a given number of particles in an agglomerate there are so many more open, non-spherical configurations than close packed spherical ones that it must be assumed that open structures occur more often. Therefore, the prevalence of close-packed, spherical agglomerates can not be explained by a higher probability of formation.

The prevelence of close-packed structures cannot be explained by a two body collision model either. In two body models there is no discrimination between agglomerate configurations, only agglomerate size. Consider the following illustrations:

(i) a primary collides with two equal weight agglomerates. One agglomerate is open and the other is in a close packed configuration. In both cases the two body model predicts the same probability of bonding success, which would lead to equal probability of continued propagation of the close and open structures.

(ii) two identical primaries collide with two identical agglomerates. The first primary attaches further from the center of mass

of the agglomerate than the second as shown in Figure 3.3. By the two body model, these two collisions have an identical probability of success. Since there is no other factor in a two-body model to distinguish between these two cases, the model would again predict equal numbers of the two configurations.

The influence of hydrodynamic forces on the bonding mechanism is inconsequential to the argument: by the two body-viscous dissipation model, increased force of collision enhances the success of a single collision. The problem is that it enhances the success of all single collisions, those that result in close-packed as well as open-packed structures. Agglomerate configuration is unaccounted for in the two body models. Again there is nothing to explain the prevelence of close-packed structures.

An alternative explanation as to why close-packed structures are favored is that these configurations survive longer than other configurations. They survive longer because they are more resistant to the breaking forces due to collisions. The stronger configurations are found in greater numbers in spite of the fact that the open-packed, weak configurations have a greater probability of forming due to random collisions. In light of this argument consider the illustrations used to argue against the two body models above:

(i) a primary particle collides with two equal weight agglomerates, one open and the other close packed. According to the proposed mechanism, the second case occurs more often but the resulting open-packed, weak agglomerate would then be destroyed by the breaking

forces, leaving the stronger agglomerate of the first case intact. The result is further propagation of the close packed configuration.

(ii) two identical primaries collide with two identical agglomerates. The first primary attaches further from the center of mass of the agglomerate than the second as shown in Figure 3.3. By the new formulation, the primary that attaches further from the center of mass would be more vulnerable to shear and be broken off before the other particle attached closer to the center of mass. Therefore, if the two configurations have even the same probability of occurring initially, the stronger of the two would survive longer and be found in greater numbers.

This mechanism also applies if several particles collide simultaneously resulting in an agglomerate. (By the two body model, there is no way for this process to occur, not even the simultaneous collision of only three primaries). Random many-body collisions should result in the formation of a random distribution of loose and open structures. In order for the close-packed to dominate, the open ones must be destroyed. Of course all of this assumes that particle rearrangement within the agglomerate does not occur.

A final point about the two-body model of agglomeration is that the survival concept does not necessarily deny the probabilistic nature of two-body collision success. The only claim is that a two body interaction is insufficient to account for the experimental evidence. Greater collision force may enhance the success of single collisions but it will enhance all collisions, those that result in weak and strong configurations.

3.1.2 Interpretation of fluidization results

Seigell (1976) postulated that the rate of agglomeration in a high temperature fluidized bed is proportional to the attractive forces and inversely proportional to particle momentum (Equation 1.5). He was lead to this conclusion because as the temperature was increased, higher gas velocities were needed to keep the bed from defluidizing. Certainly this experimental observation was confirmed in the present work. It is argued here however that the rate of agglomeration is an incomplete description of the state of agglomeration in a fluidized bed.

In the constant velocity experiments for sodium chloride, calcium chloride, and glass beads, the entire range of attractive force to breaking force ratios was covered. This was accomplished by varying the temperature from ambient (well below the minimum sintering temperature) to a temperature where fluidization was not possible at any gas velocity because of cohesion. If the state of agglomeration is determined by the ratio of attractive to breaking forces then the whole range of agglomerate types should have formed. High rates of agglomeration were clearly evident because the beds were defluidized, but close-packed, strong agglomerates were hardly observed at all.

It is possible to estimate the size of close packed agglomerates which would result in the apparent minimum fluidization velocities observed in the Sodium Chloride experiments. Figure 2.9a shows that at 600^{o}C, the gas velocity needed to keep the bed fluidized is about five times that needed at 20^{o}C. As a rough estimate, the ratio of minimum fluidization velocities can be calculated from the Ergun correlation

(see Appendix A). If the voidage and shape factor are assumed constant, then

$$U_{mf(600)}/U_{mf(20)} = (d_{agg}/d_p)^2 \qquad 3.1$$

Where d_{agg} is the diameter of the agglomerate at 600°C. Also, if the agglomerates are close-packed then Yamazaki (1987) shows that

$$d_{agg}/d_p \sim n^{1/3} \qquad 3.2$$

where n is the number of particles comprising the agglomerate. Therefore

$$n = (d_{agg}/d_p)^3 = [U_{mf(600)}/U_{mf(20)}]^{3/2} = 11.2 \qquad 3.3$$

Under these conditions then, the close packed agglomerate would be comprised of about 11 primary particles, this was clearly not the case.

It must be concluded that the breaking forces needed for the production of a large number of strong, close packed agglomerates were unattainable, and that the state of agglomeration was that of a network of very large, weak configurations. This implies that it is not simply the ratio of attractive to breaking forces which determines the state of agglomeration, but that some absolute level, or a particular type of breaking force is needed to produce a certain type of agglomerate, regardless of the strength of attractive forces. Stated alternatively, if a system has strong attractive forces and weak breaking forces, agglomeration rates will be high but the agglomerate configuration will

be weak. If both the attractive forces and the breaking forces are strong, agglomeration rates will be lower but the resulting agglomerate will be strong. If the magnitude of breaking forces overwhelms the attractive forces the results is no agglomeration or non-cohesive fluidization. It is concluded therefore that the level of breaking forces needed to produce strong agglomerate configurations at significant rates was unobtainable in the experimental systems used in this work.

This interpretation is supported by the three reports of fine type C powder agglomeration by Chioki et al.(1985), Kono et al.(1987), and Morooka et al.(1987) (see Section 1.1). At low gas velocities, the beds of fine cohesive powders were unfluidizable and channeled badly. But if the gas velocity was raised high enough, much higher than the minimum fluidization velocity of the primary particles, agglomerates formed which were fluidizable. These agglomerates were roughly spherical and strong enough to survive the dynamic forces of a well fluidized bed. The ratio of particle diameter to bed diameter was much smaller than the ratios used in the present work. Also the interparticle forces were due to Van der Waals interactions rather than the relatively strong sintering forces in the present work.

The experimental results of Huang, Arastoopour and Weil (see Section 1.4.2) might also be interpreted according to this mechanism. Initially their experimental configuration consisted only of a bubbling bed with a porous distributor. They found this arrangement unacceptable because of the formation of large agglomerates which would invariably foul the distributor. Once they changed this configuration to a hot jet

and cooler dense phase arrangement they were able to sample strong agglomerates. But the jet temperature was the same as the original bubbling bed. The jet supplied the breaking forces needed to break the large, weak agglomerates which formed in the bubbling bed.

3.1.3 Minimum fluidization and defluidization

The property of a given gas-solid system known as the minimum fluidization velocity looses its traditional meaning when the particles are cohesive. This is because the state of agglomeration of the system is dependent on the breaking forces as stated above.

Consider a bed of well fluidized particles. As long as all the particles are fluidized and regardless of the state of agglomeration or the size of the particles, the pressure drop across the bed will be relatively constant at increasing gas velocities; this is a well known fact. For non-cohesive particles, if the velocity is decreased slowly, a point will be reached where the pressure drop begins to decrease. This is the true minimum fluidization velocity of the system, U_{mf}(the lowest velocity at which all particles are kept in the fluidized state). In monodispersed systems, minimum fluidization occurs when the drag and buoyancy forces exactly balance the weight of the particles. The situation is somewhat confused when a variety of particle sizes are present. Then, the point of balance of between drag, buoyancy and gravity may not be clearly defined. But either way, the minimum fluidization velocity of all non-cohesive particle systems is dependent on those gas and particle properties which influence the drag and gravity forces. In principle then, in non-cohesive systems, U_{mf} can be

computed from single particle properties (or an average of single particle properties) and the gas properties which influence drag.

When particles are cohesive the situation is different. The results of the constant velocity experiments in Chapter Two (i.e. Figure 2.9a-c) and the results of Siegell (1976) and Tardos et al. (1985) etc. suggest that there is is a minimum velocity for fluidization of cohesive particles. But instead of being a static situation, as in the non-cohesive case, this is a dynamic equilibrium. This state of fluidization does not represent a balance of drag and gravity forces. In fact, it doesn't really represent a balance of drag, gravity and cohesion forces either, not in the traditional sense. The cohesive forces do not act against the drag forces directly but influence the state of agglomeration which in turn influences the drag and gravity forces.

It is possible then to envision two different defluidization mechanisms though it is argued below that only one can occur. The first is where the breaking forces are weak and large, weak agglomerates will dominate because they are not destroyed. The result is a kind of network of agglomerated particles which promotes the formation of channels. This is type C fluidization. In the constant velocity experiments this kind of defluidization was obtained by increasing the cohesion forces until fluidization became impossible. Clearly this is not defluidization because the agglomerates were too heavy to be supported by the drag forces: the agglomerates are interconnected and are not single entities.

In the second case, breaking forces are strong and strong, smaller agglomerates dominate because the weak ones are destroyed. These agglomerates act more like single entities and may be fluidizable.

Yamazaki et al. (1986) propose that in this case defluization occurs because the drag force can no longer balance the agglomerate weight and so the bed defluidizes in the traditional way. In other words the minimum fluidization of the solids has increased due to increased particle size. If this were true one would think that in the experiments where the relative gas velocity was high, defluidization should have occurred without the formation of channels. The results of Chapter Two however show that channels do develop when high relative velocity beds defluidize. The explanation is that as the solids agglomerate the breaking forces are attenuated because of the larger effective weight of single entities ($U-U_{mf}$ decreases). As the breaking forces get smaller the resulting agglomerate configuration reverts back to the large, weak types. The result is again type C defluidization.

In conclusion, defluidization in the particle systems studies in this work did not result from agglomerate weight exceeding the drag forces. Defluidization occurred when the agglomerate structures became large, weak and interconnected as a network.

3.2 High Temperature Interparticle Bonding

3.2.1 Mechanism of bonding

As discussed in Section 1.2, the theories of sintering mechanisms are based on the concept of stages of which the first is initial bond formation. In these models the particles are assumed to be in contact before heating. In a high temperature fluidized bed the particles come into contact at sintering temperatures and so initial bonding must depend on what happens in the short duration of collision. Based on the results of the experiments described in Chapter Two and on other studies of high temperature surfaces, it seems probable that above the minimum sintering temperature, particle surfaces are liquid-like to some extent. Moreover, the surfaces need not be in contact with other particles for this to happen, that is, the capillary pressure due to the curved interface of the bond neck is not a requirement for liquid-like behavior.

This assumption follows in part from the fluidized bed results at lower temperatures (but still above the minimum sintering temperature). For example, Figure 2.9 shows that the calcium chloride particles become cohesive at about 450^{o}C because of deviation from the Ergun correlation. But sampling did not reveal agglomerates and so significant solid bond necks really can not have formed. Also, if bond neck growth is an exponential process (see Appendix C) isothermal dilatometry results of FCC catalyst (Figure 2.21a) and calcium chloride (Figure 2.14) show that the time constants for sintering are on the order of at least ten minutes at higher temperatures and much longer at low temperatures.

These particles must have the potential to bond instantaneously because they are probably only together for a very short amount of time. A liquid interface can form a bond much faster than a solid interface because solid bond growth depends on solid state diffusion.

All of the bonding mechanisms postulated in the two-body models reviewed in section 1.4.3 assumed that agglomeration occurs between two particles only if the energy of impact can be dissipated by some process on the surface. Again it seems that only a surface which is liquid-like before contact could dissipate energy so quickly.

Adamson (1982) reviewed reports which suggest solid surfaces are mobile even in the absence of contact with other surfaces. For example, scratches on a silver plate will fill up when heated to temperatures below the melting point and irregular cavities in rock salt and metals will assume regular shapes when heated. Kuczynski (1973) states that in powder metallurgical sintering processes the grain boundaries are probably in a liquid state.

Simulation of the melting of aluminum surfaces by molecular dynamics (Stoltze et al., 1988) predicts upper surface layers to melt at about $200^{o}C$ below the bulk melting point. Figure 3.4 shows the absolute square of the structure factor, S, for the upper ten surface layers of aluminum as a function of temperature. The structure factor is a measure of crystal disorder. Here it is seen that as the the bulk melting point is approached, the thickness of the disordered layer increases. Again this surface melting process does not require the presence of a curved interface and was actually derived for a non-curved surface.

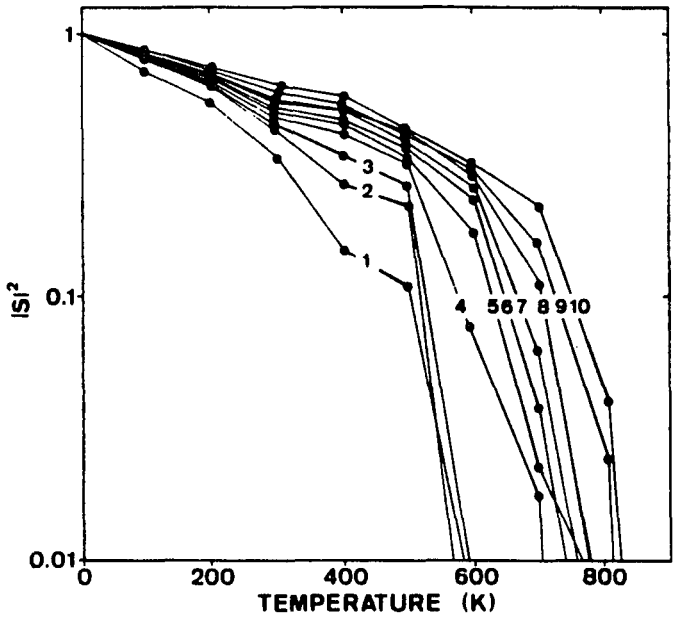

The absolute square of the structure factor of Eq. (1) for layers 1 to 10 as a function of temperature for an Al(110) surface. The sudden decrease between 500 and 800 K is an indication of a loss of order which we associate with a melting transition.

Figure 3.4. Molecular dynamics simulation of the melting of the surface of aluminum. (From Stoltze et al., 1988).

Liquid behavior on the particle surfaces would allow for the instantaneous bonding needed in the fluidized bed. Once bonded, the strength of the bond could grow by further migration of material to the bond neck. It seems unlikely that appreciable bondneck growth occurred in the experiments described here because few strong agglomerates were produced. A system where higher breaking forces are present would be needed to study this phenomena. The "type C" network defluidization mechanism described above can occur with weak initial liquid binding only.

3.2.2 Properties of the minimum sintering temperature

Traditionally, powder metallurgists claim that sintering is possible starting at about two-thirds of the melting point of a given material. This rule of thumb implies that the minimum sintering temperature should correlate with the melting point, that is, the minimum sintering temperature should be a constant fraction of the melting point - this does not appear to be the case. The experimental findings in Chapter Two show sintering to occur at a wide range of relative temperatures. Sodium Chloride showed cohesion in the fluidized bed at about 370°C, 432°C less than the bulk melting point (802°C) and calcium chloride showed cohesion at about 470°C, 370°C less than the bulk melting point (770°). Polyethylene sample C (Section 2.3.2) showed a minimum sintering temperature of 127°C compared to a melting point of 133°C.

When the minimum sintering temperature is plotted against the crystalline melting point for the polyethylene in Figure 2.24, it is

clear that the melting point does not determine the minimum sintering temperature at all. It is probably more meaningful to compare relative minimum sintering temperatures, the minimum sintering temperature divided by the absolute melting temperature, T_s/T_m ($^oK/^oK$) as shown in Table 3.1. This Table, which includes data from Siegell (1976), Andriesky (1984), and Mazzone (1986), demonstrates that minimum sintering temperatures as low as 40 and as high as 98% of the absolute bulk melting point have been measured. A value of 40% for the relative sintering temperature is also much lower than the molecular simulation of the aluminum melting predicted. (T_m-200/T_m [$^oK/^oK$] for aluminum is equal to 0.79, T_m=660^{o}C).

These lower relative sintering temperatures suggest that real particles, as opposed to the ideal aluminum suface modeled above, have greater driving forces to reduce surface energy perhaps due to surface imperfections and high curvature asperities. If these imperfections are the cause of low sintering temperatures it would be assumed that on heating the surfaces would anneal and the potential for sintering would be attenuated. This was demonstrated by use of a refluidization procedure. In this technique a well fluidized, high temperature bed is defluidized by quickly reducing the gas velocity to zero. After allowing the fixed bed to sit for a specified length of time the gas velocity is increased incrementally and the pressure drop over the bed is recorded. If there is interparticle cohesion the pressure can exceed the weight of the bed when the gas velocity is raised high enough, usually this is referred to as the "unlocking" of the bed. Obviously, this procedure is dependent on wall effect.

Table 3.1. Relative minimum sintering temperatures for a variety of materials.

Material	T_m (°C)	T_s (°C)	T_s/T_m (°K/°K)
Sodium Chloride (NaCl)	802	370	0.60
Sodium Bromide (NaBr)	755	480	0.73
Calcium Chloride ($CaCl_2$)	772	470	0.71
Calcium Fluoride (CaF_2)	1330	368[1]	0.39
Ferric Chloride ($FeCl_2$)	677	535	0.85
Magnesium Oxide (MgO)	2800	1109[1]	0.45
Polyethylene granules (Sec. 2.3.2)	125	55-98	0.82-0.98
Polyproplyene beads	162	141[2]	0.95
Polyethylene beads	135	118[2]	0.96
Polyethylene spheres	135	127[2]	0.98
Aluminum Nitride (AlN)	2150	1108[1]	0.57
Zeolite Cracking Catalyst (Sec. 2.3.1)	1260	900	0.77
Copper Shot (D_p=1.015mm)	1083	899[1]	0.86
Copper Shot (D_p=0.718mm)	1083	844[I]	0.83
Copper Shot (D_p=0.569mm)	1083	750[I]	0.75
Nickel powder	1452	4341[1]	0.41
Molybdenum powder	2620	814[1]	0.40
Boron powder	2330	1759[1]	0.78
Silicon powder	1420	1335[1]	0.95

[1] Andrievsky (1984)

[2] Mazzone (1986)

[I] Siegell (1976)

Rumpf (1977) derived the following relationship to describe the tensile strength, σ_t of a fixed bed of ideally packed spheres

$$\sigma_t = (1-\varepsilon)\cdot k\cdot F_{ad}/\pi\cdot d_p^2 \qquad (3.4)$$

where k is the coordination number and F_{ad} is the strength of each bond. Here it assumed that the maximum overpressure, ΔP_{max} is proportional to the tensile strength of the bed

$$\Delta P_{max} \sim \sigma_t = (1-\varepsilon)\cdot k\cdot F_{ad}/\pi\cdot d_p^2 \qquad (3.5)$$

The use of Equation 3.5 is limited by the non-spherical nature and the non-ideal packing of the real particles studied here (also Hobbel, 1988 warns that fixed beds do not break-up uniformly but rather by fracture). It might be possible however to compare the relative maximum pressures developed under two different conditions and attribute the difference to the difference in bond strength if the voidage and particle sizes are kept constant. Therefore

$$\Delta P_{max,1}/\Delta P_{max,2} \sim \sigma_{t,1}/\sigma_{t,2} \sim F_{ad,1}/F_{ad,2} \qquad (3.6)$$

Figure 3.5 shows the result of this procedure for sodium chloride at 450°C. Each run was consecutive in that the tests were performed one after another without changing the material or cooling back down. First the salt was set down for five minutes, on refluidization the pressure

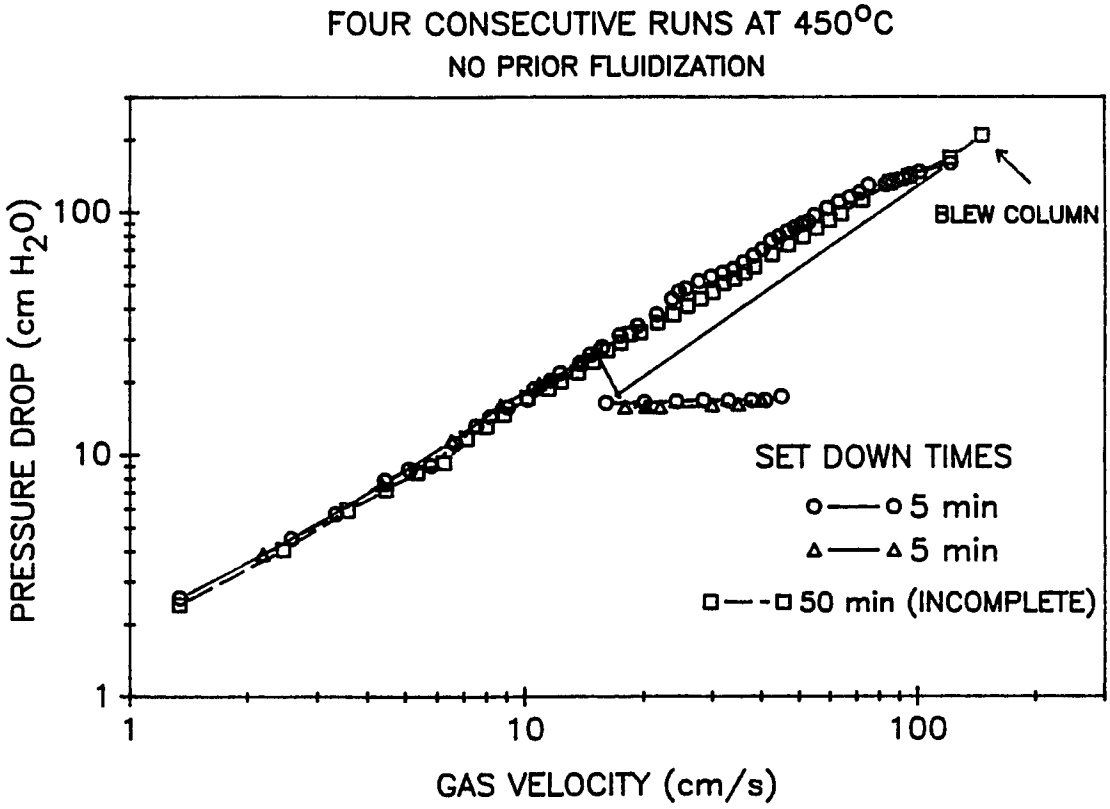

Figure 3.5. Refluidization procedure for sodium chloride (dp=40-50mesh, Temperature=450°C).

reached 170 cm H_2O before breaking up, about ten times the theoretical pressure drop. Once the bed broke, fluidization was remarkably regular and the theoretical pressure drop was reestablished. The bed was then set down again for five minutes but on refluidization an overpressure of only 2cm H_2O was obtained. At a set down time of 50min the bed was not refluidizable. The similar slopes of the pressure drop versus velocity imply that the voidage was constant in all runs; therefore the sintering potential was reduced by annealing.

The effect of annealing was seen in the FCC catalysts as well. When equilibrium catalyst was ground, new surfaces were created. The ground material showed deformations in the dilatometer which appeared in the fresh catalyst curves but not in the unground equilibrium curves.

Another property of the minimum sintering temperature seen from Table 3.1 is that ionically bonded materials exhibit lower relative sintering temperatures than covalently bonded materials. Andrievsky (1984) came to the same conclusion by comparing the relative sintering temperatures of the purely covalent solids boron and silicon to the more ionic magnesium oxide, calcium fluoride and aluminum nitride; the low relative sintering temperatures for the ionic salts in Chapter 2.2 supports this conclusion. The polymers listed in Table 3.1 also have very high relative sintering temperatures ranging from 0.82 to 0.98. Polymers are certainly more covalent in character than the ionic salts. Metals do not seem to follow any particular trend.

It is very difficult to quantify a chemical bond's ionic character. As a crude model, the degree of ionicity is assumed to be proportional to the difference in standard electronegativities of the

elements. The electronegativities used, as can be found in any elementary chemistry text, are listed in Table 3.2. The relative minimum sintering temperatures are plotted against electronegativity difference in Figure 3.6. Even with the wide variety of particle shapes, and the wide variety of conditions under which the measurements were made, a strong correlation between relative minimum sintering temperature and electronegativity difference exists.

The effect of other variables on the minimum sintering temperature have been studied. A weak dependence of the minimum sintering temperature on particle size for glass beads is seen in Figure 3.7a. A four-fold increase in diameter results in only a $10^{o}C$ increase in the minimum sintering temperature. There appears to be a stronger dependence on the compressive load on the particles for the glass (Figure 3.7b) as well as the sodium chloride particles shown in Figure 2.16a. The results of the granular polyethylene studies in Section 2.3.2 show no correlation of minimum sintering temperature with Vicat softening point.

3.2.3 Dilatometry as a Tool for Predicting Cohesion

In general, strong shrinkage in CHR dilatometry curves are indicative of surface softening and the temperature of incipient shrinkage correlates well with the temperatures of incipient cohesion in the fluidized beds. This is based on the comparison of CHR results with constant velocity fluidization results in Chapter Two (ie. Figure 2.9, etc). Exceptions to this rule have been noted, particularly the salts which exhibit increase rates of dilatation after reaching sintering temperatures (sodium chloride, sodium citrate) and materials which

Table 3.2. Electronegativity differences between elements for compounds used in sintering studies.

Material	Electronegativity Difference
CaF_2	3.0
MgO	2.3
NaCl	2.1
$CaCl_2$	2.0
NaBr	1.9
AlN	1.5
$FeCl_2$	1.2
B	0
Si	0

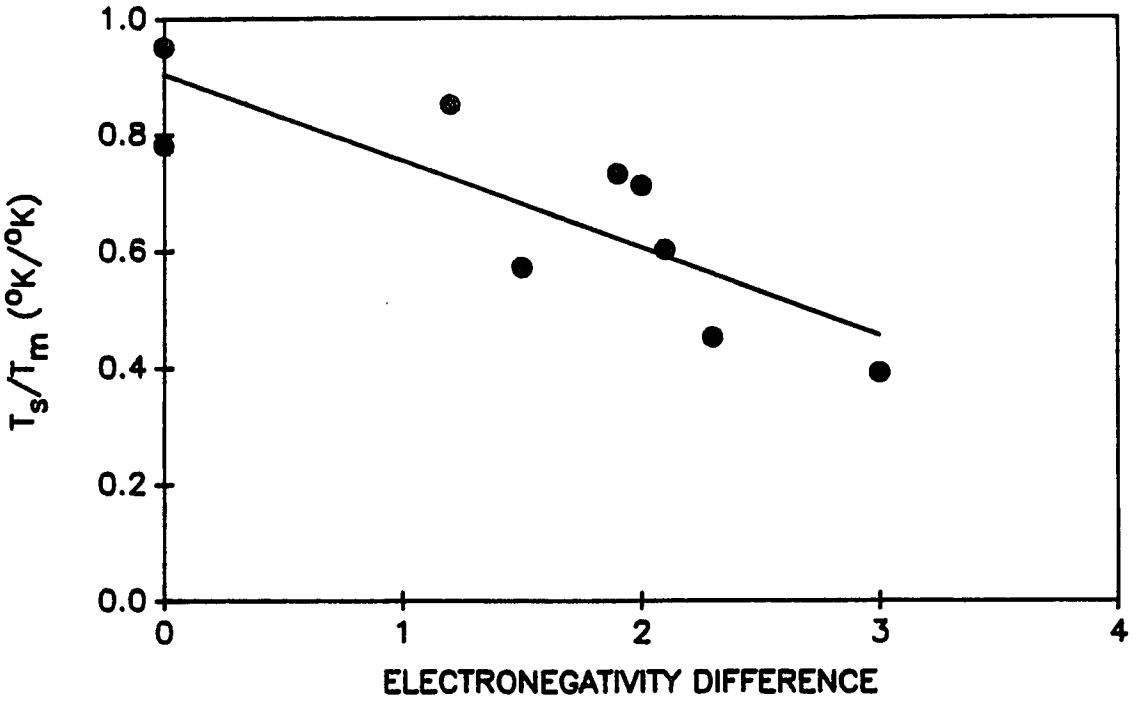

Figure 3.6. Correlation of the relative minimum sintering temperature with the electronegativity difference between elements.

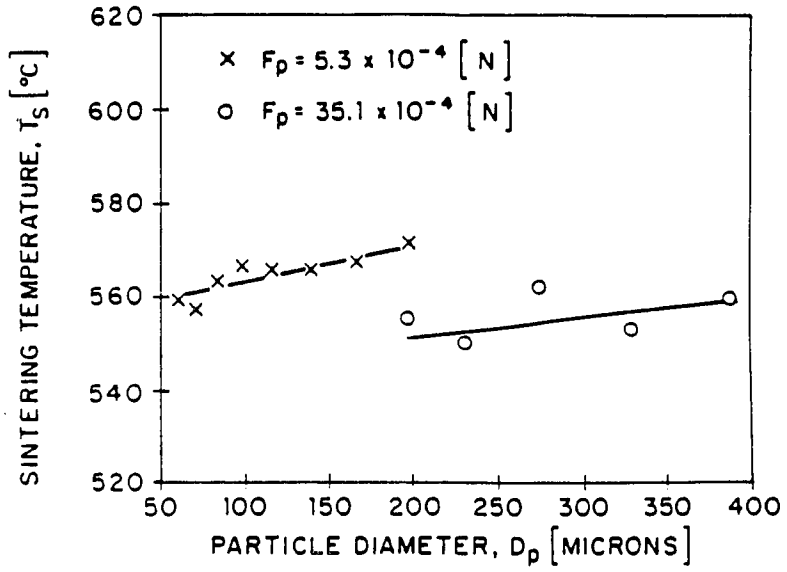

(a) Sintering temperature T_s vs. particle diameter D_p for glass particles at constant intergranular force F_p.

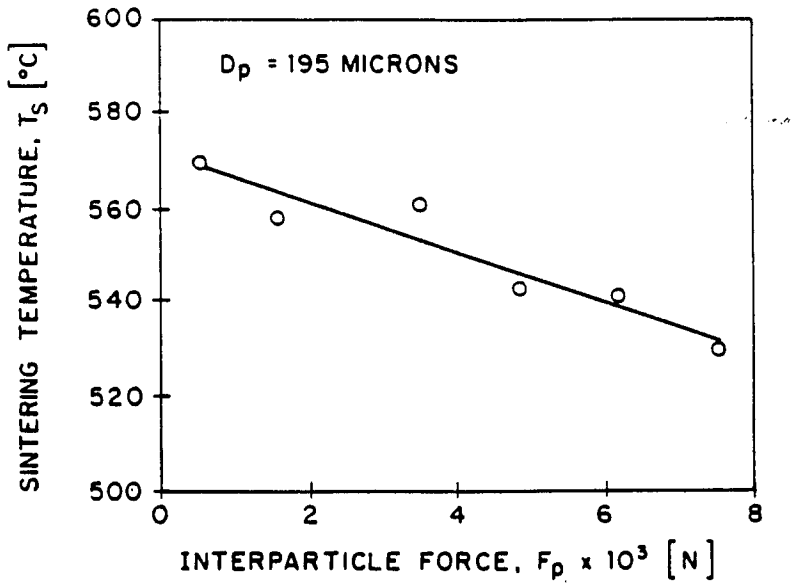

(b) Sintering temperature vs. interparticle force for glass beads.

Figure 3.7. Effect of (a) particle diameter and (b) interparticle force on the minimum sintering temperature for glass beads.

demonstrate shrinkage in the dilatometer not accompanied by surface cohesion. Also, it has been shown that the degree of shrinkage is not necessarily representative of the degree of sintering. An example of this was calcium chloride where the compaction of the voids created by the removal of lattice water caused shrinkage which is unexplainable in terms of bond neck growth.

The importance of these interpretational difficulties depends on what kind of information is desired. Obviously, some experimental technique is needed to determine the sintering characteristics of fluidizable particles. Except for the crude relationship between electronic structure and minimum sintering temperature presented above, there are no correlations of minimum sintering temperatures with particle composition, not to mention particle morphology. Even if there were correlations for pure materials, many particles of interest have non-homogenous structure; some may have unknown compositions as well.

Fluidized bed tests alone are cumbersome because only one piece of information is obtained in each run. If the relative gas velocity is kept constant as it was in the procedure described in Chapter two, only the cohesion which is strong enough to cause segregation or defluidization at that velocity will be identified. It could take numerous runs to pinpoint the temperature of incipient cohesion. The experiments with granular polyethylene showed that agglomeration problems in one fluidized bed (the industrial bed in this case) might not manifest themselves in another.

Most of the data in powder metallurgy has been obtained from isothermal measurements, but again, numerous isothermal experiments are

needed to identify the minimum sintering temperature. Because the most important high temperature agglomeration problem in industry is avoidance, the minimum sintering temperature is very important. CHR dilatometry allows for a complete scan of the temperature range of interest in one experiment.

There are alternatives to dilatometry. In particular the electrical conductance method developed by Raask (see Section 2.3.3). Further study is needed to confirm his conclusion that electrical sinter points of lignite coal ashes are truer indications of incipient bonding. The fact that powder metallurgical sintering theory predicts the first stage of sintering to occur without change in the center to center distance between particles would not seem to hold for fluidized particles in light of the arguments in Section 3.2.1, namely that in a high temperature fluidized bed, the particle surfaces are liquid-like. If the surfaces of particles are liquid-like or if initial sintering is more dependent on surface imperfections and asperities etc, the initial stage would more likely result in a decrease in the distance between particles. The good agreement between CHR dilatometry and fluidization data supports this.

In terms of finding a general method, a severe drawback of measuring electrical conductance is that its applicability is limited to those materials which conduct electricity. This rules out its use for many important materials including ceramics, oxide based catalysts, polymers, etc. In addition, Raask's device must be built; dilatometers are commercially available.

Hot stage microscopy has been utilized for the study of coal ash sintering (Katta, 1984) and coal (Klose and Lent, 1985) but the results have not been compared to fluidization data. Impact separation methods such as those suggested by Jimbo et al. (1985) might be useful, but again there is no data as yet at high temperatures.

In conclusion, CHR dilatometry may not be a foolproof technique, but interpreted correctly and in conjunction with selected fluidization experiments it can give valuable information. It can be used for initial evaluation of the fluidizability of particles or for the systematic study of a set of materials.

CONCLUSIONS AND SUGGESTIONS FOR FUTURE WORK

4.1 Conclusions

1. The process of high temperature fluidized bed agglomeration has is proposed to occur as follows: for a given level of particle-particle bond strength, random collisions in the fluidized bed result in the formation of many different agglomerate configurations, some strong and some weak. The number of weak, open configurations is far greater than the number of close packed, strong configurations. When breaking forces (ie, forces opposing particle-particle bonding) are strong, the weak agglomerates are destroyed leaving the strong, closed packed configurations. When breaking forces are weak, the weak configurations are not destroyed and since there are many more weak configurations for a given number of particles comprising an agglomerate, these weak configurations dominate. Simply stated: high temperature fluidized bed agglomeration is controlled by what survives, not by what forms.

This mechanism deviates conceptually from two-body models in that agglomerate configuration must be taken into account to fully explain the available experimental evidence. Two body models do not allow for differences in agglomerate configuration, in fact, two body models do not allow for agglomerate breakage at all. Note however that the proposed mechanism does not necessarily conflict with the basic assumption of the two-body models; that a collision between two particles will be successful if the energy of impact can be dissipated by some flow process on the surface. In fact, a conclusion of this study

is that particle surfaces are indeed liquid-like at high temperatures and that it is likely that some interfacial flow would result from particle collisions.

Experimental evidence obtained in this work suggests that it is not simply the ratio of attractive forces to breaking forces which determines the state of agglomeration in a fluidized bed and that some absolute level of breaking forces (not obtainable in the systems used in this study) are needed to obtain true close packed agglomerates.

2. The mechanism of defluidization and the meaning of the minimum fluidization velocity under cohesive conditions have been discussed in light of the proposed agglomeration mechanism. The frequent assumption, that the effect of cohesion forces is to counter the gravity force at minimum fluidization is thought to be incorrect. Cohesive forces result in agglomerate formation of some type which in turn alters the balance of forces around the solids. Minimum fluidization does not exist in the traditional sense, data suggests however that there may be a minimum gas velocity where agglomeration is balanced by breaking forces, that is a dynamic equilibrium.

Fluidization experiments showed that defluidization does not necessarily occur suddenly with the formation of channels as described by Siegell (1976). Gradual defluidization preceded by partial particle segregation, and defluidization without the formation of channels were also observed.

3. With proper interpretation, dilatometry is shown to be an effective method of predicting minimum sintering temperatures, confirming the earlier work of Siegell (1976). This conclusion is based on the comparison of constant heating rate dilatometery with high temperature fluidization data for a wide range of particle compositions and morphologies. These include inorganic salt crystals, polyethylene granules, FCC catalysts (fresh, equilibrium, and spent), a ferrous chloride powder, a beneficiated ilmenite ore, and five coal ash powders. Some difficulties in the interpretation of inorganic salt dilatometry results have been identified. The results of coal ash sintering tests confirm earlier work showing the importance of cation concentrations, in particular sodium and calcium. However, certain discrepancies between shrinkage methods (such as dilatometry) and electrical conductance methods, such as the method developed by Raask (1982) remain somewhat unresolved.

4. Properties of the minimum sintering temperature have been identified. The relative minimum sintering temperature (T_s/T_m) is shown to decrease with the degree of ionic bonding of the material. The degree of ionicity was assumed to be proportional to the electronegativity difference between elements making up the particle. Relative minimum sintering temperatures are shown to range from about 0.4 for highly ionic salts to as high as 0.95-0.98 for purely covalent solids. Certainly, the "two-thirds of the melting point for sintering" rule from powder metallurgy does not apply to these systems. In addition, the

minimum sintering temperature was shown to be a weak function of particle size.

5. It is argued in Section 3.2.1 that the surfaces of particles at high temperature are liquid-like. This accounts for the development of cohesion on very short time scales. A refluidization procedure was developed to show that interparticle cohesion is attenuated in time by annealing of the particle surfaces at high temperature.

4.2 Suggestions for Future Work

This work leads to a number of possible areas of study which can be divided into the following

* the mechanism of fluidized bed agglomeration
* the mechanism of high temperature bonding
* properties of the minimum sintering temperature
* relationship between sintering forces and other interparticle cohesive forces
* methods for prediction of high temperature cohesion

All five of these have been investigated to some extent, however there are many unanswered questions.

As discussed in Chapter one, interparticle forces due to Van der Waal's interactions and triboelectrification have been characterized to some extent. The relative strengths of these forces versus sintering forces should be investigated. Perhaps more importantly for large particles, the cohesion (if any) due to chemical changes including phase

transitions and chemical reactions should be investigated. Appendix D contains a short study of cohesion development due to the reduction of phosphogypsum to calcium sulfide. Other examples of chemically induced cohesion from industrial cases should be studied.

The relationship between the electronic structure on the minimum sintering temperature could be more accurately measured if particles of similar morphology and structure were used. One possible method would be to obtain smooth, spherical salt particles of a systematic series, for example

CaF_2	NaF
$CaCl_2$	NaCl
$CaBr_2$	NaBr
CaI_2	NaI

The effect of particle morphology on minimum sintering temperature should be measured by different particle types of the same material. Sodium chloride for example is available in many forms and is not a hydrated crystal. As shown in Section 2.2.3, measurements of sintering temperatures on hydrated crystals can be more confusing than when non-hydrated crystals are used.

The mechanism of fluidized bed agglomeration was described only in the most qualitative way in this work. The chief omission from the

discussion of agglomeration is time. Agglomeration is obviously a kinetic process and the time factor must be included in any model. In addition, agglomeration is a very general subject and data from other disciplines are available; these include, among others, fluidized bed granulation (see Ennis et al., 1989) and particle floculation (see for example the various papers by Hogg et al. at the Pennsylvania State University). Perhaps more interesting than the development of detailed models of agglomeration (many of which exist today with out taking breaking forces and agglomerate breakage into account) is to correlate the values of breaking and attractive forces with agglomerate configuration. This of course assumes the ability to put a value on attractive and breaking forces. Methods for the estimation of these forces in fluidized beds are needed. A preliminary effort in this area is reported in Appendix E, where stresses in a large two-particle agglomerate were measured using a strain gage. Another way to approach the problem might be to construct agglomerates of known yield strengths and then measure their survival rates in the fluidized bed.

It was concluded that strong, close-packed agglomerates of the particles used in this study can not be obtained in the three inch diameter equipment used. This conclusion might be tested by use of either larger equipment or smaller particles. This data would be helpful in any modeling effort.

APPENDIX

Appendix A: Review of Models of Bubbling Bed Agglomeration

Note: In the following, the forms of the equations and the nomenclature used in the original works may have been changed for consistency with the rest of this dissertation and to eliminate multiple definitions.

A number of models of cohesive fluidization and agglomeration due to thermal effects have been proposed in the literature. A common approach has been to modify the conventional equations which describe non-cohesive fluid beds as found in texts such as Kunii and Levenspiel (1971) and Geldart (1986) to include cohesive terms. The analysis starts with a force balance on the particles at minimum fluidization when the total drag force (pressure drop multiplied by the cross sectional area, A) is equal to the weight of the bed

$$\Delta P \cdot A = g(\rho_s - \rho)(1-\varepsilon_{mf})A \cdot H \qquad (A.1)$$

using the well known Ergun correlation

$$\Delta P/H = (\mu U/(\phi_s d_p)^2) \cdot ((1-\varepsilon)^2/\varepsilon^3) + (1.75\rho U^2/\phi_p d_p) \cdot ((1-\varepsilon)/\varepsilon^3) \qquad (A.2)$$

and combining Equations A.1 and A.2, leads to the well known expression

$$Ga = [150(1-\varepsilon_{mf})/\varepsilon_{mf}^3]Re_{mf} + [1.75/\varepsilon_{mf}^3]Re_{mf}^2 \qquad (A.3)$$

In an effort to correlate Siegell's (1976) defluidization data, Liss et al. (1983) proposed a semi-empirical model for the minimum fluidization velocity based on a modification of the above force balance on the particles (Equation A.3). They reasoned that in the presence of adhesive forces due to sintering, the drag force must balance interparticle adhesion as well as gravity. The adhesive stress, S, was related to the pressure drop over the bed and gravity by

$$\Delta P \cdot A = (1-\varepsilon_{mf})(\rho_s-\rho)g \cdot A \cdot H + S\pi d_p^2 \qquad (A.4)$$

Combining Equation A.4 with the Ergun correlation the following dimensionless expression was obtained

$$Ga(1+Co) = 150[(1-\varepsilon_{mf})/\varepsilon_{mf}^3]Re_{mf} + [1.75/\varepsilon_{mf}^3]Re_{mf}^2 \qquad (A.5)$$

Here the cohesive number, Co, takes the form

$$Co = 6S/(\rho_s-\rho)d_p g \qquad (A.6)$$

Clearly Equations A.4 and A.5 are not applicable to the state of fluidization; the pressure drop at U_{mf} cannot exceed the weight of the bed divided by its cross sectional area regardless of how the particles interact with each other (ignoring wall effects). If all the particles making up a bed were bonded together permanently, the drag force

necessary to lift this aggregate would precisely balance the gravity force acting downward.

What equation A.4 does describe is the increase in pressure drop over the fixed bed in excess of the weight of the particles which occurs when the superficial velocity is first raised above minimum fluidization. The greater the attraction between particles, the greater the strength of the fixed bed, the higher the velocity needed to break the stronger structure. The higher velocity results in a higher pressure drop. Sometimes this is referred to in the literature as the unlocking of the bed. When the velocity is lowered from above the minimum fluidization value, the pressure never exceeds the weight of the bed. (See Section 3.2.2).

Basu (1982) also rewrote the force balance on the particles at minimum fluidization by adding the adhesive term Ψg

$$\Delta P/H = [(1-\varepsilon_{mf})(\rho_s-\rho_s) + \Psi(T,d_p,H)]g \qquad (A.7)$$

Basu assumed that the adhesive force Ψ, acting on a particle from its surrounding (averaged over the bed), would be dependent on the height of the fluidized bed, H, in concordance with Siegell's (1976) results. This formulation differs from the result of Liss et al. only by the inclusion of the gravitational constant in the adhesive term. It is unclear how gravity could influence the strength of an interparticle bond.

In an early study on the effect of interparticle adhesion force on fluidizability, Baerns (1966) attempted to calculate a fluidizability index, FI, which is defined as the ratio of the minimum fluidization

velocity calculated from the average particle diameter, U^*_{mf},(which is a hypothetical value), to the observed minimum fluidization velocity, U_{mf}.

$$FI = U^*_{mf}/U_{mf} \tag{A.8}$$

Experimentally, Baerns measured U_{mf} for a number of small diameter cohesive powders and then measured single particle adhesive forces using an inclined rotating plate method. To explain values of FI which were less than unity the single particle adhesion force, Ψ_p, was added to the force balance on a single particle during the unlocking phase of fluidization.

$$F_d = W_p g + \Psi_p \tag{A.9}$$

He reasoned that to fluidize the particle, the drag forces imparted from the fluid, F_d, must counter both the weight of the particle $W_p$and the adhesive forces acting to keep it stationary, Ψ_2.

Equation A.9 is a correct description of the unlocking of the bed (depending on the true form of Ψ_p), but Baerns goes on by applying Equation A.9 to the condition of minimum fluidization. The drag force was related to the drag coefficient, C_D, by

$$F_d = \alpha C_D \pi d_p^2 \rho U^2/8 \tag{A.10}$$

where the superficial velocity, U, can take either the observed value (in the case of a cohesive powder) or the hypothetical value U^*_{mf} obtained from the single particle calculation

$$F_d = \alpha C_D^* \pi d_p^2 \rho (U_{mf}^*)^2/8 \tag{A.11}$$

$$F_d + \Psi_p = \alpha C_D \pi d_p^2 \rho U^2/8 \tag{A.12}$$

where C_D^* is the drag coefficient in the hypothetical case. By dividing Eq. A.8 by Eq. A.9, and assuming $C_D=24/Re$ (Re<1), the formula for the fluidizability index is obtained

$$FI = F_d/(F_d+\Psi_p) = U_{mf}^*/U_{mf} \tag{A.13}$$

This result is based on the same assumptions used by Liss et al. and Basu because of the application of a fixed bed force balance to the fluidized state. In addition, there is a question about Equations A.11 and A.12: by what mechanism is U_{mf} larger than U_{mf}^*? In this formulation the drag coefficient is the only factor which is different between the cohesive bed and its hypothetical analogue. However, the drag coefficient is only assumed to change because of the increased superficial velocity, i.e., the two are not independent.

A model of agglomeration which also involves modifications of both the force balance on the particles and the Ergun pressure drop relationship was put forth by Chaoki et al.(1985) in order to explain the unusual fluidization behavior of Ca/Al_2O_3 aerogel catalyst powders. These powders, nominally classified as group C, are not fluidizable and channel badly at expected superficial velocities calculated from the single particle diameter(~1μm). But it was found that at much higher velocities (~4cm/s) the cohesive bed structure "rearranges" by breaking into clusters which fluidize homogeneously. Photographic analysis of

the bed showed the clusters to be fairly uniform with a diameter of approximately 0.1cm. That this type of stable agglomeration and fluidization behavior has not been reported to occur with conventional group C powders was attributed to the extremely low bulk density of the aerogel ($0.066 g/cm^3$) - most group C powders have densities no lower than $0.4\ g/cm^3$.

Chaoki et al. assumed that the system may be treated as a fluidized bed of clusters where the primary particles which make up the bed do not exist singly. Accordingly equations A.1 through A.3 were rewritten (for Re<20) as

$$\Delta P \cdot A = g(\rho_c - \rho)(1-\varepsilon_c)A \cdot H_c \qquad (A.14)$$

$$\Delta P/H_c = [\mu U_c/(d_c)^2][(1-\varepsilon_c)^2/\varepsilon_c^3] \qquad (A.15)$$

$$U_c = [d_c^2(\rho_c - \rho)g/(150\mu)][(1-\varepsilon_c)/\varepsilon_c^3] \qquad (A.16)$$

where the subscript c refers to the cluster.

Using experimental values for the voidage at clustering, $\varepsilon_c = 0.53$ and the density of the clusters, $\rho_c = 0.066 g/cm^3$, which was taken as the density of the quiesent bed, a cluster equivalent diameter of 0.07cm is obtained which is in accord with the photographic estimate.

It was then attempted to relate the interparticle Van der Walls force which is exerted on a cluster by its surroundings, F_v to the drag force acting on the cluster, $F_{d,c}$. Again the force balance was applied to a cluster in the fixed bed prior to fluidization. The authors state that a cluster is fluidized by breaking out of the fixed bed as a formed

unit and that the drag force must equal the intercluster force and the weight of the cluster. But instead they write

$$F_{d,c} = g(\rho_c - \rho)d_c^3/6 = F_v \qquad (A.17)$$

There is nothing to disprove Equation A.17. It does not violate the overall force balance and it makes sense that the diameter of the cluster should increase with interparticle force. However the reasoning behind it seems arbitrary. For example there is no dependence on the forces which serve to break up the clusters, as if once they are formed there is no exchange of particles. If the interparticle bonds are that strong how do the clusters fluidize in the first place? In fact this theory implies that the forces acting on the cluster during fluidization are identical to those acting on the clusters in the fixed bed, which cannot be the case since the fixed bed is not made up of clusters at all.

The theory of Yamazaki et al. (1986) is almost identical to that of Chaoki et al. except that analytical expressions for the voidage of the clustering bed and the shape factor of the clusters were also developed. Yamazaki et al. assumed that the increase in U_{mf} of clustering partcles is due mainly to the inability of the clusters to pack well resulting in increased voidage. The poor packing was attributed to the clusters being less spherical than the primary particles of which they are comprised. The theory states that the shape factor of a cluster, Φ may be computed from the product

$$\Phi = \phi_p \phi_a \qquad (A.18)$$

where Φ_p is the shape factor of the single particles and Φ_a is the shape factor of a cluster made of spherical equivalent particles given as

$$\Phi = \Phi_p[1+0.188(n-1)/n]/[n^{1/3}] \qquad (A.19)$$

where n is the number of primary particles comprising a cluster. Equation A.19 was obtained from geometrical considerations and the assumption of closed packed spheres. There is no distinction between clusters which have the same number of particles but have different overall shapes. The relationship between voidage and the shape factor was assumed to be

$$\Phi^2(1-\varepsilon_{mf})/\ \varepsilon_{mf}^3 = K \qquad (A.20)$$

(a modified version of the voidage relation developed by Wen and Yu, 1966), where K is a constant; there was no physical meaning attributed to the constant K. The number of particles in a cluster was then related to the intergranular adhesive force ,F_{ad} by

$$F_{ad} = (k)(\text{weight of the cluster}) = kn(\pi/6)\rho_s d_p^3 g \qquad (A.21)$$

which is analogous to equation A.17 (Choaki et al.'s theory) except for the inclusion of the constant k which allows for the cluster size to be proportional to the interparticle force.

By combining equations A.18 through A.21, an expression for the voidage, f_ε, is obtained as a function of the adhesion force, etc.

$$\varepsilon_{mf}^3/(1-\varepsilon_{mf}) = f_\varepsilon(F_{ad},K,k,d_p,\ldots) \qquad (A.22)$$

Curiously, when equation A.22 was inserted into the expression for U_{mf} (Equation A.3), the single particle values for the shape factor, diameter and density were still retained, resulting in th expression

$$U_{mf} = [(\Phi_p d_p)^2(\rho_s-\rho)g/150\mu]f_\varepsilon(F_{ad},\ldots) \qquad (A.23)$$

(perhaps this was an oversight). In addition, the following observations are made:

1) Though it is true that the voidage at U_{mf} appears to increase with particle adhesion (see Lau, 1981 and Geldart et al., 1984) the effect cannot be attributed only to a difference in shape factor; the particles are also unable to pack because of hinderance of movement due to adhesion.

2) The expression for the shape factor of the clusters (eq. A.18) implies that the hydrodynamic shape factor of the cluster is proportional to the shape factor for a single particle, Φ_p which describes the hydrodynamic properties on the single particle length scale. However, the length scales of single particles and clusters are not the same. By this model then a spherically symmetrical cluster made of say, 25 non-spherical particles (Φ_p=0.6), would have a shape factor of Φ=0.24; for 50 particles, Φ=0.19; this does not make sense. The overall shape factor of a cluster must become less dependent on the shape factor of the single particles as the cluster grows larger.

3) There is no dependence on the forces which act to break up agglomerates in the fluidized state.

4) The presence of two free parameters without clear physical meaning (k in Equation A.21 and K in Equation A.18) eliminates predictive capability and also testability.

The theoretical model of defluidization devised by Tardos et al.(1985a) is a departure from the approach taken by the authors whose work has been described above. Instead of modifying the force balance on the particles and the Ergun pressure drop relationship to account for adhesion, the defluidization velocity was modeled as the velocity needed to fracture the largest possible agglomerate in the bed, i.e., an agglomerate which is equal in size to the diameter of the bed. It was assumed that if this agglomerate could be prevented from forming, the bed would remain fluidized. It is assumed that the agglomerate, which is taken as a cylinder resting close to the distributor plate, can be broken by stresses created by bubble motion. If the pressure on the agglomerate, P_{agg} exceeds the value given by

$$P_{agg,max} = \sigma_y (2h/d_{agg})^2 A_1 \qquad (A.24)$$

where σ_y is the yield strength of the agglomerate, A_1 is a constant, and d_{agg} and h are its diameter and height respectively, the agglomerate will break. The pressure on the agglomerate P_{agg} was taken to be evenly distributed over the surface, or

$$P_{agg} = 4G_v/\pi d_{agg}^2 \qquad (A.25)$$

where Gv is the total force acting on the agglomerate which was correlated by Livshits et al.(1978) as a function of the following variables

$$G_v = G_v[\rho_p, d_{agg}, D_b, H, (U-U_{mf})] \quad (A.26)$$

The vertical force, G_v, grows with increasing $(U-U_{mf})$, bubble diameter D_b, agglomerate diameter, d_{agg}, etc.. The model is not meant to predict the size of the agglomerates which would exist at velocities above this limiting defluidization velocity, but the authors maintain that as long as there is a dynamic equilibrium between breakup and formation of these agglomerates, the bed will remain fluidized.

The importance of this model is that instead of writing equations which describe the condition of a fixed bed and then applying these to fluidization, an attempt is made to relate the size of the agglomerate to the forces acting on it in the fluidized state. However, some of the assumptions used to develop this theory seem unrealistic, the most important of which is that an agglomerate with a dimension on the order of the bed diameter could never form. To demonstrate this, a rough calculation of U_{mf} for a cluster the size of the bed used during the experiments (15.2cm) would give a value of approximately 5,800cm/sec. In fact, if it can be assumed that the minimum fluidization velocity grows with particle diameter according to the Ergun correlation

$$U_{mf} \sim d_p^2 \quad (A.27)$$

the minimum fluidization velocities calculated by Tardos et al. would be sufficient to fluidize particles on the order of only twice the diameter of the primary particles used in their experiments.

Appendix B. Values of U_{mf} in the Low Temperature Range

T(^{o}C)	d_p(μm)	Bed Weight(g)	U_{mf}(cm/s)
Sodium Chloride:			
30	360	1750	9.27
155			6.8
320			6.4
400			7.8
18	360	1750	9.2
100			7.9
220			6.18
295			6.18
380			6.82
17	360	1250	9.08
225			6.43
295			6.22
350			7.4
390			8.14
23	510	1250	14.6
335			13.6
Calcium Chloride			
20	~500	500	16.7
141			13.0
245			12.0
325			12.0
430			12.2
Glass beads			
20	720	1500	21.6
118			19.1
255			15.0
404			15.2
554			14.8
605			14.6

Appendix C. Isothermal Sintering Models

Review of the literature shows that most of the mathematical models of sintering are for the isothermal case. There are numerous mechanisms by which sintering can occur. Some of these are shown below.

Frenkel (1945):

$$(b/D_p)^2 = (3\gamma/2Dp\eta)t \qquad \text{Viscous Flow} \qquad (C.1)$$

Kuczynski (1973):

$$(b/D_p)^2 = 6\alpha\gamma P_o (V_p{}^3\rho_s/2\pi(RT)^3)^{.5}\cdot t \qquad \text{Vapor phase transport} \qquad (C.2)$$

$$= (31\gamma V_p \delta D_v/RT)^{2/5}\cdot t^{2/5} \qquad \text{Volume Diffusion} \qquad (C.3)$$

$$= (96\gamma V_p D_b/RT)^{1/3}\cdot t^{1/3} \qquad \text{Grain Boundary Diffusion} \qquad (C.4)$$

$$= (56\gamma V_p D_p \delta D_s/RT)\cdot t^{2/7} \qquad \text{Surface Diffusion} \qquad (C.5)$$

Kuczynski (1973) recast these equations in a general form

$$(b/D_p)^n = \frac{F(T)}{(D_p)^m}\, t \qquad (C.6)$$

where n and m characterize the transport mechanism. Klose and Lent (1984) argue that this type of equation, where the bond neck growth is

proportional to time is hydrodynamically incorrect because it leads to an infinite bond neck diameter at large times. They rederived the equation for a viscous flow mechanism (Frenkel) arriving at

$$(b/D_p)^2 = (1-e^{-t/\tau}) \qquad \tau = 3\gamma/2\eta Dp \qquad (C.7)$$

It seems natural then to modify Kuczynski's Equation (C.6) in the same way to arrive at

$$(b/D_p)^n = k(1-e^{-t/\tau}) \qquad \tau = \Pi\, \tau_i(T) \qquad (C.8)$$

where $n = \Pi\, n_i$, and $k = k(T)$.

Appendix D: Fluidized Bed Reduction of Phosphogypsum to Calcium Sulfide

The feasability of reducing calcium sulfate (phosphogypsum) to calcium sulfide (CaS) in hydrogen at 700°C in a fluidized bed was investigated using a 3-inch bench scale fluidized bed with a porous plate distributor and controlled atmosphere dilatometry.

The overall reaction proceeds as

$$CaSO_4 \xrightarrow{N_2,H_2} CaS + H_2O \qquad (D.1)$$

A batch of phosphogypsum was obtained from the U.S. Bureau of Mines, Tuscaloosa, Alabama. The material was first sieved to 165μm and then fluidized in pure nitrogen at about 3 times the measured minimum fluidization velocity (1.4 cm/s). The temperature of the bed was brought slowly up to 700°C, keeping the gas flow rate constant, at which point a flow of hydrogen was introduced into the bed via a small tube situated directly above the distributor plate. The ratio of hydrogen to nitrogen flow was approximatly 1:3. The total pressure drop over the bed and the temperature of the bed were measured throughout the experiment.

In nitrogen,the phospogypsum fluidized well with no indication of agglomeration or particle adhesion. Steam was evolved starting at 100°C and terminating at about 280°C. Fines were produced at all temperatures and at gas velocities as low as 1.5 times minimum fluidization. Soon after the flow of hydrogen was initiated the pressure drop began to decrease quickly indicating the agglomeration of the powder and the

development of gas channels (see Figure D.1). The bed was completely defluidized after about 14 minutes.

The development of strong powder cohesion beginning with the conversion of calcium sulfate to calcium sulfide led to the conclusion that the calcium sulfide is extremely cohesive and that the calcium sulfate is not cohesive at these temperatures. A dilatometry test of the calcium sulfate confirmed the later assumption: a 165μm sample of the powder was heated in the dilatometer at about 200°C/hr and in a pure nitrogen atmosphere. The resulting curve (see Figure D.2) shows a slight increase in length after 500°C, which is probably due to thermal expansion. Inspection of the sample showed no evidence of surface softening or agglomeration. An attempt to test the calcium sulfide in the dilatometer was unsuccessful due to the cohesiveness and chemical instability of the material. An attempt to fluidize the pure calcium sulfide was also unsuccessful, even at room temperature the powder is too cohesive to initiate fluidization. This result was confirmed by the work of Austin ("Sulfur from gypsum", Proceedings of the International Symposium on Phosphogypsum, Lake Buena Vista, Florida, 1980) who reported that calcium sulfide will not flow in downcomers at 700°C and that in order to fluidize the powder it had to be mixed with sand (100 mesh) at a ratio of 3 parts sand to 1 part calcium sulfide.

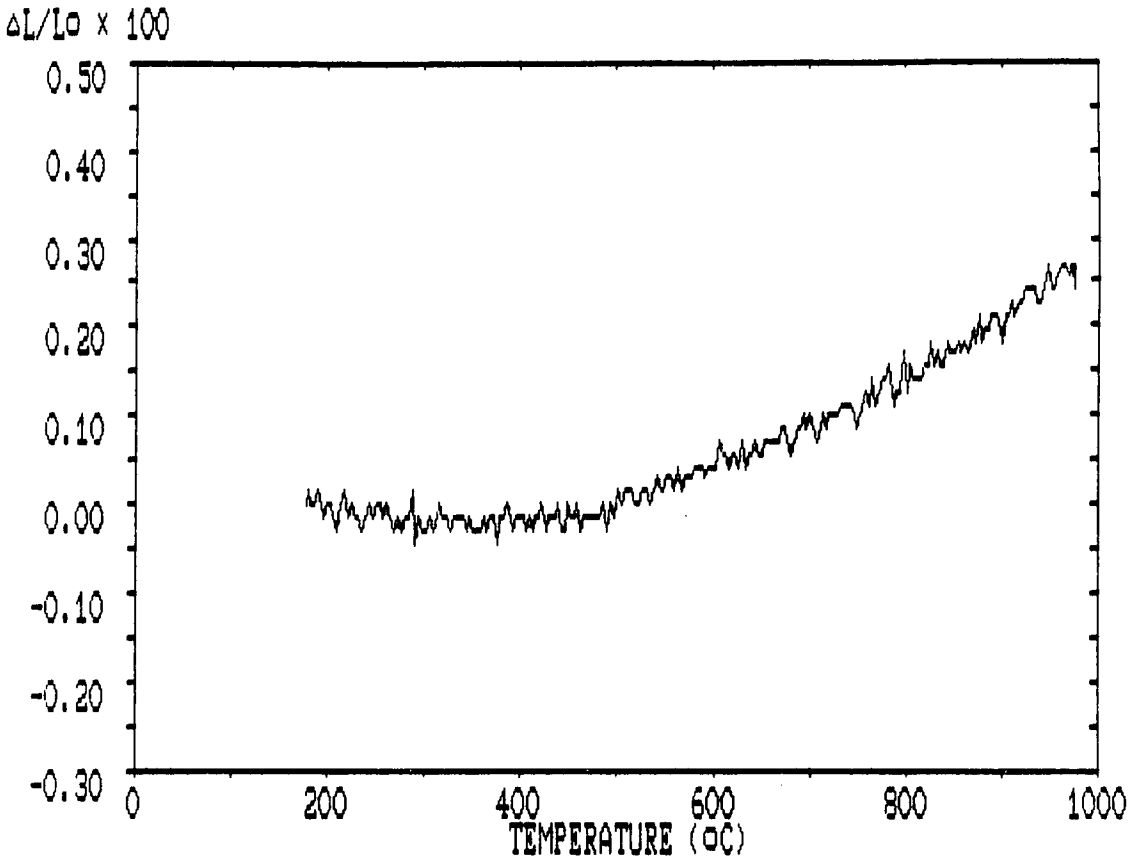

Figure D.2. CHR dilatometry for phosphogypsum.

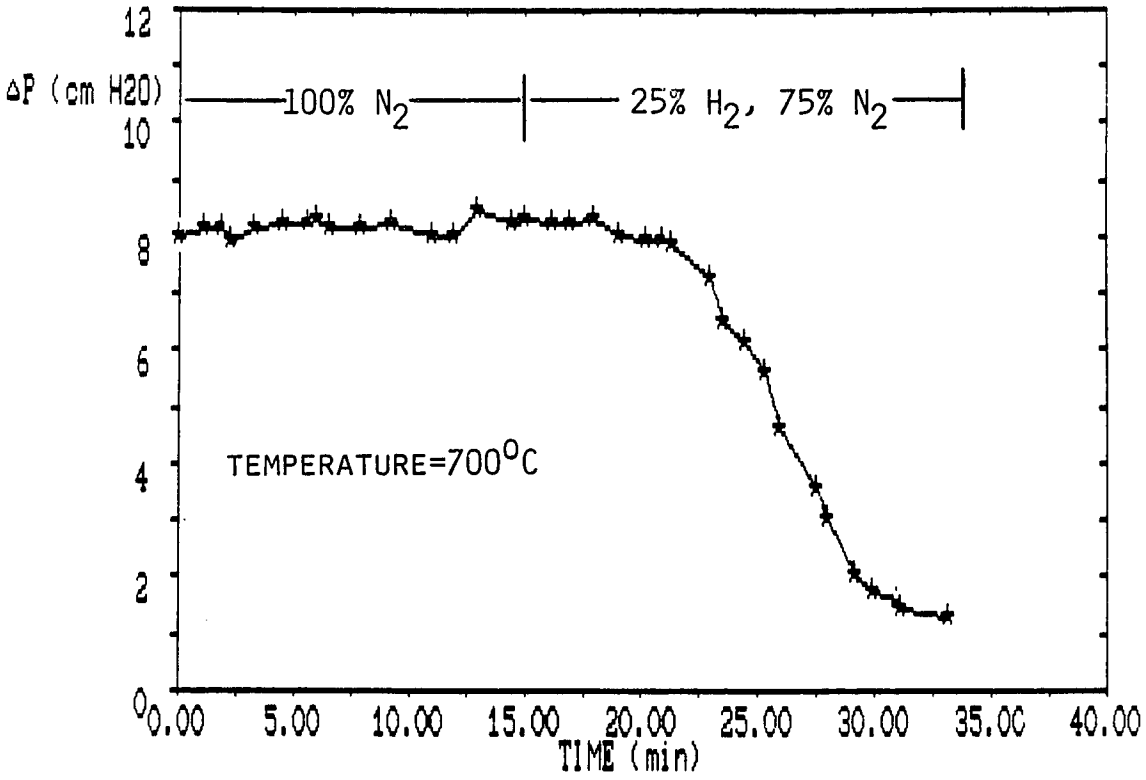

Figure D.1 DEFLUIDIZATION OF A CALCIUM SULFATE POWDER AS IT IS REDUCED TO CALCIUM SULFIDE.

Appendix E: Direct Measurement of Forces on Agglomerates

The purpose of this preliminary study was to obtain values of stresses in agglomerates in a bubbling fluidized bed. The excess pressure over a spherical agglomerate and the bending stresses in a specially designed "dumbbell" shaped and agglomerate were measured as functions of fluidization velocity. Measurements were made with the agglomerates both fixed and freely buoyant in the bed. Statistical analysis of fluctuation was used to obtain the frequency and amplitude of pressure and bending stress oscillations.

PRESSURE MEASUREMENTS ON AGGLOMERATES

To measure excess pressures on a spherical agglomerate situated in a fluidized bed of otherwise unagglomerated particles, small tubes were placed at the bottom and top of the sphere with the leads directed up through the top of the column (see Figure E.1). The tubes, being lightweight and flexible, allowed for free movement of the agglomerate in the directions parallel and perpendicular to the flow while restricting the rotational motion somewhat. For the experiments with fixed agglomerates, the sphere was attached to a heavy rod mounted on the wall of the column.

Pressures were measured for a 4.75cm diameter sphere formed from polyethylene granules which was placed in a 15.2cm diameter, air fluidized bed of the same material. The small polyethylene particles had an average diameter of 0.07cm and a density of $0.92 g/m^3$. The bed height at rest was 20.2cm and the velocity at minimum fluidization was U_{mf} =

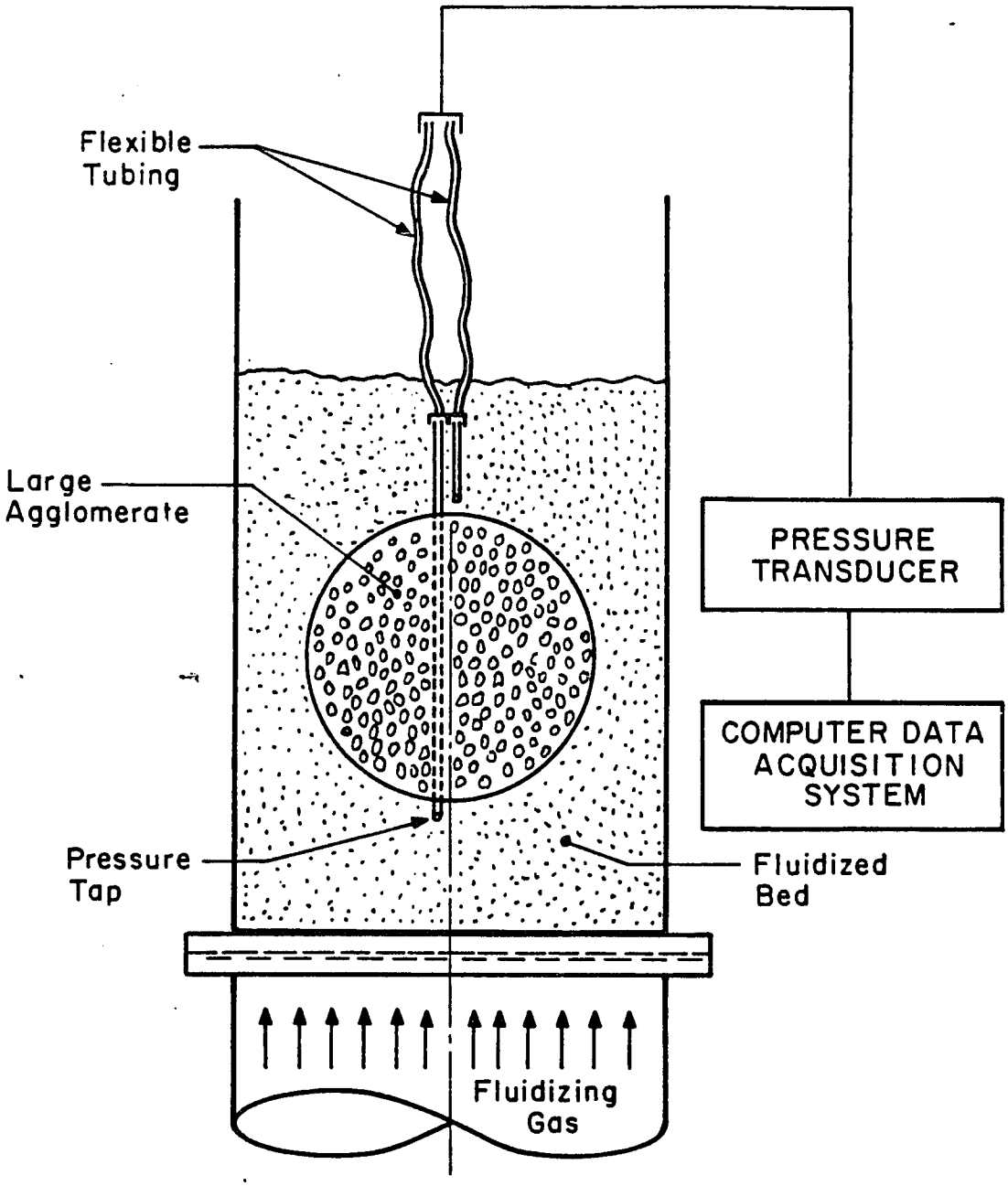

Figure E1. Pressures on a free agglomerate.

14.3cm/sec. When fixed, the center of the sphere was placed approximately 4.5cm from the distributor plate in the middle of the bed. The free agglomerate was observed to stay relatively close to this position at low velocities, while at higher velocities it moved towards the surface.

The pressure tube leads were connected to the positive and negative ports of a pressure transducer with the resulting signal amplified, and collected on the computer for analysis of the amplitude and frequency of the pressure peaks. Figure E.2 shows an example of pressure fluctuation as a function of time.

The vertical force F_v, due to over pressure on the agglomerate was obtained from

$$F_v = (\Delta P_{max})A_P \qquad (E.1)$$

where ΔP_{max} is the average value of maximum pressures (peaks in Figure E.2) and A_P is the projected area of the sphere. In Figure E.3, the vertical force F_v, is plotted as a function of dimensionless excess velocity for the fixed and the free moving agglomerate, and is compared to the total vertical force on the agglomerate G_v, obtained from a correlation taken from the literature (Livshitz et al., 1978). Results show that the pressure drop over an immersed sphere is the same for fixed and freely buoyant agglomerate. However, the total vertical force acting on the fixed body is much larger than the force due to pressure only. This indicates that particles colliding with the body is the main cause of vertical forces. The levelling off of the G_v curve with increasing velocity indicates that growing turbulence results in collisions in the positive and the negative direction.

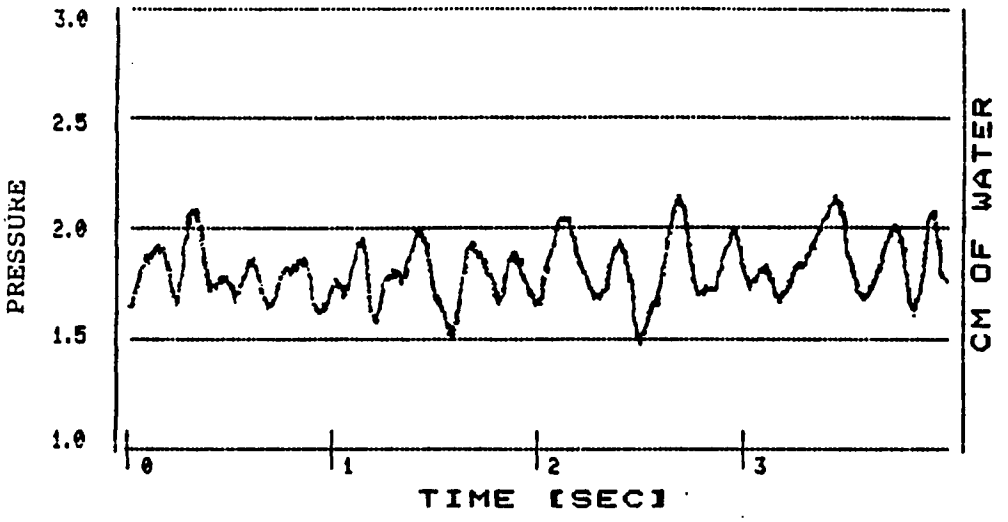

Figure E2. Pressure over a spherical agglomerate versus time, $[u/u_{mf}=2.4]$.

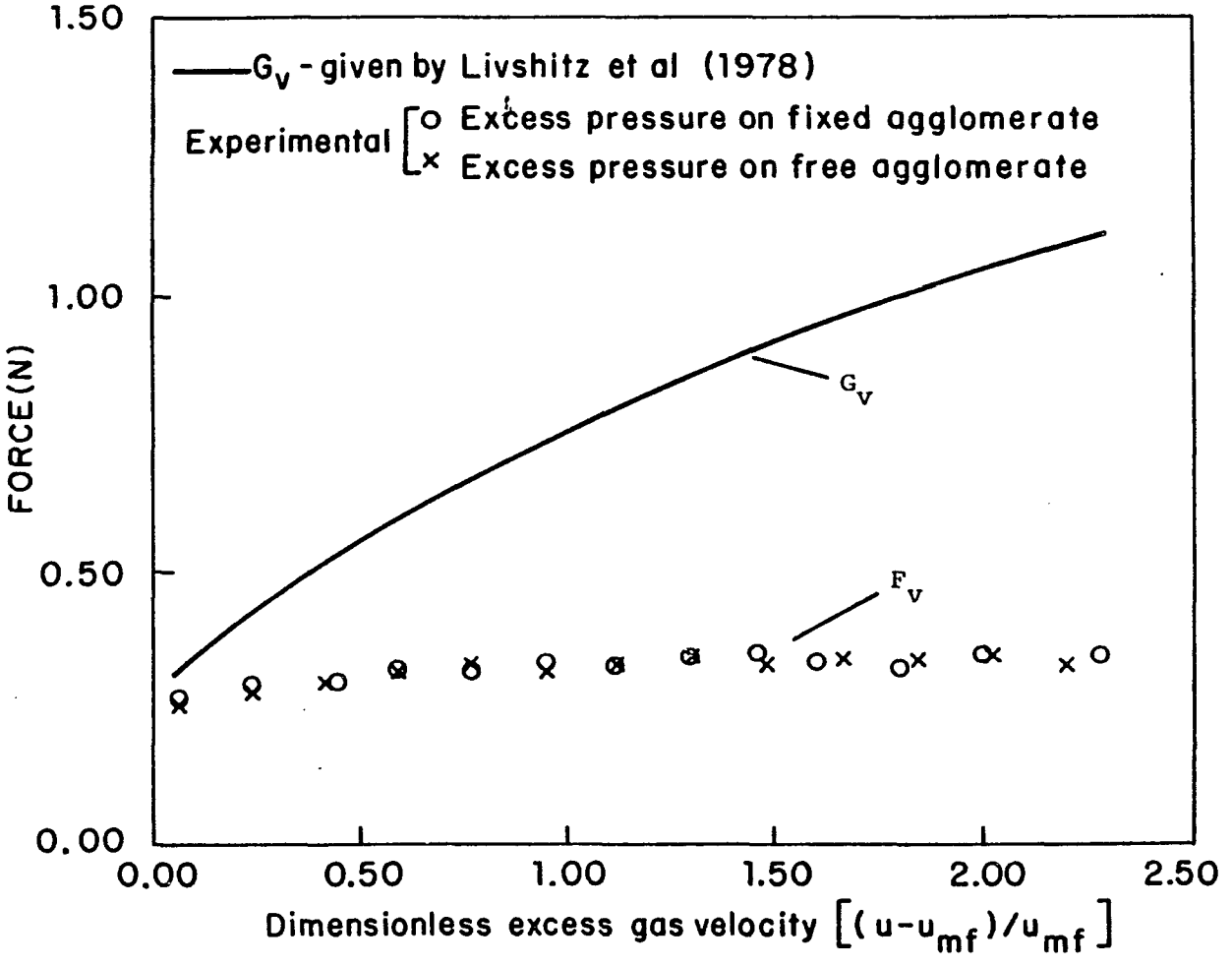

Figure E3. Vertical force vs. excess gas velocity for a spherical agglomerate.

STRESS MEASUREMENT IN AN AGGLOMERATE

Stresses were measured in the dumbbell shaped agglomerate shown in Figure E.4. A small constantan foil strain gage was mounted on a thin, hardened steel beam. Ceramic spheres (D_p = 1.2cm), attached to both ends of the beam, produced the "dumbbell" shape shown. To allow for maximum movement of the freely buoyant agglomerate - thin, stranded copper wires, coiled throughout their lengths, and introduced through the top of the column were used as the connecting leads between the strain gage and the signal amplifier. As in the procedure used for pressure measurements, the agglomerate could also be fixed in place by a heavy rod, firmly attached to the column wall.

Stress measurements were made in an air fluidized bed of alumina particles using a 7.62cm diameter column. The alumina had a density of 3.5g/cm^3 and an average size of 100μm. The bed height at rest was 50.7cm and the minimum fluidization velocity was measured to be u_{mf} = 0.705cm/s at ambient. Data was obtained with the agglomerate in three different situations: (1) freely buoyant; (2) fixed horizontally in the center of the column with the spheres directed in a line perpendicular to the gas flow and (3) fixed vertically in the center of the column with the spheres in line, parallel to the flow. When fixed, the agglomerate was located 40cm above the distributor plate and when unattached, the agglomerate moved freely throughout the upper 15 or 20cm of the bed. The stress in the beam between the spheres was calculated from

$$\sigma = Mc/I \qquad (E.2)$$

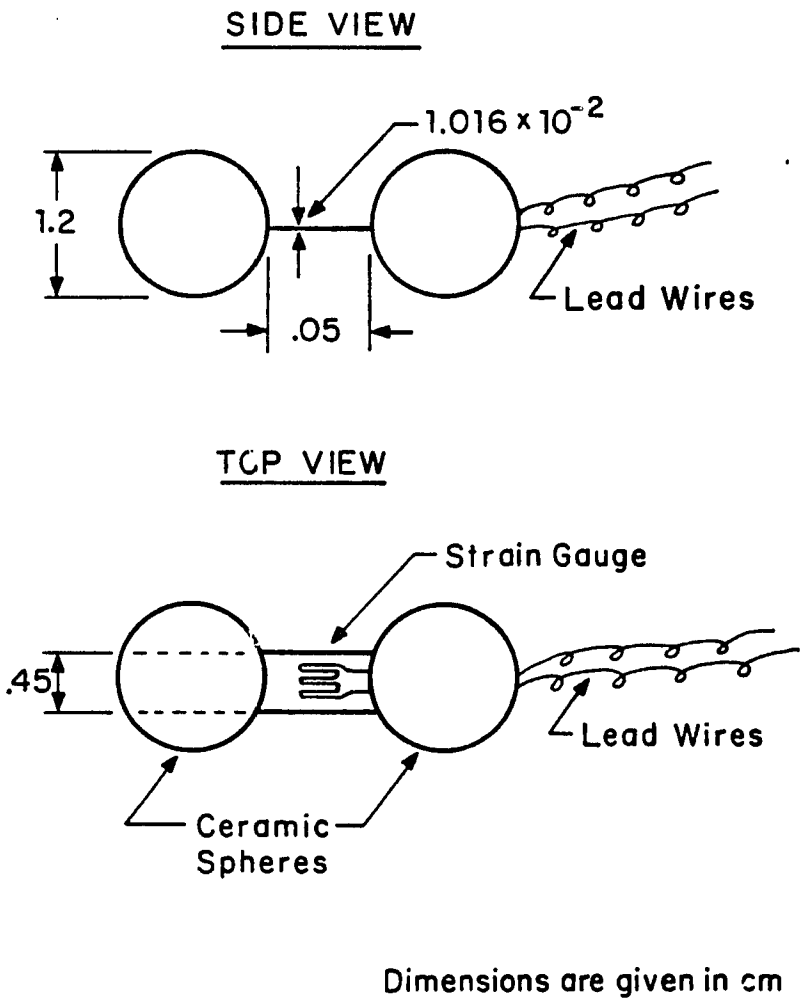

Figure E4. Dumb- bell shaped agglomerate with strain gauge

where M is the bending moment, c is half the thickness of the beam and I is the moment of inertia. In order to obtain moments, the system was initially calibrated using known forces.

An example of stress versus time data for the freely buoyant agglomerate is shown in Figure E.5. In this case, the gas velocity was twenty times the minimum fluidization velocity. Figure E.6 shows maximum average stresses for the three cases (freely buoyant, fixed horizontally and fixed vertically) as a function of dimensionless fluidization velocity. At low velocities, stresses are of similar magnitude for all three cases. At higher velocities, however, the fixed agglomerates show increasing stress while the force in the free agglomerate remains relatively constant. The wide fluctuations in the data for the vertically fixed case result from chaotic motion in the bed at high velocities. The large magnitude of some of these points demonstrates that horizontal forces on immersed bodies are significant.

NOTATION

A_p	Projected area, cm^2
c	One half the thickness of connecting beam, cm
d_p	Particle diameter, cm
G_v	Total vertical force acting on an object in a fluidized bed, N
F_v	Vertical force due to pressure acting on an object, N
I	Moment of inertia, cm^4
L_o	Bed height at rest, cm
M	Bending moment, N-M
u	Superficial fluidization velocity, cm/s
u_{mf}	Minimum superficial fluidization velocity, cm/s

REFERENCE

Livshits, Y.Y., Tamanin, A.I. and Zabrodsky, S.S., Fluid Mechanics - Soviet Res., 7, 30, (1978).

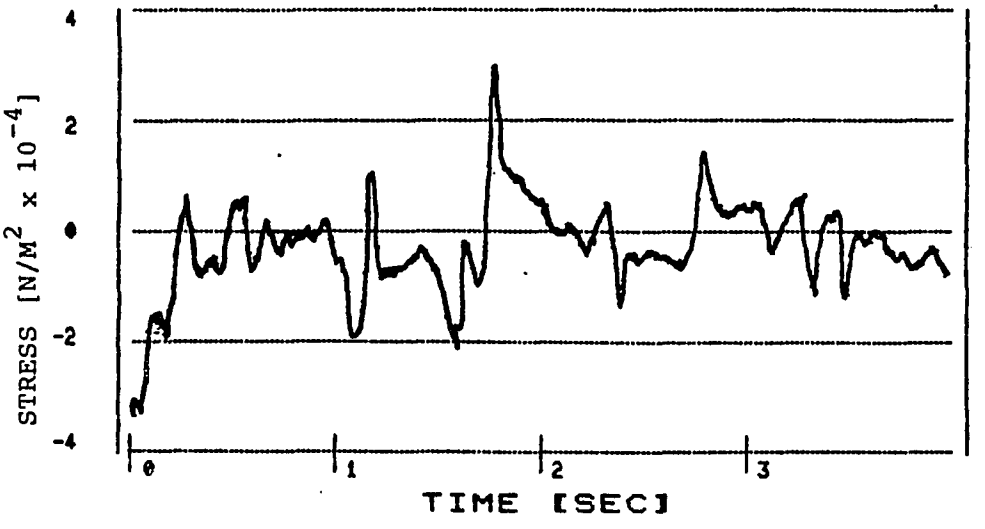

Figure E5. Maximum stress versus time for a freely buoyant agglomerate, [u/u_{mf}=11.9].

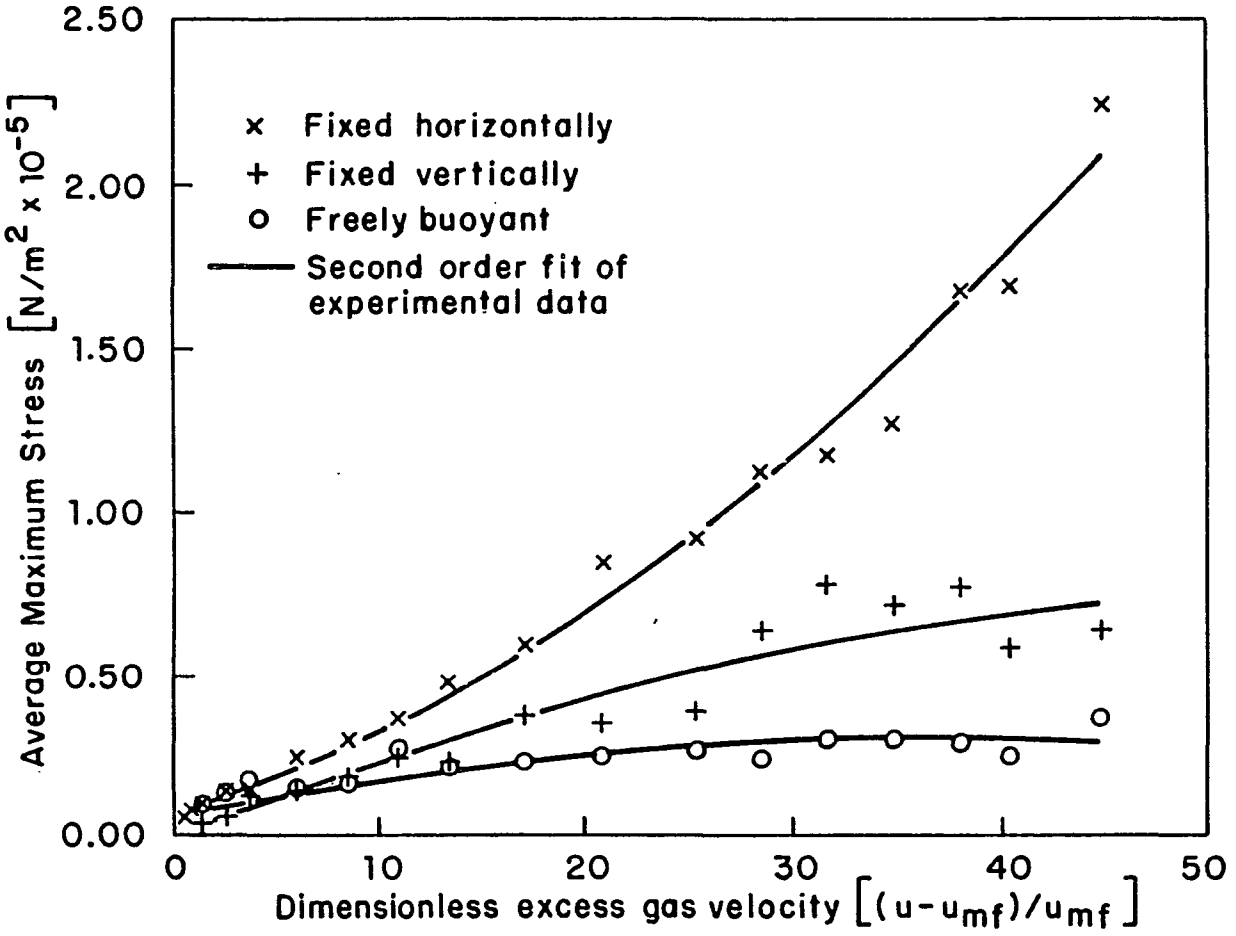

Figure E6. Internal stress vs. excess fluidization velocity in the dumb-bell shaped agglomerate.

6. REFERENCES

Adamson, A.W., Physical Chemistry of Surfaces. 4th ed. Wiley, New York (1982).

American Society of Testing Materials, Annual Book of ASTM Std., Phila., Designation D, 1857-68(1978).

Anderson, T.B. and R. Jackson, "Fluid Mechanical Description of Fluidized Beds", Ind. Eng. Chem. Fundamentals 7, 12(1968).

Andrievsky, R.A., "Sintering Behavior and Electronic Structure of materials", in Sintered Metal-Ceramic Composites, Upadhyaya ed., p. 25 (1984).

Arastoopour, H., C.S. Huang and S.A. Weil, "Fluidization Behavior of Particles Under Agglomerating Conditions", Chem. Eng. Sci. 43(11), 3063(1988).

Baerns, M., "Effect of Interparticle Adhesive Forces on Fluidization of Fine Particles", Ind. Eng. Chem. Fundamentals 5, 508(1966).

Barringer, E.A., R. Brook and H.K. Bowen, "The Sintering of Monodispersed TiO_2", in Sintering and Heterogeneous Catalysis, ed. Kuczynski et al., 1(1984).

Baskakov, A.P., V.G. Tuponogov and N.F. Filippovsky, "A Study of Pressure Fluctuations in a Bubbling Fluidized Bed", Powder Technology 45, 113(1986).

Basu, P., "A Study of Agglomeration of Coal-Ash in Fluidized Beds", Can. J. Chem. Eng. 60, 791(1982).

Basu, P. and A. Sarka, "Agglomeration of Coal Ash in Fluidized Beds",Fuel 61, 924 (1983).

Benson, S.A., F. Karner and G. Groblirsch, "Bed Agglomerates Formed by Atmospheric Fluidized Bed Combustion of a North Dakota Lignite", Proceedings of A.C.S., Division: Fuel Chemistry. Las Vegas, Nevada. 174-181(1982).

Blake, T.R. and B. Liss, "An Assessment of Process Modeling for Fluidized Bed Coal Gasifiers", Final Report: DOE Contract #DE-AC21-83MC20440, (1985).

Botterill, J.S.M., Y. Teoman and K.R. Yunegin, "The Effect of Operating Temperature on the Velocity of Minimum Fluidization, Bed Voidage and General Behavior", Powder Tech. 31, 101(1982).

Chaouki, J., C Chavarie, D. Klvana and G. Pajonk, "Effect of Interparticle Forces on the Hydrodynamic Behavior of Fluidized Aerogels", Powder Tech 43, 117(1985).

Clift, R., "Particle-Particle Interactions in Gas-Particle Systems," I. Chem. E. Symposium Series No. 91, 27(1985).

Compo, P., G.I. Tardos, D. Mazzone, and R. Pfeffer,"Minimum Sintering Temperatures of Fluidizable Particles", Particle Characterization 1,171(1984).

Compo, P., R. Pfeffer and G. Tardos,"Minimum Sintering Temperatures and Defluidization Characteristics of Fluidizable particles",Powder Technology 51, 85(1987).

Conn, R.E. and L.G. Austin, "Studies of Sintering of Coal Ash Relevant to Pulverized Coal Utility Boilers", Fuel 63,1664(1984).

Cumming, J.W. and A. Sanyal, "The Electrical Resistance of Coal Ash at Elevated Temperatures", J. Inst. Energy 53, 153(1980).

Davidson, J.F., R. Clift, and D. Harrison, Fluidization, 2cd ed., Academic Press, London(1985).

Easterling, K.E. and A.R. Tholen, "A Study of Sintering Using Hot-Stage Election Microscopy", Met. Sci. J. 4, 130(1970).

Ennis et al., "Growth Mechanisms in Fluid Bed Granulation Processes", (in press, 1989).

Exxon, "Review of Ash Agglomeration in Fluid Bed Gasifiers", Draft Final Topical Report, U.S. DOE Contract DE-AC21-82MC19265,(1984).

Falcone-Miller, S and D.P. Kalmanovitch, "Relation of Slag Viscosity and Surface Tension to Sintering Potential", Pre. Pap. Am. Chem. Soc., Fuel Division, 33(2), 42(1988).

Fan, L.T., S. Hiraoka, T.C. Ho and W.P. Walawender, "Pressure Fluctuations in a Fluidized Bed", AIChE J 27, 388(1981).

Fan, L.T., Y.W. Huang, D. Neogi and N. Yutani, "Statistical Analysis of Temperature Effects on Pressure Fluctuations in a Gas-Solid Fluidized Bed", Fluidization '85, Second China-Japan Symposium, Kunming, China, April (1985).

Fitzgerald, T., D. Bushnell, S. Crane and Yeong-Cheng Shieh, "Testing of Cold Scaled Bed Modeling for Fluidized Bed Combustors", Powder Tech. 38, 107(1984).

Foscolo, P.U., L.G. Gibilaro, R. DiFelice and S.P. Waldram, "The Effect of Interparticle Forces on the Stability of Fluidized Beds", Chem. Eng. Sci. 40(12), 2379(1985).

Geldart, D., "Types of Gas Fluidization", Powder Tech.7, 285(1973).

Geldart, D., N. Harnby and A.C. Wong, "Fluidization of Cohesive Powders", Powder Tech.37, 25(1984).

Geldart, D., ed., Gas Fluidization Technology, John Wiley & Sons, New York, (1986).

Gluckman, M.J., J. Yerushalmi and A.M. Squires, "Defluidization Characteristics of Sticky or Agglomerating Beds", in Fluidization Technology, Vol. II, D.L. Keairns (ed.), Hemisphere Publishing, New York, 395 (1975).

Hartman, M. and K. Svoboda, "Predicting the Effect of Operating Temperature on the Minimum Fluidization Velocity", Ind. Eng. Chem. Process Des. Dev. 25, 649(1986).

Harvey, R.D., J.M. Masters, and J. Yerushalmi, "Behavior of Coal Ash in Gasification Beds of Ignifluid Boilers", Illinois Minerals Note 61, (1975).

Hobbel, E.(E.I. Dupont Co., Wilmington De.) Personal communication (1989).

Huang, C., "Fundamentals of Agglomeration in a Fluidized Bed", Ph.D. Thesis - Ill. Inst. Tech.,(1985).

Jen, C.O., and K.C. Tsao, "Coal Ash Agglomeration Mechanism and its Application in High Temperature Cyclones", Separation Science and Technology 15(3), 263(1980).

Jimbo, G., R. Yamazaki and J. Tsubaki, "The Factors which Affect the Adhesion Force of Powder Particles", in 4th International Symposium on Agglomeration, Toronto, 697(1985).

Katta, S., "Sintering Behavior of Coal Ash on the Hot Stage Microscope", Appendix A. Quarterly Progress Report, Oct. 1, 1983-Dec. 1, 1983. DOE Report No. FE-19122-38, (1984).

Klose, W. and M. Lent, "Agglomeration Kinetics of Caking Coal Particles During the Softening Phase", Fuel 64, 193(1985).

Kono, H.O., C.C. Huang, E. Morimoto, T. Nakayama, and T. Hikosaka, "Segregation and Agglomeration of Type C Powders from Homogenously Aerated Type A-C Powder Mixtures During Fluidization" Powder Tech.53, 163(1987).

Kuczynski, G.C., "Physics and Chemistry of Sintering", Advan. Colloid Interface Sci. 3, 275(1972).

Kwauk, M., Personal Communication to Peter Compo, May 7th (1984).

Latimer, W.M. and J. Hildebrand, Reference Book of Inorganic Chemistry. Macmillan Co. (1940).

Lau, I.T., "Defluidization Characteristics in Sticky Beds of Caking Coals", paper presented at the Second World Congress of Chemical Engineers, Montreal (1981).

Lau, I.T. and B.J.P. Whallen, "A Differential Thermal Probe for Anticipation of Defluidization of Caking Coals", Fuel Processing Technology 4, 101(1980).

Ledesma, R., P. Compo and L.L. Isaacs, "Thermal Characterization of Coal Ash Powders", Materials Research Society Symposia Proceedings 86, 127(1987).

Levenspiel, O. and D. Kunii, Fluidization Engineering, Wiley, New York (1969).

Liss,B., T.R. Blake, A.M. Squires, and R.Bryson, "Incipient Defluidization of Sinterable Solids", Fourth International Conference on Fluidization, Japan, June (1983).

Mazzone, D., Ph.D. Thesis, the City College of the City University of New York (1986).

Raask, E., "Coal Ash Sintering Model and the Rate Measurements", Prep. Pap. Am. Chem. Soc. Div. 27(1), 145(1982).

Rehmat, A., C. Huang, R.Carty, H. Hariri, and H. Arastoopour, "Modeling of Agglomeration in a Fluidized Bed", Prepr. Pap.-Am. Chem. Soc., Div. Fuel Chem., 33(2), 176(1988).

Rietema, K., "Powders, What are They?", Powder Tech. 37, 5(1984).

Rumpf, H., "Particle Adhesion", in Agglomeration 77, K.V.S. Sastry (ed.), AIME, 97(1977).

Schobert, H.H., S.A. Benson, and L.G. Austin, "Relationship Among Fusing and Sintering Behavior, Strength and Composition of Slag Deposits from U.S. Lignites", 1987 International Conf. on Coal Science, Moulijn et al. (ed.), Elsevier, Amsterdam,(1987).

Seville, J.P.K. and Clift, R., Powder Tech. 37, 117(1984).

Siegell,J.H., Ph.D. Dissertation, the City University of New York(1976).

Siegell,J.H., "High Temperature Defluidization", Powder Tech. 38, 13(1984).

Squires, A.M., "Iron and Steel with Hydrogen", Atomic Energy Commission Symposium Series, 14, 181(1969).

Stallmann, J.J. and R. Neavel, Fuel 59, 584(1980).

Stoltze, P., J.K. Norskov, and U. Landman, "Disordering and Melting of Aluminum Surfaces", Physical Review Letters, 61(4), 440(1988).

Svoboda, K., J. Cenmak, M. Hartman, J. Drahos and K. Selucky, "Pressure Fluctuations in Gas-Solid Fluidized Beds at Elevated Temperatures", Ind. Eng. Chem. Process Des. Dev. 22, 514(1983).

Tardos, G.I., D. Mazzone and R. Pfeffer, "Measurement of Surface Viscosities Using a Dilatometer", Can. J. Chem. Eng. 62, 884(1984).

Tardos,G.I., D. Mazzone and R. Pfeffer, "Destabilization of Fluidized Beds Due to Agglomeration, Part I: Theoretical Model", Can. J. Chem. Eng.63, 377 (1985a).

Tardos,G.I., D.Mazzone and R.Pfeffer, "Destabilization of Fluidized Beds Due to Agglomeration ,Part II:Experimental Verification", Can. J. Chem. Eng.63, 377 (1985b).

Touloribian et al. (ed.), Thermophysical Properties of Matter, Vol. 13 - Non-Metallic Solids. Plenum, New York, 1000(1977).

Waldron, M.B. and B.L. Daniell, Sintering, Heyden Press, London and Philadelphia (1978).

Yamazaki, R., N. Veda and G. Jimbo, "Mechanism of Incipient Fluidization in Fluidized Beds at Elevated Temperature" J. of Chem. Eng. of Japan 19(4), 251(1986).

Yan, M.F., "Sintering of Ceramics and Metals", Advances in Powder Technology, G.Y. Chin (ed.), Amer. Soc. of Met., Metals Park, OH, 99(1982).

Yang, W., D.C. Chitester, R.M. Kornosky and D.L. Keairns, "A General Methodology for Estimating Minimum Fluidization Velocity at Elevated Pressure and Temperature", AIChE J. 31(7), 1086(1985).